Report No.332

epaResearch
Climate - Water - Sustainability
Identifying pressures • Informing policy • Developing solutions

OPTI-SDS: An Investigation of the OPTImum Specification for Soil Depressurisation Systems (Active and Passive) That Take Account of Irish Building Practices

Authors: Le Chi Hung, Jamie Goggins, Marta Fuente and Mark Foley

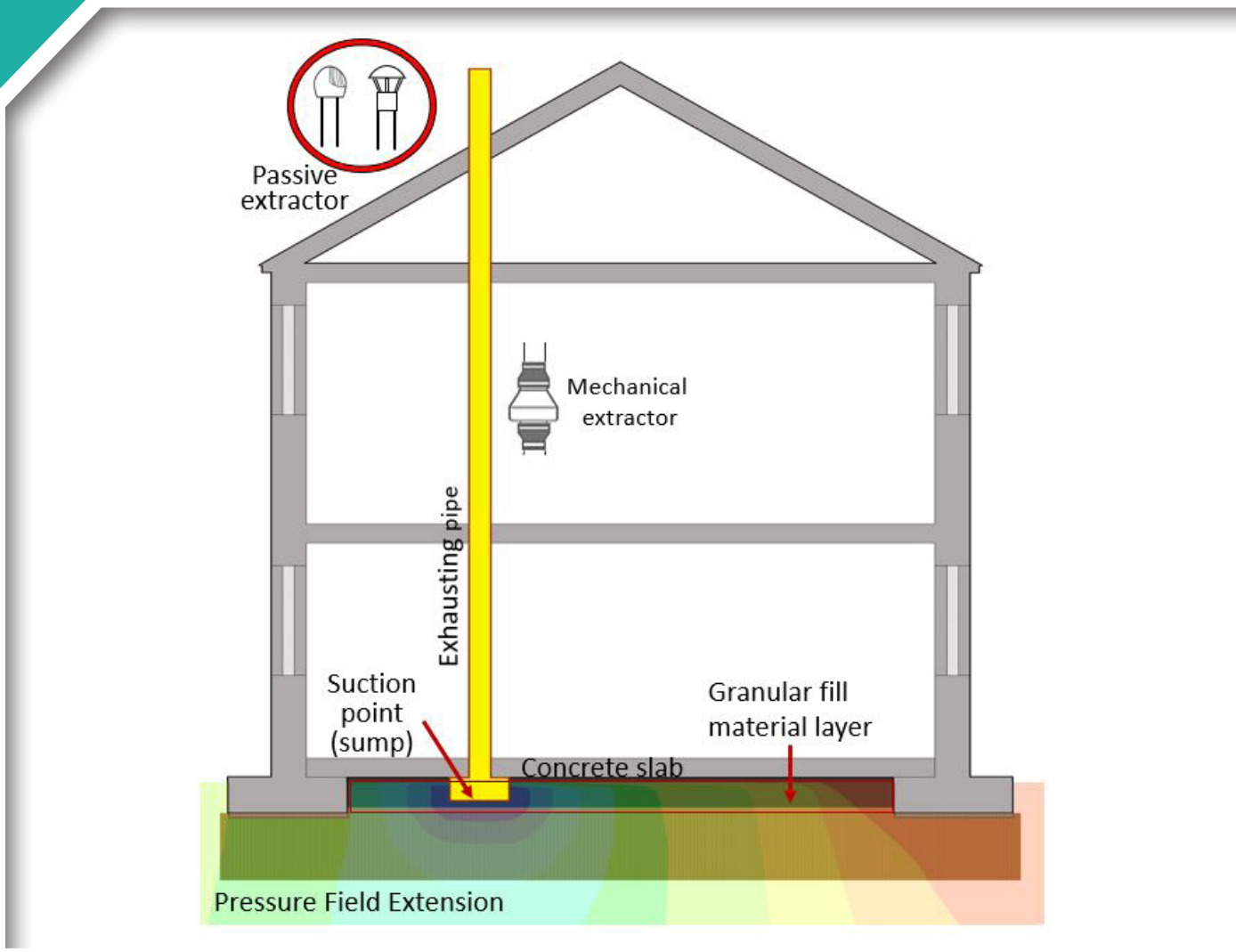

www.epa.ie

Rialtas na hÉireann
Government of Ireland

ENVIRONMENTAL PROTECTION AGENCY

The Environmental Protection Agency (EPA) is responsible for protecting and improving the environment as a valuable asset for the people of Ireland. We are committed to protecting people and the environment from the harmful effects of radiation and pollution.

The work of the EPA can be divided into three main areas:

Regulation: *We implement effective regulation and environmental compliance systems to deliver good environmental outcomes and target those who don't comply.*

Knowledge: *We provide high quality, targeted and timely environmental data, information and assessment to inform decision making at all levels.*

Advocacy: *We work with others to advocate for a clean, productive and well protected environment and for sustainable environmental behaviour.*

Our Responsibilities

Licensing

We regulate the following activities so that they do not endanger human health or harm the environment:

- waste facilities *(e.g. landfills, incinerators, waste transfer stations)*;
- large scale industrial activities (*e.g. pharmaceutical, cement manufacturing, power plants)*;
- intensive agriculture *(e.g. pigs, poultry)*;
- the contained use and controlled release of Genetically Modified Organisms *(GMOs)*;
- sources of ionising radiation *(e.g. x-ray and radiotherapy equipment, industrial sources)*;
- large petrol storage facilities;
- waste water discharges;
- dumping at sea activities.

National Environmental Enforcement

- Conducting an annual programme of audits and inspections of EPA licensed facilities.
- Overseeing local authorities' environmental protection responsibilities.
- Supervising the supply of drinking water by public water suppliers.
- Working with local authorities and other agencies to tackle environmental crime by co-ordinating a national enforcement network, targeting offenders and overseeing remediation.
- Enforcing Regulations such as Waste Electrical and Electronic Equipment (WEEE), Restriction of Hazardous Substances (RoHS) and substances that deplete the ozone layer.
- Prosecuting those who flout environmental law and damage the environment.

Water Management

- Monitoring and reporting on the quality of rivers, lakes, transitional and coastal waters of Ireland and groundwaters; measuring water levels and river flows.
- National coordination and oversight of the Water Framework Directive.
- Monitoring and reporting on Bathing Water Quality.

Monitoring, Analysing and Reporting on the Environment

- Monitoring air quality and implementing the EU Clean Air for Europe (CAFÉ) Directive.
- Independent reporting to inform decision making by national and local government *(e.g. periodic reporting on the State of Ireland's Environment and Indicator Reports)*.

Regulating Ireland's Greenhouse Gas Emissions

- Preparing Ireland's greenhouse gas inventories and projections.
- Implementing the Emissions Trading Directive, for over 100 of the largest producers of carbon dioxide in Ireland.

Environmental Research and Development

- Funding environmental research to identify pressures, inform policy and provide solutions in the areas of climate, water and sustainability.

Strategic Environmental Assessment

- Assessing the impact of proposed plans and programmes on the Irish environment *(e.g. major development plans)*.

Radiological Protection

- Monitoring radiation levels, assessing exposure of people in Ireland to ionising radiation.
- Assisting in developing national plans for emergencies arising from nuclear accidents.
- Monitoring developments abroad relating to nuclear installations and radiological safety.
- Providing, or overseeing the provision of, specialist radiation protection services.

Guidance, Accessible Information and Education

- Providing advice and guidance to industry and the public on environmental and radiological protection topics.
- Providing timely and easily accessible environmental information to encourage public participation in environmental decision-making *(e.g. My Local Environment, Radon Maps)*.
- Advising Government on matters relating to radiological safety and emergency response.
- Developing a National Hazardous Waste Management Plan to prevent and manage hazardous waste.

Awareness Raising and Behavioural Change

- Generating greater environmental awareness and influencing positive behavioural change by supporting businesses, communities and householders to become more resource efficient.
- Promoting radon testing in homes and workplaces and encouraging remediation where necessary.

Management and structure of the EPA

The EPA is managed by a full time Board, consisting of a Director General and five Directors. The work is carried out across five Offices:

- Office of Environmental Sustainability
- Office of Environmental Enforcement
- Office of Evidence and Assessment
- Office of Radiation Protection and Environmental Monitoring
- Office of Communications and Corporate Services

The EPA is assisted by an Advisory Committee of twelve members who meet regularly to discuss issues of concern and provide advice to the Board.

EPA RESEARCH PROGRAMME 2014–2020

OPTI-SDS: An Investigation of the OPTImum Specification for Soil Depressurisation Systems (Active and Passive) That Take Account of Irish Building Practices

(2015-HW-MS-5)

EPA Research Report

Prepared for the Environmental Protection Agency

by

National University of Ireland Galway

Authors:

Le Chi Hung, Jamie Goggins, Marta Fuente and Mark Foley

ENVIRONMENTAL PROTECTION AGENCY
An Ghníomhaireacht um Chaomhnú Comhshaoil
PO Box 3000, Johnstown Castle, Co. Wexford, Ireland

Telephone: +353 53 916 0600 Fax: +353 53 916 0699
Email: info@epa.ie Website: www.epa.ie

ACKNOWLEDGEMENTS

This report is published as part of the EPA Research Programme 2014–2020. The EPA Research Programme is a Government of Ireland initiative funded by the Department of Communications, Climate Action and Environment. It is administered by the Environmental Protection Agency, which has the statutory function of co-ordinating and promoting environmental research. The support of the SFI MaREI Centre (Grant no. 12/RC/2302) is also recognised.

The authors would like to acknowledge the members of the project steering committee, namely David Fenton (EPA), Eamonn Smyth (Department of Housing, Planning and Local Government), Stephanie Long (EPA) and Simon McGuinness (Department of Housing, Planning and Local Government), and the collaborators Luis Santiago Quindos Poncela and his research group at the University of Cantabria, and Eugene Monahan at All Clear Radon Ltd for his advice on the passive depressurisation test set-up. The authors would also like to acknowledge the important contributions made to the project by Peter Fahy, Colm Walsh, Dermot McDermott and Aodh Dalton of the School of Engineering, National University of Ireland Galway.

DISCLAIMER

This report is based on research carried out/data from June 2016 to June 2019. More recent data may have become available since the research was completed.

The EPA Research Programme addresses the need for research in Ireland to inform policymakers and other stakeholders on a range of questions in relation to environmental protection. These reports are intended as contributions to the necessary debate on the protection of the environment.

EPA RESEARCH PROGRAMME 2014–2020
Published by the Environmental Protection Agency, Ireland

ISBN: 978-1-84095-925-3 July 2020

Price: Free Online version

Project Partners

Dr Le Chi Hung
School of Physics/School of Engineering
National University of Ireland Galway
Galway
Ireland
Email: lchhung@gmail.com

Dr Jamie Goggins
School of Engineering and the MaREI Centre
National University of Ireland Galway
Galway
Ireland
Email: jamie.goggins@nuigalway.ie

Dr Marta Fuente
School of Physics
National University of Ireland Galway
Galway
Ireland
Email: m.fuentelastra1@nuigalway.ie

Dr Luis Santiago Quindos Poncela
Radon Group
University of Cantabria
Spain
Email: luis.quindos@unican.es

Dr Mark Foley
School of Physics
National University of Ireland Galway
Galway
Ireland
Email: mark.foley@nuigalway.ie

Contents

List of Figures

List of Tables

Executive Summary

The National Radon Control Strategy (NRCS) for Ireland has identified several knowledge gaps, including the optimum specifications for soil depressurisation (SD) systems (active and passive) that take account of Irish building practices. Few publications exist on this issue in the Irish context and this limits policy development and implementation, as well as hindering the use of novel technologies in the development of “radon-safe” new buildings. Studies from other countries have indicated that the effectiveness of passive sumps is enhanced by appropriate sealing across the base of the building (passive SD systems). Research is required in this field to take account of Irish building practices. The “OPTI-SDS: an investigation of the OPTImum specification for Soil Depressurisation Systems (active and passive) that take account of Irish building practices” project examined the characterisation of the T1 Struc and T2 Perm specified granular fill materials for SD systems for buildings.

The project was divided into two experimental laboratory test phases. In phase 1, a series of small-scale experimental laboratory tests were conducted to quantitatively investigate the characterisation of the T1 Struc and T2 Perm granular fill materials for SD systems for radon reduction under buildings. The characterisation included determination of grading curves and measurement of air permeability, porosity and the effective particle diameter of the fill material. A test apparatus was developed to measure the air permeability of the granular fill materials under different compaction degrees. Test results showed that the T1 Struc and T2 Perm specified granular fill materials could be classified as well-graded and poorly graded granular materials, respectively. The air permeability and porosity of T1 Struc decrease with an increase in compaction degree and are strongly affected by the change in moisture content. However, the air permeability of T2 Perm was found to be independent of the compaction degree and variation in moisture content.

In phase 2, a series of large-scale experimental tests was performed to examine the flow behaviour of the T1 Struc and T2 Perm materials with active and passive depressurisations. Materials were compacted and tested at various compacted thicknesses. Compaction works were performed using a field compactor and the compaction degrees of the materials were found to be higher than those induced by a standardised small-scale compactor. The air permeability values of the materials were obtained with active depressurisation. It was found that the overall trend in air permeability tended to decrease with the increase in the compacted thickness of the materials, which was consistent with the results obtained using the small-scale test apparatus. Furthermore, passive depressurisation tests were performed to examine the performance of different common chimney cowls available on the market for use in passive depressurisation systems. The rotating cowls performed best, followed by a static open pipe and a pipe with a cap.

Computational fluid dynamic simulations were developed and validated to simulate the flow behaviour of the T1 Struc and T2 Perm materials. The key parameters for simulating the flow behaviour of the materials were confirmed to be air permeability, porosity and effective particle diameter. Benchmark input parameters for the design of the T1 Struc and T2 Perm materials are provided in this study.

In addition to the laboratory tests, a case study was conducted in a pilot house with high radon levels in Spain to examine the ability and efficiency of active and passive SD systems. Radon concentration and pressure field extension (PFE) under the slab were monitored to examine radon reductions as a function of depressurisation. A relatively homogeneous pressure distribution was found under the slab of the house and the PFE analysis showed that the pressure drop with distance from the suction point of the SD system has a linear dependence on the depressurisation generated under the slab. Radon reductions in excess of 85% were achieved for the different SD systems tested. Based on the radon reduction results obtained from active SD, under the conditions considered it was found that a 20-W mechanical fan is sufficient to achieve SD producing radon reductions of above 85%.

1 Introduction

1.1 Overview

This report outlines (1) the characterisation of T1 Struc and T2 Perm granular materials for soil depressurisation (SD) systems under buildings using small- and large-scale experimental tests and computational fluid dynamics (CFD) simulations and (2) the characterisation of passive cowls for SD systems to mitigate the radon gas concentration inside buildings. The report also presents a case study that was conducted in a pilot house with high radon levels in Spain to examine the ability and efficiency of active and passive SD systems.

Radon (^{222}Rn) is a product from the decay chain of uranium (^{238}U) present in soils and rocks. It is a colourless, odourless, tasteless gas that has been identified as a human carcinogen by the World Health Organization (WHO), the International Agency for Research on Cancer (IARC) and the US Environmental Protection Agency (US EPA) (ICRP, 2010). Studies have shown that the outdoor radon concentration globally is between 5 and 15 Bq/m^3 and does not pose a health risk (Gunning *et al*., 2014; WHO, 2016). However, indoor concentrations can be significantly higher and have been shown to cause lung cancer through the decay of radon's short-lived daughter products, which results in pulmonary cell DNA damage.

It is estimated that indoor radon levels account for 9% of deaths from lung cancer, 2% of all deaths from cancer in Europe and approximately 21,000 deaths per year in the USA (Darby *et al*., 2005; Vogeltanz-Holm and Schwartz, 2018). The indoor radon concentration should be lower than 300 Bq/m^3 and indoor radon concentration mitigation is recommended when the radon level exceeds 300 Bq/m^3 (EU, 2014).

Reduction of the indoor radon concentration is an important issue in buildings (WHO, 2009). To minimise the indoor radon concentration, different mitigation techniques may be used: active and passive SD, sealing of surfaces, barriers and membranes, ventilation of unoccupied spaces and ventilation of occupied spaces (WHO, 2009). Among these techniques, the active and passive SD methods have been proven to be the best (Gadgil *et al*., 1991; Bonnefous, 1992; WHO, 2009; Abdelouhab *et al*., 2010; Vazquez *et al*., 2011). In Ireland, all buildings built after July 1998 have been required to include an SD system, regardless of the indoor radon concentration (DEHLG, 1997). The granular fill materials used beneath the floors and foundations of buildings are standardised, namely T1 Struc and T2 Perm granular fill materials (NSAI, 2016a). These materials are used to increase the bearing capacity of the foundations, as well as to avoid the expansion of the underfloor caused by the existence of pyrite-bearing material.

However, the National Radon Control Strategy (NRCS) for Ireland has identified several knowledge gaps, including the optimum specifications for passive SD systems that take account of Irish building practices (Fuente *et al*., 2020). Few publications exist on this issue in the Irish context and this limits policy development and implementation, as well as hindering the use of novel technologies in the development of "radon-safe" new buildings. Studies from other countries such as Spain and France (Abdelouhab *et al*., 2010; Vazquez *et al*., 2011) have indicated that the effectiveness of passive sumps is enhanced by appropriate sealing across the base of the building. Research is required in this field to take account of Irish building practices.

1.2 Objectives

The objectives of this study were to:

- Characterise the Irish T1 Struc and T2 Perm granular fill materials, including determination of the grading curves, compaction degree, air permeability and porosity of the materials. The characterisation included small-scale and large-scale experimental tests. New test apparatus was developed to complete this objective.
- Develop CFD models to design the SD system in practice. The models were validated using experimental tests. Detailed input parameters and boundary conditions for the design of SD systems using CFD simulations are presented.

- Investigate the performance of different common cowls used for passive SD systems. Two rotating and three static cowls were examined.
- Benchmark Spanish granular fill materials and establish the effectiveness of radon mitigation by SD in a Spanish pilot house.
- Examine radon concentration reductions and pressure field extension (PFE) under a slab of a pilot house as a function of the depressurisation.

1.3 Dissemination of the OPTI-SDS Project

The authors acknowledge that the contents of this report are published, in full or in part, in the following contributions.

1.3.1 International peer-reviewed journal articles

- Hung, L.C., Goggins, J., Fuente, M. and Foley, M., 2018. Characterisation of specified granular fill materials for radon mitigation by soil depressurisation systems. *Construction and Building Materials* 176: 213–227. https://doi.org/10.1016/j.conbuildmat.2018.04.210
- Hung, L.C., Goggins, J., Fuente, M. and Foley, M., 2018. Investigation of sub-slab pressure field extension in specified granular fill materials incorporating a sump-based soil depressurisation system for radon mitigation. *Science of the Total Environment* 637–638: 1081–1097. https://doi.org/10.1016/j.scitotenv.2018.04.401
- Fuente, M., Rabago, D., Herrera, S., Quindos, L., Fuente, I., Foley, M. and Sainz, C., 2018. Performance of radon monitors in a purpose-built radon chamber. *Journal of Radiological Protection* 38: 1111–1127. https://doi.org/10.1088/1361–6498/aad969
- Hung, L.C, Goggins, J., Croxford, C. and Foley, M., 2019. Large-scale experimental investigations of specified granular fill materials for radon mitigation by active and passive soil depressurisations. *Journal of Environmental Radioactivity* 207: 27–36. https://doi.org/10.1016/j.jenvrad.2019.05.018
- Fuente, M., Muñoz, E., Sicilia, I., Goggins, J., Hung, L.C., Frutos, B. and Foley, M., 2019. Investigation of gas flow through soils and granular fill materials for the optimisation of radon soil depressurisation systems. *Journal of Environmental Radioactivity* 198: 200–209. https://doi.org/10.1016/j.jenvrad.2018.12.024
- Fuente, M., Rabago, D., Goggins, J., Fuente, I., Sainz, C. and Foley, M., 2019. Radon mitigation by soil depressurisation case study: radon concentration and pressure field extension monitoring in a pilot house in Spain. *Science of the Total Environment* 695: 133746. https://doi.org/10.1016/j.scitotenv.2019.133746
- Fuente, M., Long, S., Fenton, D., Hung, L.C., Goggins, J. and Foley, M., 2020. Review of recent radon research in Ireland, OPTI-SDS project and its impact on the National Radon Control Strategy. *Applied Radiation and Isotopes* 109210. https://doi.org/10.1016/j.apradiso.2020.109210

1.3.2 Conference contributions

- Hung, L.C., Goggins, J. and Foley, M., 2016. OPTI-SDS: an investigation of the optimum specification for soil depressurization systems (active and passive) that take account of Irish building practices. *ROOMS 2016*, Concarneau, France, October 2016.
- Foley, M., Fuente, M., Goggins, J. and Hung, L.C., 2016. OPTI-SDS: an investigation of the optimum specification for soil depressurisation systems (active and passive) that take account for Irish building practices. *EPA conference, Environment and Health: Our Environment – Our Wellbeing*, Dublin, Ireland, November 2016 (poster).
- Hung, L.C., Goggins, J., Fuente, M. and Foley, M., 2017. An investigation of the optimum specification for soil depressurisation systems (active and passive) that take account for Irish building practices (update). *ROOMS 2017*, Galway, Ireland, October 2017.
- Fuente, M., Muñoz, E., Foley, M. and Frutos, B., 2017. Behaviour study of air flow through gravels based on laboratory experimentation and contrast with FEM models. *ROOMS 2017*, Galway, Ireland, October 2017.
- Foley, M., Goggins, J., Fuente, M. and Hung, L.C, 2018. An investigation of the optimum specification for soil depressurisation systems (active and passive) that take account for Irish building practices. *ENVIRON 2018 conference*, Cork, Ireland, March 2018.

- Croxford, C., Hung, L.C., Foley, M. and Goggins, J., 2018. Development of a test tank to investigate the pressure field extension for specified granular fill materials for radon mitigation by soil depressurisation systems. *Civil Engineering Research in Ireland 2018 (CERI2018) conference*, Dublin, Ireland, 29–30 August 2018.
- Fuente, M., Hung, L.C., Goggins, J. and Foley, M., 2018. Radon mitigation in Spanish pilot house: results overview and measurement plan. *Civil Engineering Research in Ireland 2018 (CERI2018) conference*, Dublin, Ireland, 29–30 August 2018.
- Hung, L.C., Croxford, C., Goggins, J., Fuente, M. and Foley, M., 2018. OPTI-SDS Project: an experimental investigation of the pressure field extension in a granular fill material for radon mitigation by soil depressurisation systems. *ROOMS 2018*, Lugano, Switzerland, September 2018.
- Fuente, M., Goggins, J., Hung, L.C. and Foley, M., 2018. Ongoing research on radon mitigation by soil depressurisation in a Spanish pilot house. *ROOMS 2018*, Lugano, Switzerland, September 2018.
- Foley, M., Long, S., Fenton, D., Hung, L.C., Goggins, J. and Fuente, M., 2019. EPA funded radon research in Ireland and its impact on the National Radon Control Strategy. *10th Annual Scientific Meeting of the Irish Association of Physicists in Medicine*, Dublin, Ireland, March 2019.

1.3.3 Outreach activities

- RTE's *10 Things to Know About … Earth's Crust*: The EPA-funded OPTI-SDS project featured in the season 3 opener on 13 November 2017. Excerpt from the press release: "Dr Mark Foley and his team at NUI Galway are investigating different building materials that could be placed under concrete foundations of houses, to improve radon ventilation before it enters our homes".
- An 8-week school project was carried out at Scoil Íde, Salthill, Galway, with 30 children from the 4th class to highlight the importance of raising awareness of radon and mitigation measures that could be undertaken to reduce radon levels in homes and schools. The project was presented at the Galway Science & Technology Festival 2017 (in excess of 20,000 attendees) on 26 November 2017 and it was awarded the top prize in the Physics & Chemistry Primary School project category.
- Participation at the Engineering Our Future: Family Fun Day on 24 February 2018 (>700 attendees) in the Alice Perry Engineering Building, National University of Ireland Galway. Among different science and engineering shows, workshops and activities, there was a stand about radon to raise awareness of radon as a public health issue. The co-ordinator of the overall event was Dr Jamie Goggins, OPTI-SDS co-principal investigator.
- A workshop on Radioactivity: The Science of the Invisible was conducted at Scoil Íde, Salthill, Galway, to explain to children the basic concepts of radioactivity and particle detection. A DIY cloud chamber was built in the classroom to help indirectly observe radiation, including radon alpha tracks. The workshop was showcased at the Galway Science & Technology Festival 2018 on 25 November 2018.
- Participation at the Engineering Our Future: Family Fun Day on 2 March 2019 (>1400 attendees) in the Alice Perry Engineering Building, National University of Ireland Galway. The co-ordinator of the overall event was Dr Jamie Goggins, OPTI-SDS co-principal investigator.

2 Literature Review

2.1 Objective

The objective of the literature review was to comprehensively review existing national and international publications on the issues of indoor radon concentrations and SD systems.

2.2 Methods

To conduct the literature review, searches for publications were carried out in online databases including Scopus (Elsevier), ScienceDirect, Wiley Online Library and Springer. Searches were also undertaken on ResearchGate, Google Scholar and the EPA website, as well as in the *WHO Handbook on Indoor Radon: A Public Health Perspective* (WHO, 2009). In addition, citations in relevant publications were also checked and reviewed. These steps were repeated frequently during the project to ensure that the latest relevant publications were included.

2.3 Review of the Literature

2.3.1 Representative previous studies of soil depressurisation

Previous studies have shown that SD systems are the most effective radon mitigation techniques. The principle of an SD system is to generate suction pressure in the granular fill material layer placed beneath the floor of a building to reverse the entry path of radon gas from the soil into the building (Figure 2.1) (Jiránek and Svoboda, 2007; Jiránek, 2014; Diallo *et al*., 2015, 2018; Collignan, 2018). The active SD system can reduce the indoor radon level (Jelle, 2012; Long *et al*., 2013; Jiránek, 2014) by up to 92%.

Jiránek and Svoboda (2007) adapted three different finite element programs (i.e. Press 3D, Wind 2D and Radon2D) to study radon concentrations in the subsoil using SD systems. They began by stating that the effectiveness of the SD systems is influenced by different factors such as airtightness, the air permeability of the soil and hardcore layers, the number and capacity of the fans, and the location and size of the sumps and pipes. Data measured from a family home were analysed. The air permeability values of both the hardcore and the subsoil layers, the crack/leakage area and the underpressure within the hardcore layer were the main factors investigated. The authors found that the radon concentration is influenced strongly by the air permeability of both the subsoil and the hardcore layers, as well as the area of crack/leakage.

Abdelouhab *et al*. (2010) performed an extensive experimental investigation to study the ability and efficiency of SD systems to mitigate radon concentrations. They experimentally quantified that the passive SD system is much more cost-effective than the active SD system if a proper design is produced. The tests were carried out in a pilot house that had a basement area of 81 m^2 (9 m × 9 m). A 40-cm-thick hardcore gravel layer was placed below the concrete slab to depressurise the subsoil. A bitumen membrane was installed under this concrete slab. Ten different holes were drilled from the slab into the soil to set up the measurement sensors for pressure induced during the operation of the SD systems. The authors found that the soil extract flow of the passive SD system was similar to that of the active SD system. The study showed that the passive SD system could be run mainly during the cold season. This finding was also experimentally confirmed by Diallo *et al*. (2015). In addition, Abdelouhab *et al*. (2010) found that the type of extractor used plays an important role in the effectiveness of the passive SD system.

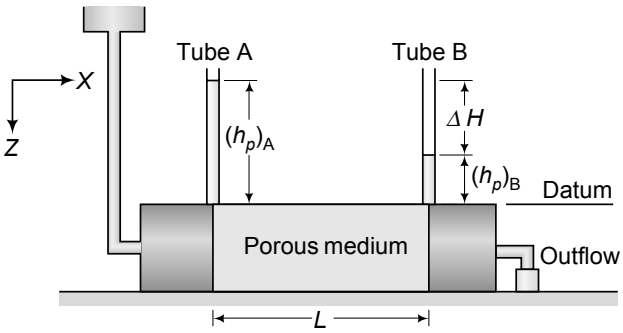

Figure 2.1. Darcy's law of airflow through a porous medium. Source: Budhu, 2010. Copyright © 2011, 2007, 2000 John Wiley & Sons, Inc. All rights reserved.

Vazquez *et al*. (2011) conducted a series of experimental tests on a prototype house to investigate the effectiveness of passive and active SD systems, as well as the location of the radon sump. The test house had an area of 25 m^2 and two radon sumps (one was located at the centre of the house and the other was located at the side of the house). The SD system consisted of a 10-cm-thick concrete slab, under which was a 15-cm-thick gravel layer. No radon membrane was used. A rotating cowl was used for the passive SD system. Similar conclusions to those from the work of Abdelouhab *et al*. (2010) were made.

Several different factors can influence the effectiveness of the SD system, including the air permeability of the granular fill material (k_{ah}) and the native soil (k_{as}) beneath the floor, cracks in the floor, the radon sump size, the sealing, the moisture content, the fan speed and atmospheric conditions. Studies have shown that the k_{ah} significantly affects the effectiveness of the SD system (Bonnefous *et al*., 1994; Gadgil, *et al*., 1994; DETR, 1997a, b; BRE, 1998; Jiránek and Svoboda, 2007). In addition, the granular fill material layer beneath the floor should satisfy the bearing capacity and serviceability criteria and should be permeable to ensure the effectiveness of the SD system.

Diallo *et al*. (2015) developed an analytical model to design the SD systems. In contrast to previous analytical models (e.g. Reddy *et al*., 1991), which simply assume that the SD system is a homogeneous cylinder layer with impermeable layers at the top and the bottom of the cylinder, the analytical model developed by Diallo *et al*. (2015) covers a wide range of boundary conditions existing in an SD system, such as the thickness of the slab, the permeability of the slab, the crack and the stack effect. The extracted air flow rate and suction pressure measured in a passive SD system were compared with the numerical model proposed by the authors. The authors confirmed the significant impacts of the air permeability of the slab, soil and hardcore and the environmental temperature on the efficiency of the SD system.

2.3.2 Air permeability and porosity of porous materials

Permeability is a property of a porous material that governs the ability of a fluid (liquid or gas) to transmit through the porous material. The convective and diffusive transport of air through a porous material is governed by the air permeability. This transport occurs if a pressure gradient is applied to the porous material; the air velocity through the material can be solved using Darcy's law (Springer *et al*., 1998; Ball and Schjonning, 2002; Shukla, 2014). The principle of Darcy's law for airflow can be expressed in equation 2.1 and Figure 2.1 as follows:

$$Q = k_a A \frac{\gamma_w g}{\eta} \frac{\Delta H}{L} \tag{2.1}$$

where Q is the volume of air passing through the porous material (m^3/s); k_a is the air permeability of the material (m^2); A is the cross-sectional area of the medium (m^2); γ_w is the density of water (kg/m^3); g is the gravitational acceleration constant (m/s^2); η is the viscosity of air (kg/m·s); ΔH is the air pressure difference = $(h_p)_A - (h_p)_B$; $(h_p)_A$ is the inlet pressure head (m); $(h_p)_B$ is the outlet pressure head (m); and L is the flow length (m).

Porosity is the ratio of the total volume of the pore space within the medium to the total volume of the medium, as shown in equation 2.2.

$$n = \frac{V_{pore}}{V_{total}} \tag{2.2}$$

where n is the porosity, V_{pore} is the total volume of the pore space and V_{total} is total volume of the medium. The typical porosity can range from 0–0.1 for rock to 0.4–0.7 for clay (Freeze and Cherry, 1979; Terzhaghi *et al*., 1996; Budhu, 2010).

Permeability is strongly dependent on the material type, shape and arrangement of the grain, roundness, grain size, sorting, pore size distribution, internal surface area, continuity of the pores, compacting degree, water content of the material, etc. (US EPA, 1993; Terzaghi *et al*., 1996; Ball and Schjonning, 2002). However, there is a poor correlation between air permeability and porosity (US EPA, 1993; Detmer, 1995) as a porous medium, which has high porosity but less continuity, may have low air permeability.

The Department of the Environment, Transport and the Regions (DETR, 1997a,b) examined the effectiveness of different types of hardcore to be used in passive ventilation for minimising the indoor concentrations of carbon dioxide and methane gases in buildings. The hardcore materials were well-sorted 20-mm single-sized gravel and well-graded granular material,

namely MOT Type 1. The DETR concluded that the minimum size of the particle should be 20 mm, with a minimum thickness of 300 mm. The well-graded granular material MOT Type 1 was not suitable as a material for hardcore for passive ventilation. Figure 2.2 shows that air permeability is independent of porosity and is strongly influenced by sorting and distribution of grain size. Air permeability increases with increase in the sorting degree. The distribution of grain size has a significant effect on air permeability: the coarser the grain size the higher the permeability. In contrast, porosity is dependent only on the sorting degree – it increases with the increase in sorting. Porosity is independent of the grain size distribution.

Selley (2000) also stated that the shape, sorting of grain and grain compaction all play an important role in air permeability. A well-sorted soil has a higher permeability and porosity than a poorly sorted soil. The effect of grain compacting on air permeability and porosity is shown in Figure 2.3.

Other studies have indicated that, for a given porous material at a specific porosity, the air permeability is largely controlled by the water content (Springer *et al*., 1998; Ball and Schjonning, 2002). Figure 2.4 shows the relationship between water content and permeability. Permeability decreases as the water content increases. At a lower-boundary water content of about 10% and an upper-boundary water content of approximately 30% the air permeability is slightly and significantly reduced, respectively. This reduction in air permeability can be explained by the blockage of water in the macropores within the porous medium.

Another important factor that influences the air permeability and porosity of porous materials is the compaction degree (DETR, 1997a). The compaction required for the hardcore layer below the slab/ shallow foundation should satisfy the bearing capacity and settlement criteria of the foundation. The gas dispersion ability of a granular material is reduced with the decrease in air permeability caused by the increase in the compaction degree. However, to the authors' knowledge, there has been no study that has systematically investigated the effect of the compaction degree on the air permeability of porous materials.

Typical values for the porosity and air permeability of different granular materials from a variety of studies are presented in Tables A1.1 and A1.2, respectively. These values can be used as reference values for primary analysis of SD systems if actual data are not available. Where available, the standards used to obtain these values in each study are listed in Tables A1.1 and A1.2.

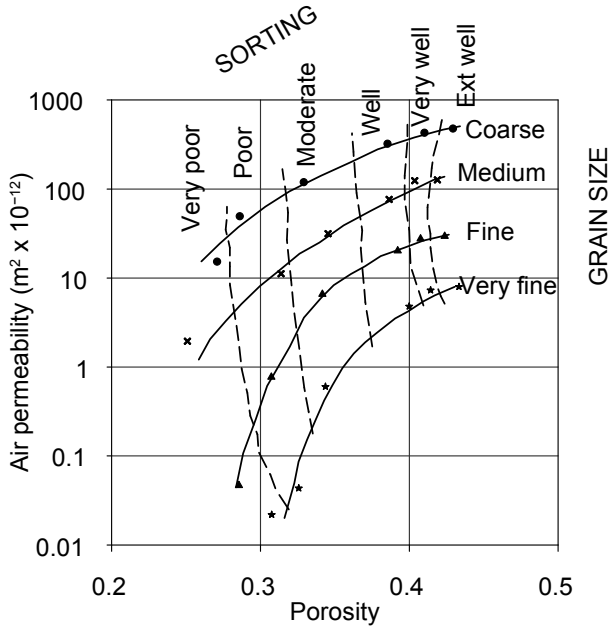

Figure 2.2. Relationship between porosity, permeability and sorting and sand grain size (modified from Nagtegaal, 1978. Courtesy of the Geological Society of London).

2.3.3 Design of the radon sump, pipe and fan

Radon gas does not drain into the sump of an SD system; however, under suction pressure created by an externally powered fan, wind force, etc., radon gas will be collected into the sump and drawn through the exhaust pipe.

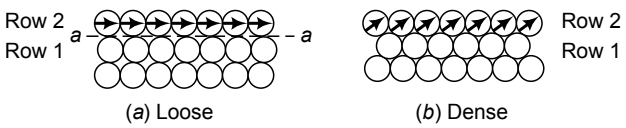

Figure 2.3. Effect of grain compacting on permeability and porosity: (a) low grain compacting (high permeability and porosity); (b) high grain compacting (low permeability and porosity). Source: Budhu, 2010. Copyright © 2011, 2007, 2000 John Wiley & Sons, Inc. All rights reserved.

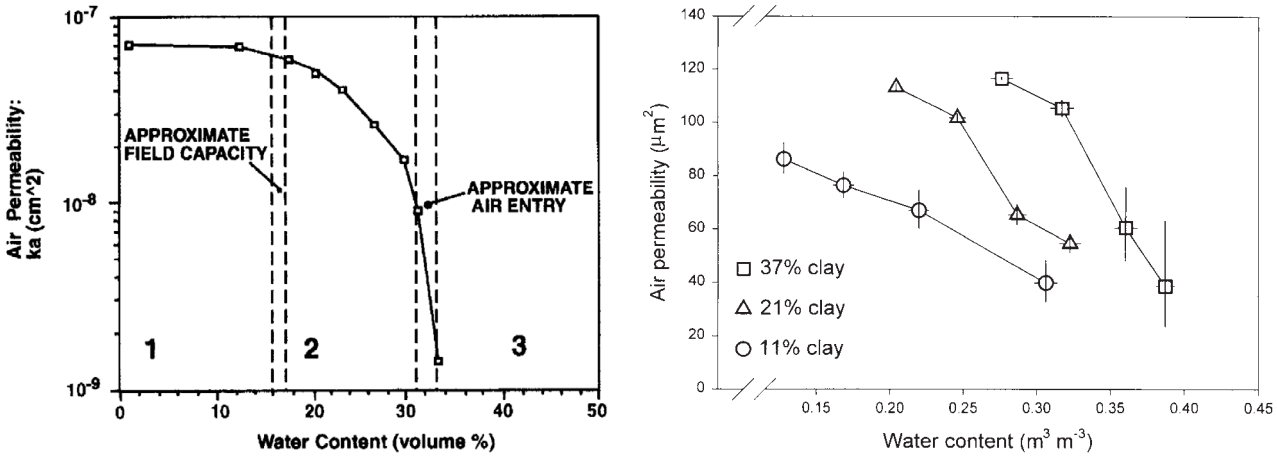

Figure 2.4. Effect of water content on the air permeability of different soils. L-B, lower bound; U-B, upper bound. (a) Source: Springer *et al.*, 1998, © 1998 National Groundwater Association; (b) source: Ball and Schjonning, 2002, © 2002 by the Soil Science Society of America, Inc.

Several existing codes and manuals provide guidelines on the design of the sump, pipe and fan for an SD system. A sump is a void that collects gas beneath the ground floor. An SD system will work effectively if a sump is included, especially in the case of very high indoor radon concentrations of greater than 1200 Bq/m^3 (BRE, 1998). The size of the sump can be varied; one radon sump can cover an influence area of 250 m^2 or a distance of 15 m from the sump centre (DEHLG, 1997). However, to the best of the authors' knowledge, this assumption has not been investigated quantitatively.

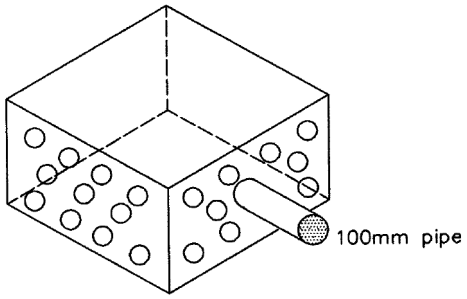

Figure 2.5. Schematic of a prefabricated radon sump (extracted from DEHLG, 2002).

Figure 2.5 shows a schematic of a prefabricated sump. The exhaust pipe that connects to the sump is usually a 100- to 150-mm-diameter polyvinyl chloride (PVC) pipe. The maximum suction pressure created by the fan should be between 150 Pa and 250 Pa at the sump (BRE, 1992).

3 Research Methodology

3.1 Overview

This research involved small-scale (phase 1) and large-scale (phase 2) experimental tests, a monitoring study carried out in a pilot house and numerical simulations obeying CFD. A configuration of the laboratory test set-up is shown in Figure 3.1. The following sections outline the research methodology.

3.2 Materials

Based on the Irish standards IS 888:2016 (NSAI, 2016a) and S.R. 21:2014+A1:2016 (NSAI, 2016b), the hardcore materials used under concrete floors in buildings in Ireland are T0 Struc, T1Struc and T2 Perm. T3 Blind is used as the cover layer to prevent the sharp projection of the hardcore through the radon membrane. T1 Struc and T2 Perm were selected as the hardcore materials for use in this research (Figure 3.2).

Two types of standard Spanish granular fill materials were benchmarked against the Irish T1 Struc and T2 Perm: garbancillo 4/12 and standard Spanish gravel 4/20 (Figure 3.3).

3.3 Particle Size Distribution Test

Sieve analysis was performed to determine the grading curves for the T1 Struc and T2 Perm granular fill materials. The test was conducted in accordance with the standard British Standard (BS) 1377 − Part 2 (BSI, 1990a).

3.4 Compaction Test

In buildings, the bearing layer beneath the foundation and floor should be compacted before any superstructure is built. This increases the density of the bearing layer, thus ensuring that the bearing capacity and serviceability criteria are met. Therefore, understanding the degree of permeability of compacted granular fill material layers beneath the floor and foundation is fundamental. In addition, the granular fill material might experience a range of moisture content (w_n) after compaction during its service life. The moisture content of the granular fill material could be dry, partially saturated or fully saturated, depending on the environmental conditions, the water table and the geological conditions. Compaction degrees of the T1 Struc and the T2 Perm materials were determined by performing small-scale and large-scale (field) compaction tests.

3.4.1 Small-scale compaction tests (phase 1)

These tests were performed following the standard BS 1377 − Part 4 (BSI, 1990b) using the BS standard compactor. At the beginning of the test, the material was mixed with water using a 0.5-m^3 revolving drum mixer. The compaction moisture content (w_{nc}) was

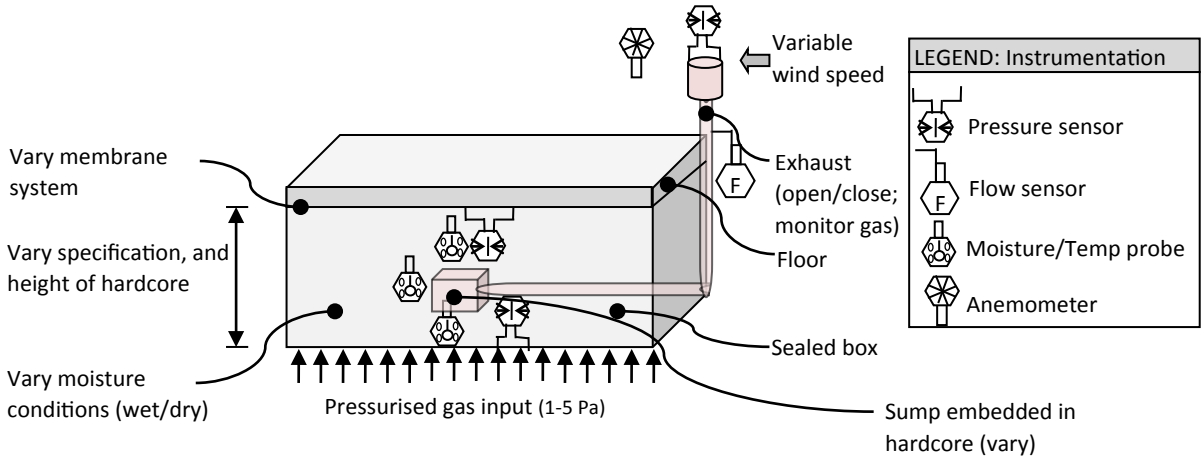

Figure 3.1. Configuration of the laboratory test set-up.

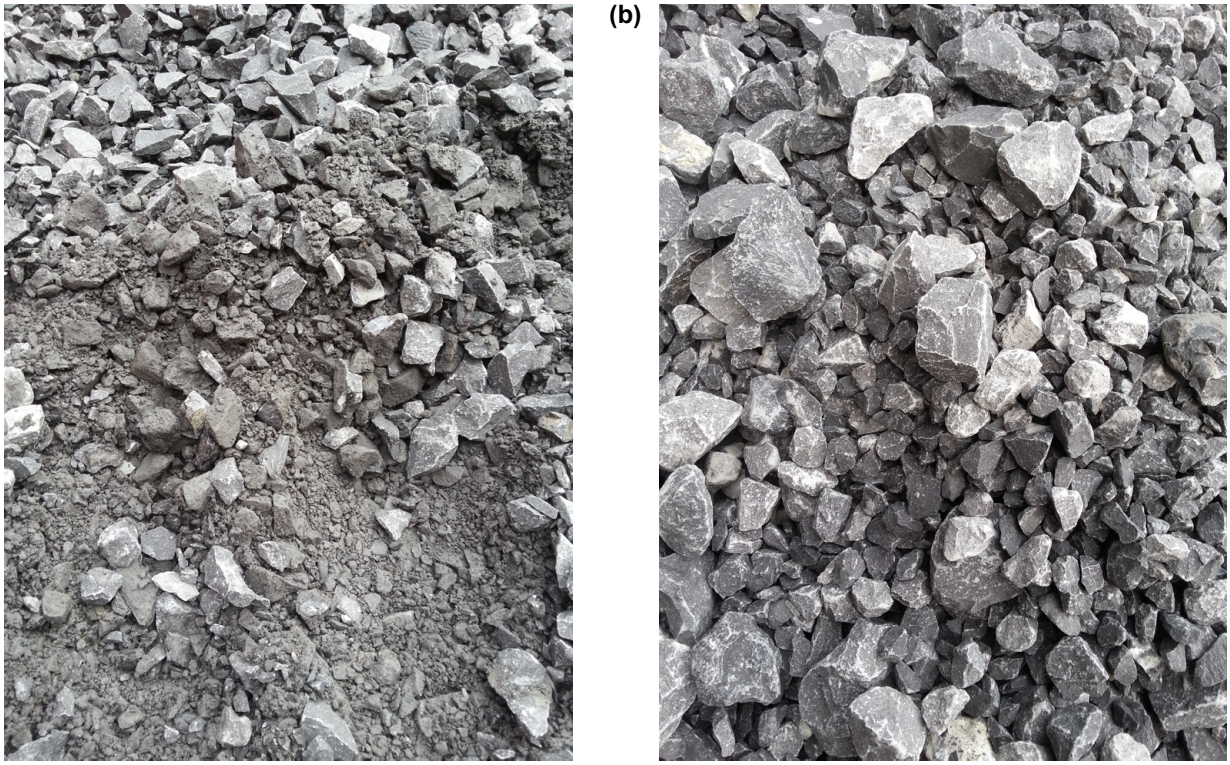

Figure 3.2. Photographs of (a) T1 Struc and (b) T2 Perm granular fill materials.

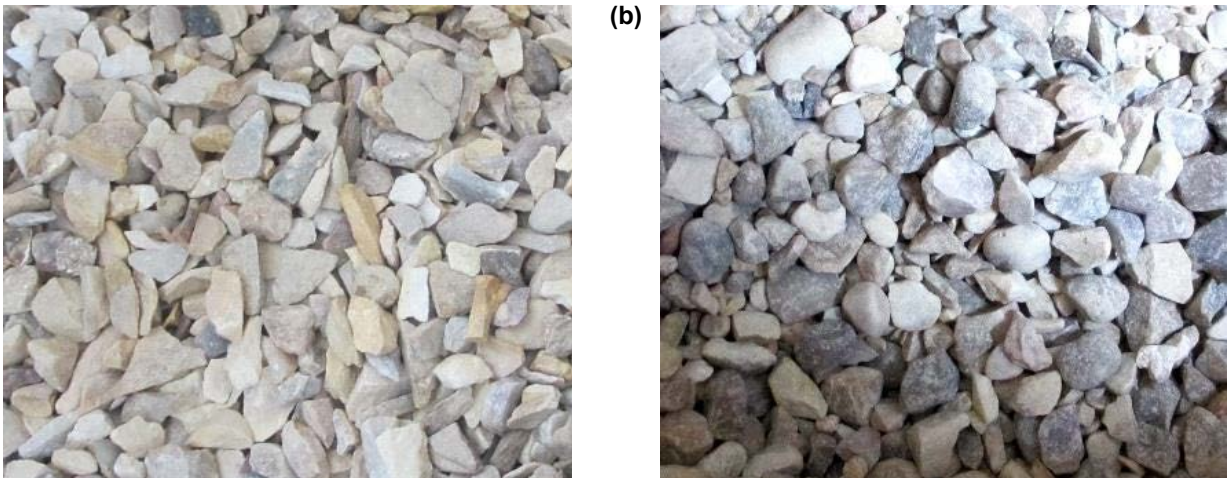

Figure 3.3. Photographs of (a) garbancillo 4/12 and (b) standard Spanish gravel 4/20.

controlled by adding a fixed amount of water. The material was then compacted with the compactor. Three small samples of the material were taken, the samples were dried using an oven dryer for 24 hours and the w_{nc} was determined for each sample. The optimum w_{nc} was determined by gradually increasing the amount of water in the materials.

3.4.2 Field compaction tests (phase 2)

The field compaction tests were carried out in accordance with the Irish standard IS 888:2016 (NSAI, 2016a) using a field compactor. For the T1 Struc material, the compaction was performed at its natural moisture content (i.e. 3–4%) to reflect real construction practice. For the T2 Perm material, water was sprayed onto the material before compacting to prevent fly

dust for health and safety reasons, as the material was extremely dry at the time of testing. The materials were compacted in layers, with each layer having an initial thickness, $t_{(initial)}$, of 110 ± 10 mm, 150 ± 10 mm or 225 ± 10 mm (see Table A2.1). The compaction degree was obtained by measuring the initial (before compaction), $t_{(initial)}$, and final (after compaction), $t_{(final)}$, thickness of each layer of material.

3.5 Development of the Experimental Test Apparatus

3.5.1 Phase 1: development of a small-scale test apparatus to measure the air permeability of granular fill materials

In phase 1, a small-scale test apparatus was developed to measure the k_{ah} and porosity (n_h) values of T1 Struc and T2 Perm (Figure 3.4). The working principle of the test apparatus was adopted following ASTM International standard D6539 (ASTM International, 2013) and previous studies by Gadgil *et al*. (1991) and BRE (1998). The main difference with the test apparatus in the current study is that it enabled the measurement of k_{ah} and n_h values of the granular fill materials under different compaction degrees, as well as for different values of w_n. The test apparatus consisted of a plastic pipe with a 150 mm inner diameter, a length of 3250 mm and a wall thickness of 5 mm. The inner diameter of 150 mm was chosen as this is similar to the BS standard compaction mould used in the compaction tests. The pipe was split into different segments, including inlet (1.5 m length) and outlet (0.25 m length) chambers and three sample segments (0.5 m length/segment). These segments were joined by four flexible couplings during testing to prevent air leakage.

Two air pressure sensors (model 26PCBFA6G, Honeywell, Golden Valley, MN, USA) were placed at the inlet and outlet chambers to measure the gas pressure difference in the test sample. Calibration of the pressure sensors was conducted by measuring the pressures derived from different fixed water column heights, e.g. a 1-cm water column height corresponds to 98.1 Pa. The water column heights were varied from 0.5 cm to 150 cm. Based on the calibration results, the following correlation was introduced to obtain the theoretical pressure measured in the tests:

$$P_{theoretical} = m \times P_{reading} \quad (3.1)$$

where $P_{theoretical}$ is the theoretical pressure associated with the water column height, $P_{reading}$ is the pressure recorded by the pressure sensors and m is the correction factor; $m = 1.304$ and 1.1073 for the sensors P_1 and P_2, respectively. These m factors were obtained with a correlation factor between $P_{theoretical}$ and $P_{reading}$ of $R^2 = 0.999$.

To determine the airflow rate (Q_m) through the test samples, three air flowmeters (VFA-3, Dwyer, Michigan City, IN, USA; PRM−1, Cole-Parmer, London, UK; and RF1MHAI46, Influx Measurements, Eastleigh, UK) were used to measure different flow rates, i.e. from 4.68×10^{-6} m³/s to 3.34×10^{-3} m³/s. In addition, a velocity sensor (F900, Degree Controls, Milford, NH, USA) was used to measure higher Q_m (i.e. $Q_m > 3.34 \times 10^{-3}$ m³/s). A compressed air regulator was

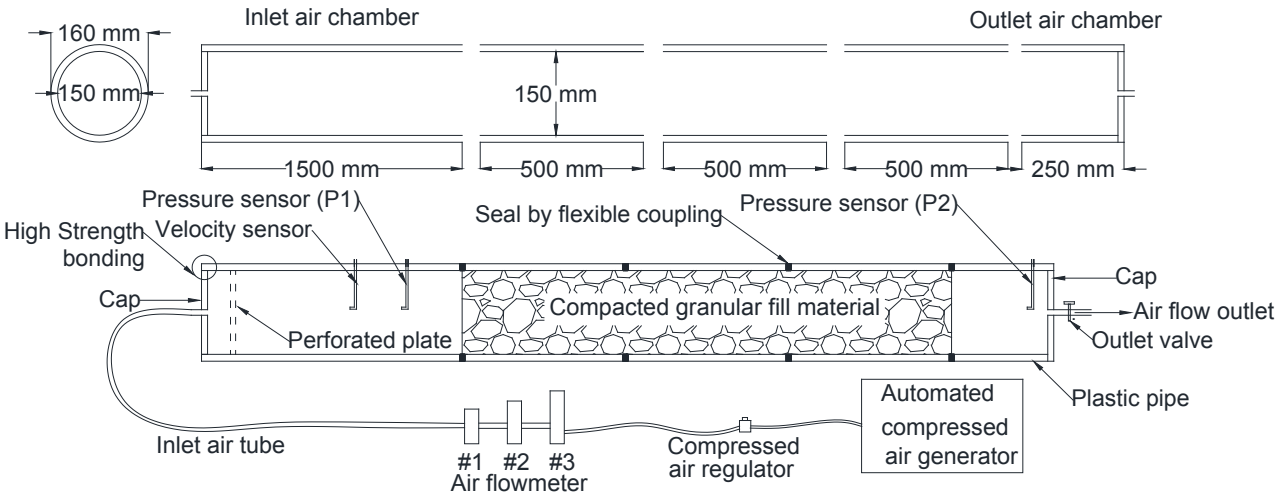

Figure 3.4. Diagram of the air permeability test apparatus used in this study (not to scale).

used to control the Q_m of the pressurised air at the air inlet chamber.

Air leakage in the test apparatus was carefully examined by introducing pressurised (20 kPa) air into the test apparatus when it was empty. After pressurising the air into the test apparatus, all valves were closed and the pressure trapped inside the apparatus was monitored for 5 minutes. No pressure drop was observed, meaning that the test apparatus was sufficiently sealed. However, tests were conducted at a maximum pressure of 12 ± 1 kPa at the inlet gas chamber. Measurements were interpreted and recorded using the National Instruments NI 9237 data logger and the LabVIEW program version 2016 (National Instruments, Austin, TX).

Experimental tests were performed as follows. A fixed air flow rate Q_m was pressurised into the air inlet chamber using an automated compressed air generator. This fixed Q_m was controlled by a compressed air regulator. The Q_m was obtained by reading the airflow rate value from an air flowmeter or air velocity meter. After the fixed Q_m had been specified, the regulator was locked to ensure that a constant Q_m was maintained during testing.

Each test was recorded for approximately 350 seconds. In the tests, P_1 and P_2 increase gradually and an equilibrium condition is observed. At this stage, P_1 and P_2 are constant (Figure 3.5) and constant values of P_1 and P_2 are averaged. The average values of P_1 and P_2 were used to calculate the pressure difference as $\Delta P = P_1 - P_2$. This ΔP was related to the degree of permeability of the material: the lower the degree of permeability, the higher the ΔP and vice versa. Each test sample was tested at least three times to minimise uncertainty.

To benchmark Spanish granular fill materials, a similar test apparatus was developed consisting of three different parts: an inlet chamber, a testing sample chamber and an outlet chamber. In this case, it was made of Perspex and PVC pipes with a diameter of 125 mm, walls of 3.2 mm thickness and a total length of 3050 mm (Figure 3.6). The diameter of the pipe was chosen to suit samples with particle sizes of less than 30 mm; for larger particle sizes the pipe diameter should be increased to avoid any surface effects.

Several differential pressure sensors were placed at different points along the sample chamber, as well as at the inlet and outlet chambers, to measure the pressure drop along the sample and the inlet–outlet pressure difference. The pressure sensors used were the Energy Conservatory DG-700 Pressure and Flow Gauge (TEC, Minneapolis, MN; measuring range from −1250 Pa to 1250 Pa, accuracy ±1%) and the Honeywell HSCDRRD006MDSA3 model (operating pressure ±6 mbar, accuracy 0.25%). A pitot tube (Testo 0635 2145, West Chester, PA; measuring range from +1 to +100 m/s) for measuring flow velocity and a hot wire anemometer [Testo 425; measuring range from 0 to +20 m/s, accuracy ±(0.03 m/s + 5% of mv) and resolution 0.01 m/s] were used to measure the Q_m in the inlet chamber. The gas source chosen was a compressed air generator and a needle valve was used to regulate the inlet air.

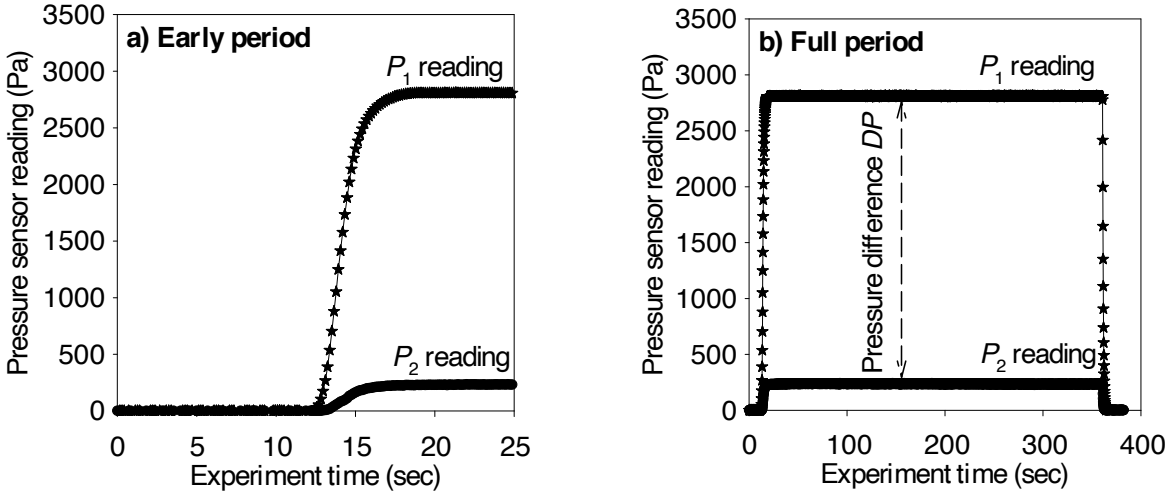

Figure 3.5. Example of the experiment time for test sample T1#4-1 at $Q_m = 1.67 \times 10^{-4}$ m³/s. See section 3.6.1 for an explanation of the test ID.

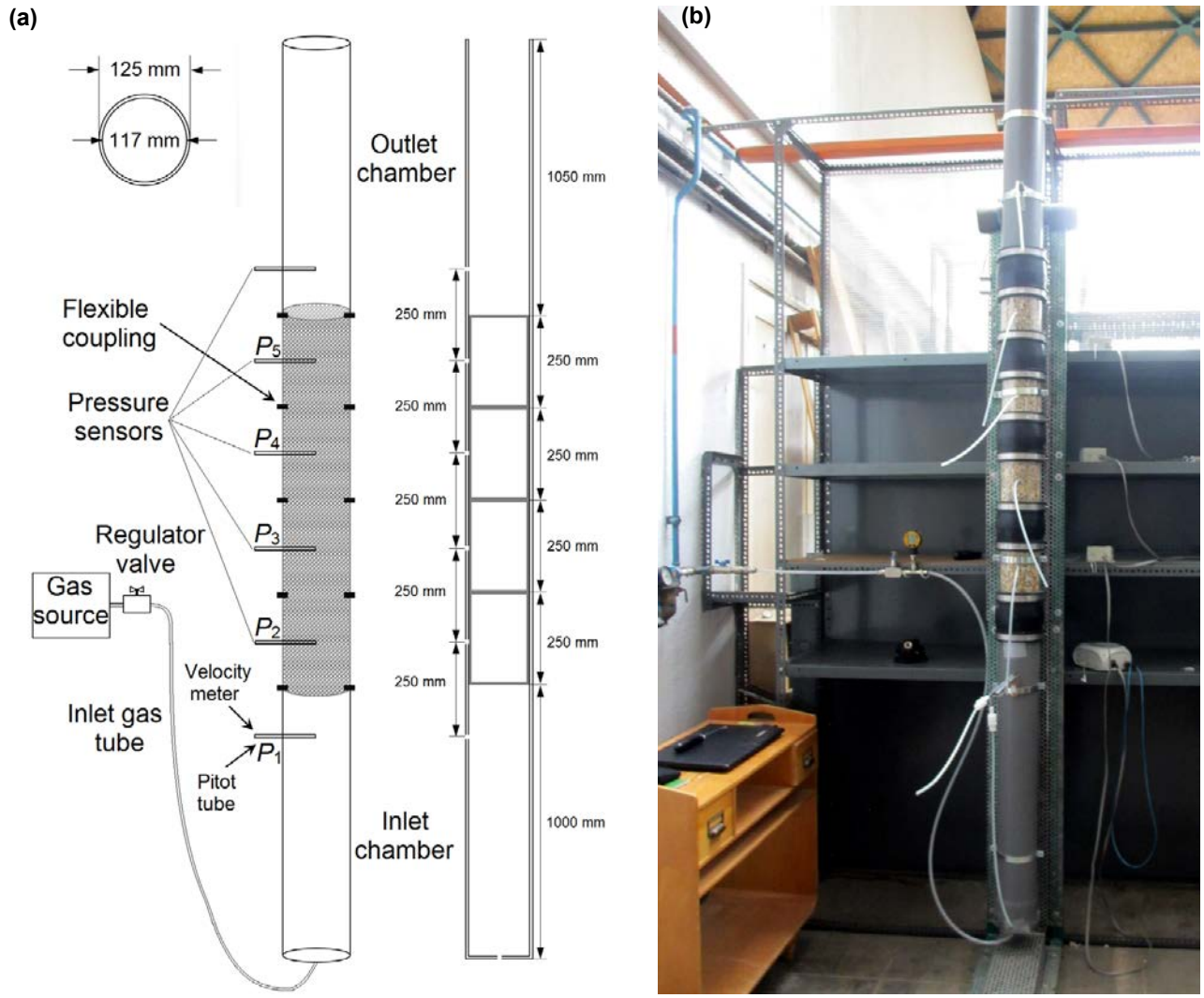

Figure 3.6. (a) Diagram of the test apparatus used in this study to benchmark the air permeability of Spanish granular fill materials (not to scale); (b) photograph of the test apparatus set-up.

3.5.2 Phase 2: development of a large-scale tests apparatus to measure the air permeability of granular fill materials

A large-scale steel test tank was developed to measure the field compaction degree, k_{ah} and n_h values of the T1 Struc and T2 Perm materials (Figure 3.7). The tank consisted of a cylinder, a base, a lid and a raised floor. The base and lid can be tightly connected to the cylinder using 80 M19 bolts. The working principle of the test tank was the same as that of the small-scale test apparatus reported in Hung *et al*. (2018a,b), with the main difference being that the tank developed in this study had a large diameter of 2000 mm compared with a diameter of 150 mm in the study by Hung *et al*. (2018a,b). The height of the tank was 1400 mm. The granular materials were added and compacted in the tank using a field compactor.

Double layers of rubber gaskets were attached on the top and the bottom of the cylinder before tightly attaching it to the base and the lid of the tank to make a perfect seal. Each M19 bolt was torqued at a final force of 18 Nm to ensure identical contact of the gaskets with the lid and the base of the tank. The perfectly sealed tank was carefully examined by both pressurising and depressurising the empty tank when the tank was fully closed. No significant pressure drop was observed, meaning that the test tank was sufficiently sealed. This sealed tank set-up was applied for all tests.

The tank had two inlet ports (12 mm inner diameter for each) and an outlet port (110 mm inner diameter). Suction pressures were generated using a controllable electric outlet fan (for active depressurisation tests) or chimney cowls (for passive depressurisation

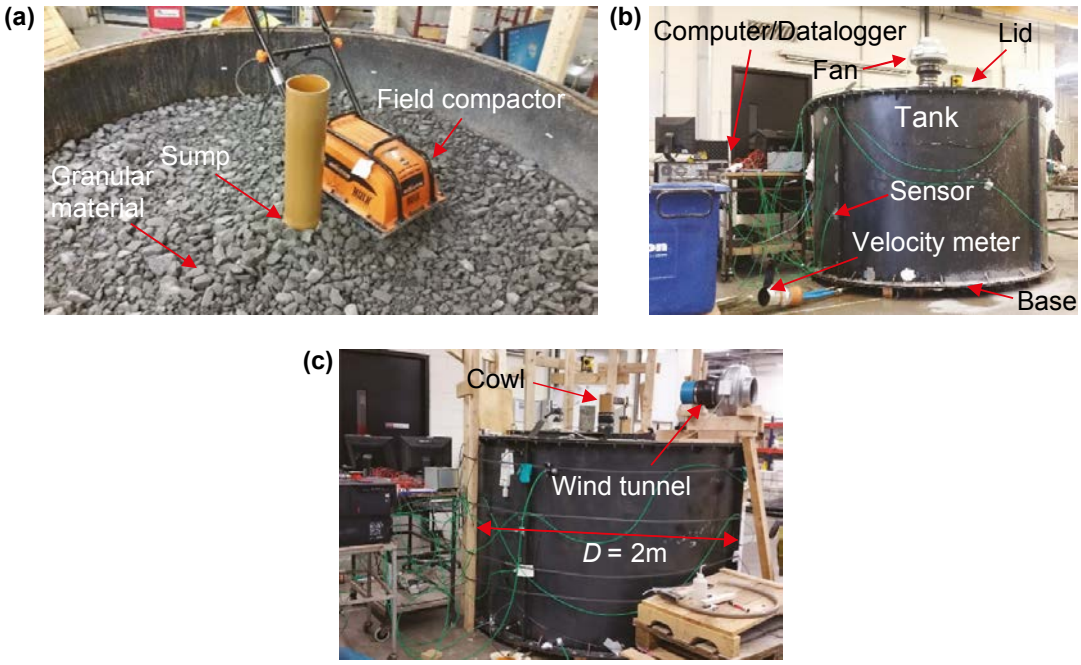

Figure 3.7. Typical set-up of the test tank with compacted material: (a) compaction work; (b) active depressurisation test set-up; (c) passive depressurisation test set-up.

tests). Fifteen high-accuracy pressure sensors (HSCDRRN002NDAA5, Honeywell TruStability™) were used and placed on the top and bottom of the tank and in the compacted material layer at different depths inside the tank.

An air velocity meter (Testo 417) was used to measure the extract Q_m through the compacted materials. The air velocity meter was placed at the inlet ports to measure Q_m for active depressurisation tests and placed at different locations around the cowl for passive tests. A fixed Q_m value was created by fixing a fan speed. The airflow through the compacted material induced pressures of P_{m1}, P_{m2} and P_{mi} at the top, at the bottom and along the depth of the tank, respectively.

The pressure difference (ΔP) between the top and the bottom of a compacted material is an important parameter to determine its k_{ah}. ΔP can be calculated as $\Delta P = P_{m1} - P_{m2}$. The suction pressure ($P_m$) inside the tank was recorded using a computer interfaced with a National Instruments NI 6210 data logger through the interpretation interface coded in the LabVIEW program version 2016. All P_m values presented in this study were taken from the pressure sensors placed immediately below the lid of the tank, unless stated otherwise. Preliminary experimental tests were carefully conducted to verify the reliability of the tank before performing experimental tests on the materials.

3.6 Phase 1: Testing Programme

3.6.1 Test sample preparation

Test samples for experimental tests in phase 1 were prepared at different w_{nc} and w_n values. The preparation procedure was as follows:

1. The material was mixed with water using a 0.5-m^3 revolving drum mixer. The compaction moisture content, w_{nc}, was controlled by adding a fixed volume of water.
2. The material derived from step 1 was compacted into the pipe segment following BS 1377 − Part 4 (BSI, 1990b). In addition, three different samples of the material obtained from step 1 were taken to determine the w_{nc} for each test by drying the samples in an oven dryer for 24 hours.
3. Sample segments derived from step 2 were connected to each other using flexible couplings. Primary tests showed that there was no difference in the k_{ah} values if the material was compacted separately (i.e. sample pipe segments are connected after compaction) or compacted connected (i.e. pipe segments are connected before compaction).

Each test is defined by a test ID, as shown in Table A2.2. For example, test T1#8-1 is the first test of

sample 8 for the T1 Struc material, with a w_{nc} of 3.94%. Test T1#8-2 is the second test of sample 8 derived by drying the sample T1#8-1 using an oven dryer for 24 hours to produce a w_n of 1.72%. Test T1#8-3 has a much higher w_n of 4.17%. This high moisture content was obtained by adding a fixed volume of water (e.g. 300–400 ml) into sample T1#8-2. After adding the water, the sample was kept standing vertically for 4 hours. This ensured that the water inside the sample had enough time to distribute by either capillary action or gravitational force. These procedures were repeated for other samples to investigate the effect of the change in w_n on k_{ah}.

3.6.2 Determination of the porosity of the granular materials

Theoretically, the porosity (n_h) of a porous material influences its degree of permeability. The porosity can be determined as the ratio of the total volume of the pore space within the medium to the total volume of the material, as shown in equation 3.2.

$$n_h = \frac{V_{total} - V_{solid}}{V_{total}} = 1 - \frac{\gamma_{dry}}{G_s \gamma_w} \quad (3.2)$$

where V_{solid} is the volume of the solid phase (m^3); V_{total} is the total volume of the material (m^3); γ_{dry} is the dry unit weight of the material (kN/m^3); G_s is the specific gravity of the material; and γ_w is the unit weight of water ($g_w = 9.81\ kN/m^3$).

In this study, the n_h values of T1 Struc and T2 Perm were obtained by either measuring the volume of the pore space of the compacted granular fill material or using equation 3.2. To measure the volume of the pore space, the material was compacted into the 500-mm pipe segment, as shown in Figure 3.8. Sample preparation for this measurement was the same as that discussed in section 3.6.1. After preparation of the sample, the material was taken out and poured into a tank of known volume. The tank was then immediately filled with water. The volume of the solid material was obtained by subtracting the total volume of the tank by the volume of the fill water. However, this measurement was carried out only for T1 Struc at $w_{nc} \geq 3\%$ and T2 Perm. This is because a significant amount of the fine content of T1 Struc at dryer conditions will absorb water and, thus, measurement of the solid volume using the method above will be incorrect. Therefore, an approximate value of G_s of 2.69 was obtained from back-calculation to determine the n_h values for dryer compacted material.

3.6.3 Determination of the air permeability of the granular materials

Four well-known equations were used to determine the k_{ah} of the granular fill materials. These equations are the Darcy, Ergun, ASTM International and Darcy–Forchheimer (D–F) equations. Each equation is described briefly below.

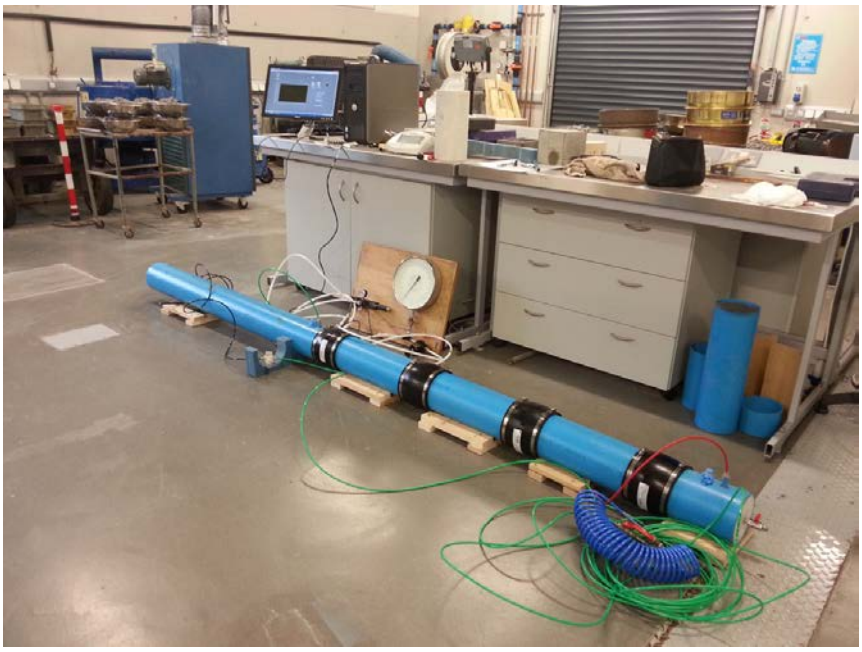

Figure 3.8. Typical test set-up of the air permeability test apparatus.

Darcy (1856) proposed a simple linear equation to present the flow of fluid through a porous medium using his experimental tests. The Darcy equation is written as:

$$Q_m = \frac{A \times k_{ah}}{\mu} \times \frac{\Delta P}{L} \quad (3.3)$$

or

$$\frac{\Delta P}{L} = \frac{\mu}{k_{ah}} \times v \quad (3.4)$$

where Q_m is the measured airflow rate (m^3/s); k_{ah} is the air permeability of the granular fill material (m^2); μ is the dynamic viscosity of the air (Pa·s); A is the cross-sectional area of flow (m^2); ΔP is the pressure drop = $P_1 - P_2$ (Pa); P_1 and P_2 are the measured pressures at the air inlet chamber and the air outlet chamber, respectively; L is the flow length (m); and v is the airflow velocity (m/s).

Ergun (1952) reviewed the flow of fluid through granular porous material. He stated that pressure loss is a result of the kinetic and viscous energy losses. Ergun suggested the following equations:

$$\frac{\Delta P}{L} = 150 \frac{\left(1 - n_h\right)^2 \mu V}{n_h^3 d_{ef(Erg)}^2} + 1.75 \frac{\left(1 - n_h\right) G V}{n_h^3 d_{ef(Erg)}} \quad (3.5)$$

$$\frac{1}{k_{ah}} = 150 \frac{\left(1 - n_h\right)^2}{n_h^3 d_{ef(Erg)}^2} \quad (3.6)$$

where $d_{ef(Erg)}$ is the Ergun effective diameter (m), which can be calculated as $d_{ef(Erg)} = d_{ef}/1000$; d_{ef} is the effective particle size of the granular fill material, which can be determined from the grading curve (mm); and G is the mass flow rate ($kg/m^2 \cdot s$).

ASTM International (2013) suggested equations to determine the k_{ah} of porous materials when k_{ah} is between 1.0×10^{-15} m^2 and 1.0×10^{-10} m^2. The data required to calculate k_{ah} are the calculated average flow rate (Q_{av}) and ΔP, and should lie within ±25%. The equation is valid only for a relatively small flow rate, i.e. $Q_{av} = 1.67 \times 10^{-5}$ m^3/s. The ASTM International equations are as follows:

$$Q_{av} = Q_m \times \frac{P_s}{\left(P_I + P_B - \frac{\Delta P}{2}\right)} \times \frac{T}{T_S} \quad (3.7)$$

$$k_P = \frac{Q_{av}}{\Delta P} \times \frac{L}{A} \times \mu \times 1.013 \times 10^{12} \quad (3.8)$$

$$k_{ah} = 9.869 \times 10^{-13} \times k_P \quad (3.9)$$

where Q_{av} is the average airflow rate (m^3/s); P_B is the barometric pressure or atmospheric pressure (Pa), taken to be 101,325 Pa; P_I is the air inlet pressure, which is equal to P_1 in this study; P_s is the standard reference pressure (101,300 Pa), T_S is the reference temperature in kelvin (293 K); T is the room temperature in kelvin; and k_P is the air Darcy permeability (Darcy).

Forchheimer (1901) suggested an equation that considers a high flow rate in porous material. The equation is also known as the D–F equation. Forchheimer (1901) observed that the relationship between pressure drop and flow rate in a specimen is not linear because there is an inertial effect on the kinetic energy of the flow at a high flow rate. Forchheimer added the inertial effect term into the Darcy equation, as follows:

$$\frac{\Delta P}{L} = \frac{\mu}{k_{ah}} \times v + c \times \frac{p}{k_{ah}} \times v^2 \quad (3.10)$$

where c is the Forchheimer constant, which depends on the material.

3.6.4 *Benchmark of Spanish granular fill materials: testing programme*

The procedure to conduct the experimental test of the Spanish granular fill materials was as follows:

- Air leakage was tested prior to any tests being carried out.
- The sample chamber was filled with the uncompacted material under study and all of the sensors were set up.
- A controlled airflow rate was pressurised into the gas inlet chamber and measurements from pressure sensors and the velocity meter were recorded.
- Pressure at the inlet was increased gradually, with each sample being tested for a range of pressures from 20 to 600 Pa.

3.7 Phase 2: Testing Programme

3.7.1 *Test sample preparation*

Test samples for the experimental tests in phase 2 were prepared as follows.

Experimental tests were performed with the T1 Struc, T2 Perm and Hybrid (combination of the T1 Struc material followed by the T2 Perm material) materials, as defined in Figure 3.9. The radon sump used for the phase 2 tests is shown in Figure 3.9d.

For compaction tests, a total of six layers were compacted for both T1 Struc and T2 Perm, labelled from T1−Layer #1 to T1−Layer #6 and from T2−Layer #1 to T2−Layer #6 (refer to Table A2.1). The Hybrid material was formed by compacting an additional layer of the T2 Perm material (T2−H−Layer #7) on top of T1−Layer #6.

Measurements of P_m were conducted after compacting each granular fill material layer. Tests presented in this study were carried out mainly with set-up type (a) in Figure 3.10. Other tests were performed to examine the effect of suction point types in practice (Figure 3.10b–d). To complete the testing programme, the following test procedures were adopted:

1. The granular material was filled into the tank to a required initial thickness.
2. Compaction work and embedment of the radon sump (if required) were performed following the measurement of the compaction degree.
3. Measure P_m with variation in Q_m with active or passive depressurisation (cowl tests).
4. Repeat steps 1–3 for each compacted layer for all tests.

A summary of the experimental testing programme is presented in Table A2.3.

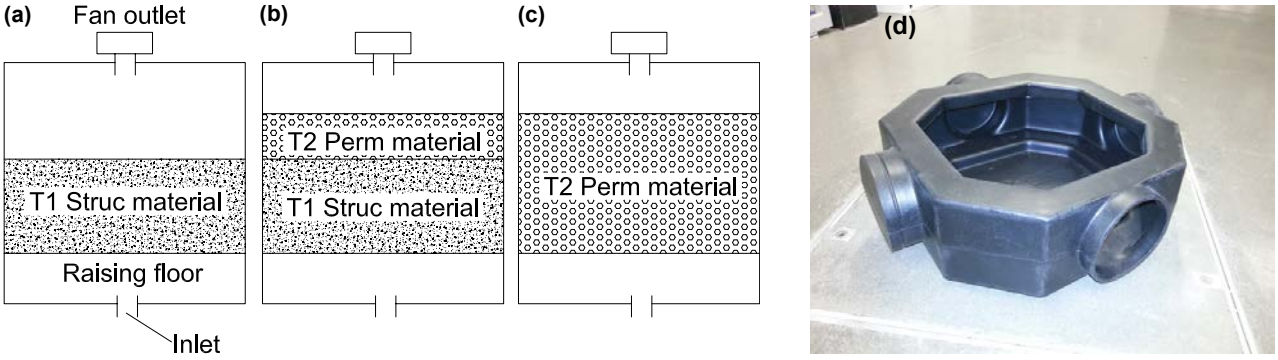

Figure 3.9. Depiction of the compaction test cases in this study: (a) compaction with T1 Struc only; (b) Hybrid − compaction with T1 Struc followed by T2 Perm; (c) compaction with T2 Perm only. Part (d) shows the radon sump used for the phase 2 tests.

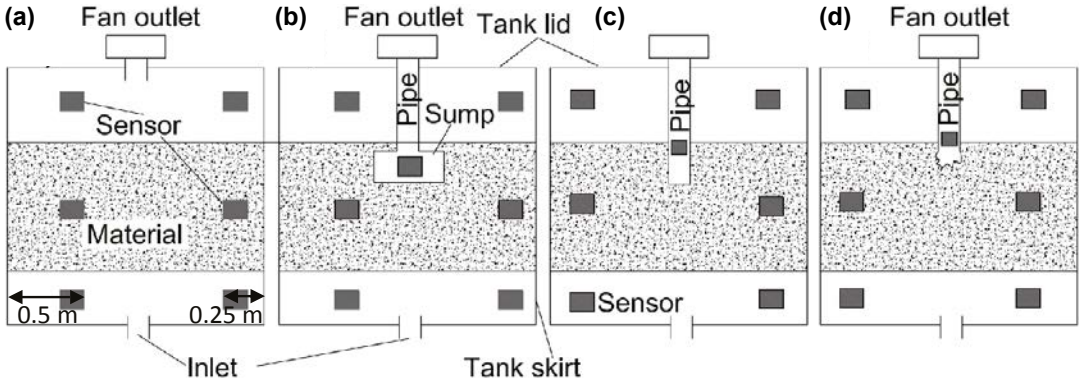

Figure 3.10. Schematic diagram of the test set-up and test cases investigated in this study: (a) type a – air extracted directly at the outlet on the lid; (b) type b – air extracted out through a radon sump; (c) type c – air extracted out through an embedded pipe; (d) type d – air extracted out through an embedded pipe that had been partially pulled up compared with that in (c). Distances of the sensors to the left-hand side and right-hand side of the skirt of the tank were 0.5 m and 0.25 m, respectively (not to scale).

3.7.2 *Determination of the air permeability of granular materials*

The k_{ah} values reported in phase 2 were calculated using the D−F equation (Forchheimer, 1901), as this equation has been shown to be the best for determining the k_{ah} of the T1 Struc and T2 Perm granular materials, as found in phase 1 (see Chapter 4 for details).

3.7.3 *Determination of the porosity of the compacted material*

The porosity of the materials in the phase 2 tests were calculated using equation 3.2.

3.7.4 *Experimental tests of the cowls connected on the pipe with the bend*

Experimental tests of the different types of cowls, as described in section 3.7.1, were performed.

3.8 Numerical Simulations using Computational Fluid Dynamics

Simulations using CFD could be a useful tool in the design of an SD system. They allow engineers and researchers to understand the working mechanism of a system, thus enabling them to design a system without conducting trial experimental tests. The commercial CFD package Ansys FLUENT version 15.0 (Ansys Inc., 2013) was used in this study. The SD systems were adopted following the configuration defined in IS 888:2016 (NSAI, 2016a) for radon mitigation. An urban family house of 64 m^2 (8 m × 8 m) was simulated. The typical numerical mesh of the house is shown in Figure 3.11. The SD system includes a 15-cm-thick concrete slab and a 50-mm-thick sand layer above the granular fill layers. Details of the granular materials will be discussed in the following section.

All simulations were performed under transient analysis obeying the Reynolds-averaged Navier−Stokes (RANS) realisable $k-\omega$ turbulence model, where k is the turbulent kinetic energy and ω is the specific dissipation rate. However, all results were obtained once steady-state conditions were reached. The $k-\omega$ turbulence model was adopted because it is more accurate than other models, e.g. laminar, $k-\varepsilon$ and Reynolds stress models (Ansys Inc., 2014). The quadrilateral element type was applied for meshing. Numerical mesh was generated by applying a maximum size of 5 mm. However, in the crack area, where the SD system domain size was changed with the change in the width of the wall crack (w_{crack}), the mesh size was remotely divided to be smaller than 5 mm. For example, for a w_{crack} of 7.5 mm, the mesh size in this crack area was reduced to 3.75 mm. If a crack had a width of 1 mm, the mesh size in this crack area was defined as 1 mm. This procedure was applied for all simulations conducted in this study. To ensure a numerical converged solution, the residual convergence criterion for velocity was set at 10^{-4} and the scaled energy residual was 10^{-6} in all simulations (Ansys Inc., 2014).

By applying symmetrical conditions, only half of the entire system was simulated. The bottom and the left side of the system were fixed with the wall boundary conditions, i.e. no airflow was allowed. The opening

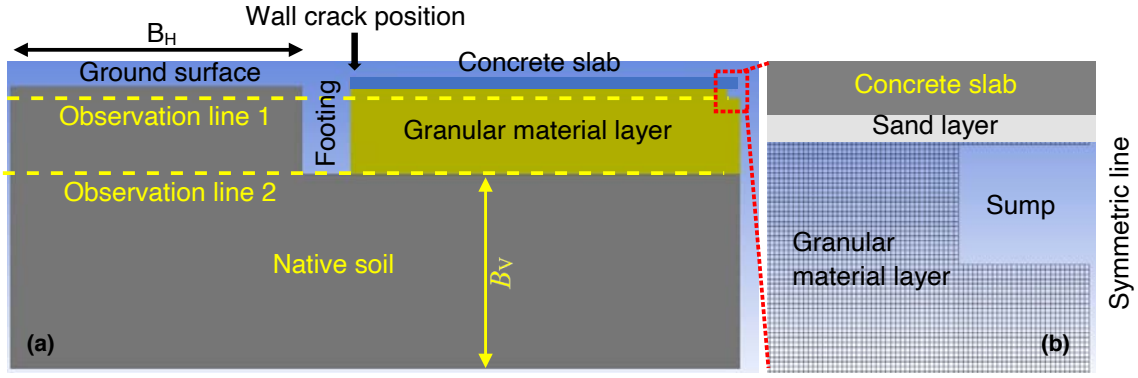

Figure 3.11. (a) Typical numerical domain geometry of an SD system; (b) a typical mesh with a 5-mm mesh size (extracted at the sump area).

boundary condition was applied at the ground surface. This boundary condition was also applied for the wall crack and the imperfectly sealed slab. Suction pressure, P_{sump}, was applied at the side and the bottom of the sump. All boundary conditions applied in CFD simulations are summarised in Table A2.4. B_V and B_H, indicated in Figure 3.11, are the distances to the vertical and horizontal boundaries measured from the bottom and the side of the footing, respectively. Preliminary CFD simulations were conducted to determine the optimum values for B_V and B_H and the numerical mesh so that they do not affect the final results. The optimum B_V and B_H values were found to be 2 and 3.5 times the total thickness, t (i.e. $t = 90$ cm), of the granular fill layer.

3.9 On-site Tests in the Spanish Pilot House

A 1-year monitoring study was conducted in a pilot house with very high radon levels to investigate the ability and efficiency of active and passive SD to mitigate radon levels (Fuente *et al.,* 2019b).

3.9.1 Pilot house: location and design

The pilot house chosen for the case study is located in Saelices el Chico, Salamanca (Spain), on the land of a former uranium mine managed by the company ENUSA Industrias Avanzadas, S.A., now under reclamation activities (Figure 3.12). The experimental house was selected because of the high radon exhalation rate and the high radium content in the soil in this area, resulting in the accumulation of high radon levels inside the building. An average radium concentration of 1600 Bq/kg was quantified from different soil samples taken onsite; this value is 40 times in excess of the average worldwide concentration of approximately 40 Bq/kg (Vazquez *et al*., 2011).

The experimental house was designed to represent a space large enough to be characteristic of a room in a typical dwelling house. It consists of two storeys, a partially below-grade so-called basement and a ground floor, connected by a standard door. The dimensions of the rooms are 5×5 m^2 and there are two windows on the ground floor level, one in the front wall next to the main door and another one in the opposite wall. The front wall of the house faces north.

Figure 3.12. Map of Spain and a plan of the mining facilities indicating the location of the pilot house, and a recent picture of the building.

Two SD systems are installed in the house, both of which consist of a 1-m^2 and 0.5-m-deep sump and an exhaust pipe. One system is located in the centre of the experimental house, with the sump placed in the aggregate layer below the concrete slab, and the other is placed on one of the sides of the house (Figure 3.13).

Materials used for the construction of the house followed Spanish building practices. A 15-cm-thick aggregate layer was placed below a 10-cm-thick concrete slab. Standard clay bricks were used for the walls and conventional perforated clay bricks were used to build the sumps of the SD systems (Vazquez *et al*., 2011).

3.9.2 Monitoring system and experimental methodology

To continuously monitor the radon concentration, several active radon monitors were used, including the Radon Scout (SARAD GmbH, Dresden, Germany), Radon Scout Home (SARAD GmbH) and AlphaE (Bertin Instruments) detectors. The performance of the radon monitors used in the experiment at the pilot house was tested in a purpose-built radon chamber (Fuente *et al*., 2018). Radon concentrations were recorded in the basement and on the ground floor.

A pressure sensor system was installed to monitor the distribution of pressure under the slab of the house. The pressure sensor system was specifically developed for this experiment at the pilot house in collaboration with a research group at the Institute for Physical and Information Technologies (ITEFI) within the Spanish National Research Council (CSIC), Madrid (Spain). It is an acquisition system designed with segmented architecture and a capacity of up to 15 pressure sensors. It consists of an adaptor board for the pressure sensor units and contains a series of Honeywell pressure sensors (HSCDRRD006MDSA3, operating pressure ±6 mbar, accuracy 0.25%) with SPI (Serial Peripheral Interface) communication. The units are connected with Ethernet cables in parallel and the adaptor board is connected to a PC via an input/output USB card type LabJack U3. The actual system installed in the house for this experiment consisted of a total of eight pressure sensor units. Five pressure sensors were distributed along the basement area in different holes drilled through the concrete slab to measure the pressure difference in the aggregate layer under the slab and the inhabited volume of the basement, at distances (*d*) of 1, 2 and 2.4 m from the central sump. The remaining three pressure sensors were placed at the sump and pipe of the central SD system and at room level for reference.

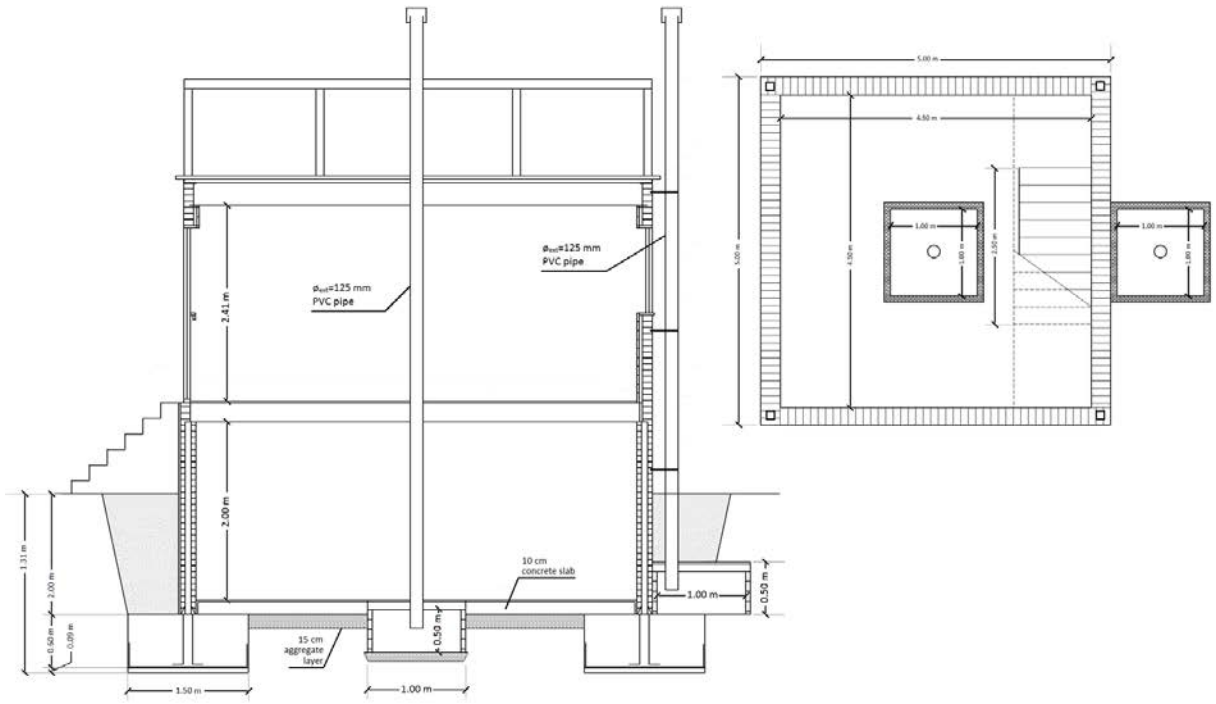

Figure 3.13. Section view of the house and plan of the basement after installation of mitigation measures. Source: Vazquez *et al*., 2011.

To record atmospheric conditions locally at the house site, a local weather station (PCE-FWS20, PCE Instruments) was installed on the rooftop. Variables recorded were wind velocity, outdoor temperature, atmospheric pressure, relative humidity percentage and accumulated rainfall. Both the pressure sensor system and the weather station were accessible remotely, which facilitated data collection.

The initial monitoring plan was to alternate testing phases of SD performance (active or passive) with periods in which the house remained completely closed, in order to record radon concentration increases and decreases over the different phases, along with the PFE induced under the slab.

The monitoring study commenced in June 2018, with the house closed during a first phase to foster accumulation of radon gas. All testing phases with this setting, in which the house remained closed and the pipes of the SD systems were capped to foster radon accumulation in the building, will be referred to as closed periods. After the first closed period (phase 1), phase 2 involved passive SD performance evaluation. A subsequent series of closed periods was followed by evaluation of active SD performance, for up to nine phases, with different active SD settings, ending in April 2019.

Only the central SD system was used for the investigation of SD during the SD testing phases. A rotating cowl was used for the passive SD operation; for the active SD performance, a mechanical fan (RP145i, RadonAway; 80 W max.) was installed in the central SD system pipe. The mechanical fan was modified by adding a potentiometer to control the extraction airflow, which in terms of velocity ranged from 0 to 4 m/s. A hot wire anemometer [Testo 440; measuring range 0–30 m/s, accuracy ±(0.3 m/s + 4% of mv) and resolution 0.01 m/s] was used to measure the extraction velocity of the mechanical fan. A schema of the experimental house settings for the different phases is shown in Figure 3.14.

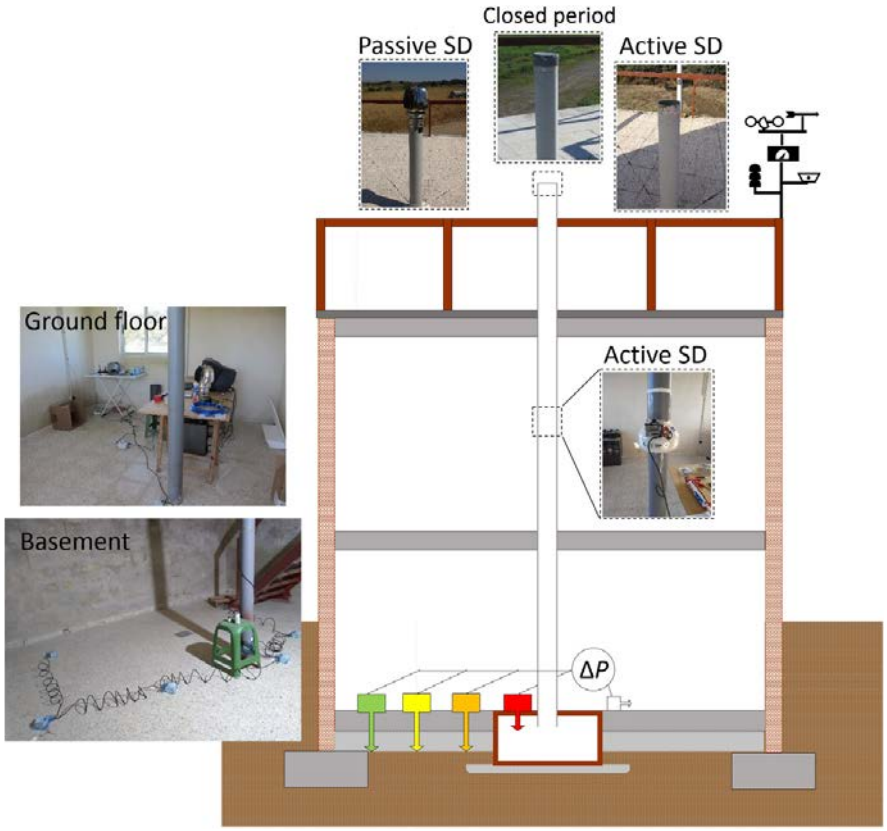

Figure 3.14. Schema of the pilot house for the closed periods and active SD and passive SD testing phases. The cross-sectional view of the house shows the pressure sensor system in the basement (same for all phases), the mechanical fan installed on the central pipe (for the active SD performance) and the top of the exhaust pipe in the house rooftop, with a cap, with a rotating cowl or opened, depending on the testing phase.

The duration of the different phases varied, depending on access to the site and technical problems experienced with the sensors or the power supply. The monitoring study was stopped at some point and resumed later. A summary of the testing phases, including dates and incidents, is presented in Table A2.5.

From February 2019, the monitoring study focused on investigation of the mechanical fan extraction impact on SD effectiveness. Short periods (1–2 weeks) of active SD were followed by closed periods, with a gradual increase in mechanical fan extraction by controlling the airflow rate.

4 Results

4.1 Phase 1: Experimental Test Results

4.1.1 Particle size distribution

Figure 4.1 shows the particle size distribution curves for each granular fill material. Based on the test results, T1 Struc and T2 Perm can be classified as well-graded and poorly graded granular fill materials, respectively. The grading curves of three British granular fill material types (MOT Type 1 sub-base and 20-mm and 40-mm granular fill materials), described by BRE (1998), were also plotted for comparison. The particle size distribution curve of MOT Type 1 is similar to that of T1 Struc. A similar observation was found for the British 20-mm and 40-mm materials and T2 Perm. This finding suggests that characterisation of the Irish T1 Struc and T2 Perm granular fill materials could apply to the British MOT Type 1 and the 20-mm and 40-mm granular fill materials, respectively, and vice versa.

4.1.2 Small-scale compaction test results

Small-scale compaction test results for T1 Struc and T2 Perm are shown in Figure 4.2. The optimum compaction moisture content, $w_{nc(opt)}$, for compaction of T1 Struc is approximately 5.75%, inducing a maximum dry unit weight $\gamma_{dry(max)}$ of about 23 kN/m^3 (Figure 4.2a). However, the optimum compaction degree for T2 Perm is relatively independent of moisture content (Figure 4.2b). This is because T2 Perm is a poorly graded material and therefore it is relatively difficult to compact this type of material with the small-scale laboratory compaction test apparatus. This assumption was confirmed using the large-scale experimental test in the second phase of this project.

4.1.3 Effect of w_{nc} and w_n on the k_{ah} values

Figures 4.3 and 4.4 show examples of the test results for samples T1#4-1 and T2#3-1, respectively. The results plotted in these figures were selected randomly from 55 test specimens. Test results for other samples show a similar trend and thus are not presented here. The figures show that there is excellent agreement between the D−F equation and the test results, inducing a correlation factor R^2 of 0.99 for both materials, whereas the Ergun equation gives an R^2 of 0.86 and 0.89 for T1 Struc and T2 Perm, respectively. The ASTM International and Darcy equations are applicable for a low flow rate only, i.e. laminar airflow. Therefore, the k_{ah} values derived from the D−F equation are recommended for use in practical design, as these accurately represent the wider range of airflow rates that might be experienced in an SD system during its service life.

The k_{ah} values derived from all of the equations are presented in Table A2.2.

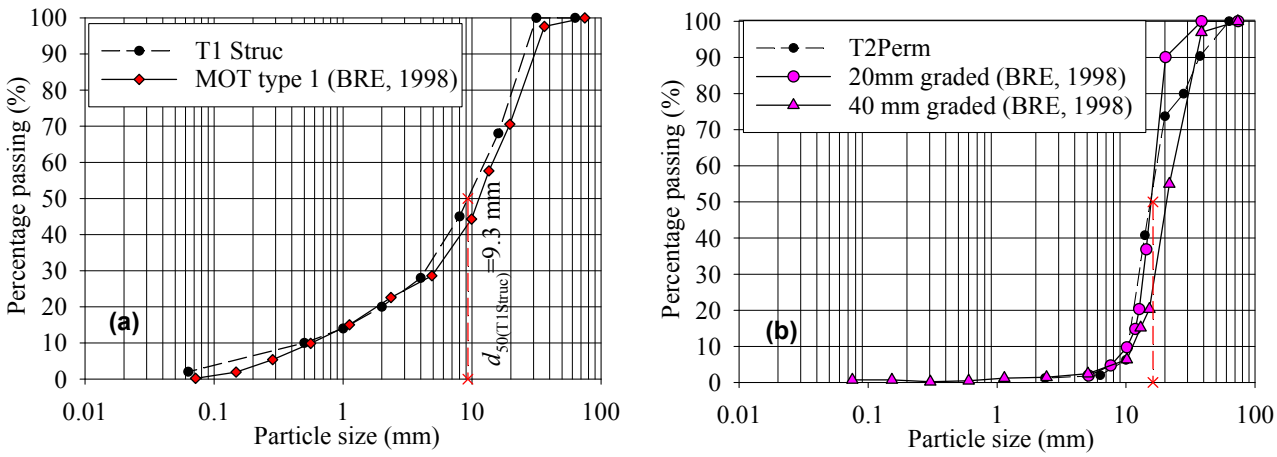

Figure 4.1. Particle size distribution of the Irish T1 Struc and T2 Perm and British granular fill materials.

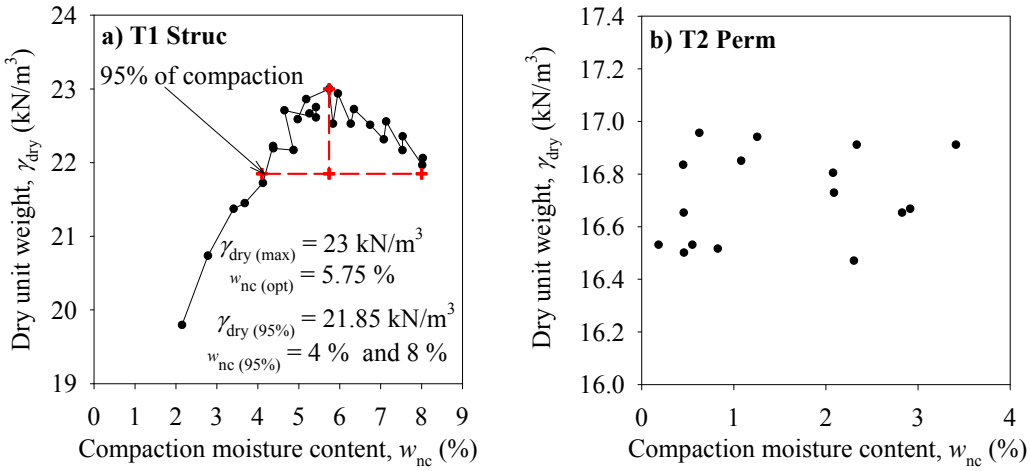

Figure 4.2. Small-scale compaction test results for (a) the T1 Struc and (b) the T2 Perm granular fill materials.

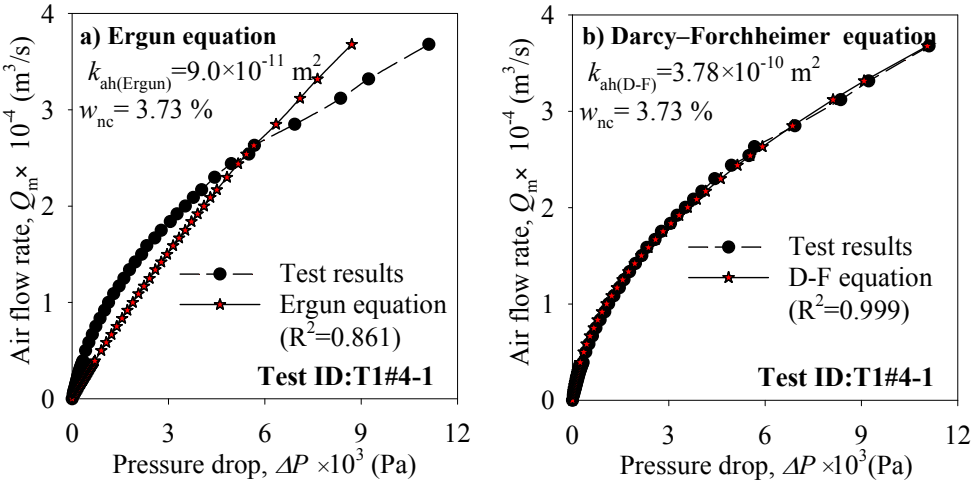

Figure 4.3. Relationship between *ΔP* and airflow rate for sample T1#4-1. These test results were selected randomly from 49 measurements for T1 Struc. Test results for other samples show a similar trend and thus are not presented here.

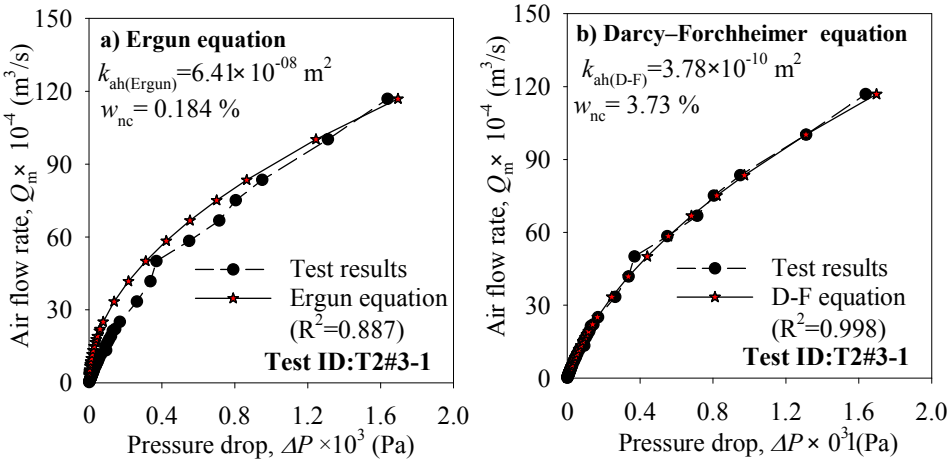

Figure 4.4. Relationship between *ΔP* and airflow rate for sample T2#3-1. These test results were selected randomly from six measurements for T2 Perm. Test results for other samples show a similar trend and thus are not presented here.

Figure 4.5 shows the variation in k_{ah} values obtained from the D−F equation measured at different values of w_{nc}, denoted as $k_{ah(w_{nc})}$ in the figure. For T1 Struc, the k_{ah} values decrease with increase in w_{nc}, whereas for T2 Perm the k_{ah} values do not vary significantly with increase in w_{nc}. The reason for this is that T1 Struc is a well-compacted material. When it is compacted, the pore space tends to reduce, thus reducing its k_{ah}. In contrast, T2 Perm is not well compacted with the small-scale laboratory compaction test apparatus and therefore the k_{ah} values do not show a clear trend with variation in w_{nc}. An average value of $k_{ah(w_{nc})}$ of approximately $(22.5 \pm 7.2) \times 10^{-9}\,m^2$ can be used for T2 Perm, whereas the value for T1 Struc can be interpolated using equation 4.1:

$$k_{ah(w_{nc})} = 20 \times 10^{-9} e^{-1.25 w_{nc}} \text{ for } 1\% \le w_{nc} \le 4.5\% \qquad (4.1)$$

Figure 4.6 presents the effect of w_n on the k_{ah} of T1 Struc in terms of normalisation:

$$N_k = \frac{k_{ah(w_n)}}{k_{ah(w_{nc})}} \qquad (4.2)$$

and

$$N_W = \frac{W_n}{W_{nc}} \qquad (4.3)$$

An N_k of 1 represents the air permeability of the granular fill material measured at w_{nc}, i.e. $N_w = 1$. "Dry side" means that the moisture content of the material was reduced by drying the sample in the oven dryer for 24 hours, whereas "wet side" presents the increase in moisture content from adding water into the sample. As shown in Figure 4.6, w_n strongly influences k_{ah}, as expected. For example, if w_n reduces below w_{nc}, then k_{ah} generally increases, up to 2.5 times $k_{ah(w_{nc})}$ on the dry side. On the other hand, adding moisture to the granular fill material after compaction decreases the permeability of the fill material, with an average value of N_k being 0.37 for specimens tested up to 1.8 times w_{nc} (i.e. "wet side").

The above finding shows that the degree of permeability of T1 Struc during its service life is dependent on the change in its moisture content. For material that is susceptible to an increased moisture content during the service life of the building, e.g. because of the presence of the water table within the depth of the material, it is suggested that the permeability of the material for the design of an SD system should be assumed to be 0.37 times the initial permeability of the compacted material (bottom right quadrant of Figure 4.6). On the other hand, if

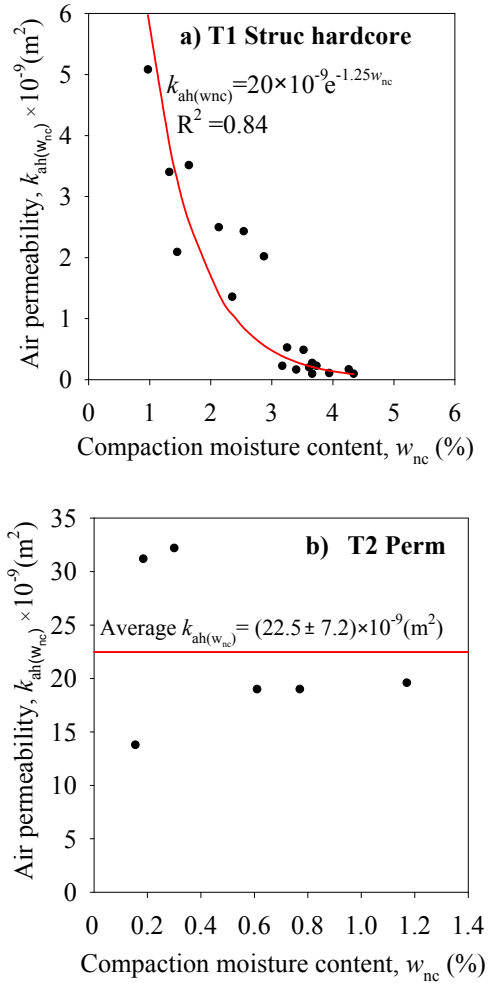

Figure 4.5. Variation in $k_{ah(w_{nc})}$ with w_{nc} for (a) the T1 Struc and (b) the T2 Perm granular fill materials.

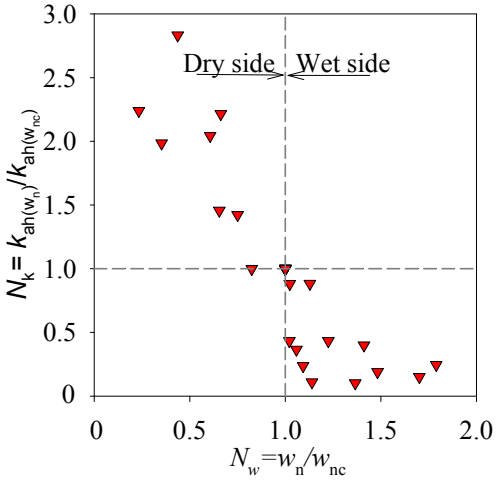

Figure 4.6. Effect of w_n on the k_{ah} of T1 Struc.

the moisture content of the material reduces after compaction, e.g. as a result of drying, the permeability of the material is expected to increase. However, for the conservative design of an SD system, it is recommended that the permeability of the material at compaction is used.

4.1.4 Test results for porosity

As discussed previously, the n_h values of T1 Struc and T2 Perm were obtained by either measuring the volume of the pore space of the compacted granular fill material or using equation 3.2. Variations in the n_h values of T1 Struc and T2 Perm with w_{nc} and γ_{dry} are presented in Figures 4.7 and 4.8, respectively, and Table A2.2. For T1 Struc (Figure 4.7a), the n_h values are constant at approximately 0.23 when $w_{nc} \leq 2$. At $2\% < w_{nc} \leq 6\%$ the n_h values decrease, and when $w_{nc} > 6\%$ the n_h values slightly increase. These trends are expected, as γ_{dry} increases up to the optimum moisture content ($w_{nc(opt)}$) of approximately 6% (as shown in Figure 4.2a), whereas it decreases when the moisture content is larger than $w_{nc(opt)}$ (Figure 4.2). As w_{nc} increases, water will fill the void space within the compacted material, which causes a small increase in n_h at $w_{nc} > 6\%$. On the other hand, the n_h values for T2 Perm are relatively constant at approximately 0.37 (Figure 4.7b). This is because T2 Perm is relatively difficult to compact with the standard compaction hammer used in the laboratory.

Figure 4.8 shows the relationship between n_h and γ_{dry} for T1 Struc obtained from the test results. The n_h values decrease linearly with the increase in γ_{dry}, as expected. Porosity values calculated using equation 3.2 are plotted for comparison. The porosity calculated from the curve fit (dashed line in Figure 4.8) is approximately $0.95 \times n_h$, as calculated in equation 3.2.

Based on the test results presented in Figures 4.7 and 4.8, the following equations are proposed to determine the n_h values of T1 Struc and T2 Perm at different values of w_{nc}:

For T1 Struc:

$$n_h = 0.23 \text{ when } w_{nc} \leq 2\% \quad (4.4a)$$

$$n_h = 0.23 - 0.03 w_{nc} \text{ when } 2\% < w_{nc} \leq w_{nc(opt)} \quad (4.4b)$$

$$n_h = 0.95\left(1 - \frac{\gamma_{dry}}{G_s \gamma_w}\right) \text{ when } 2\% < w_{nc} \leq 8\% \quad (4.4c)$$

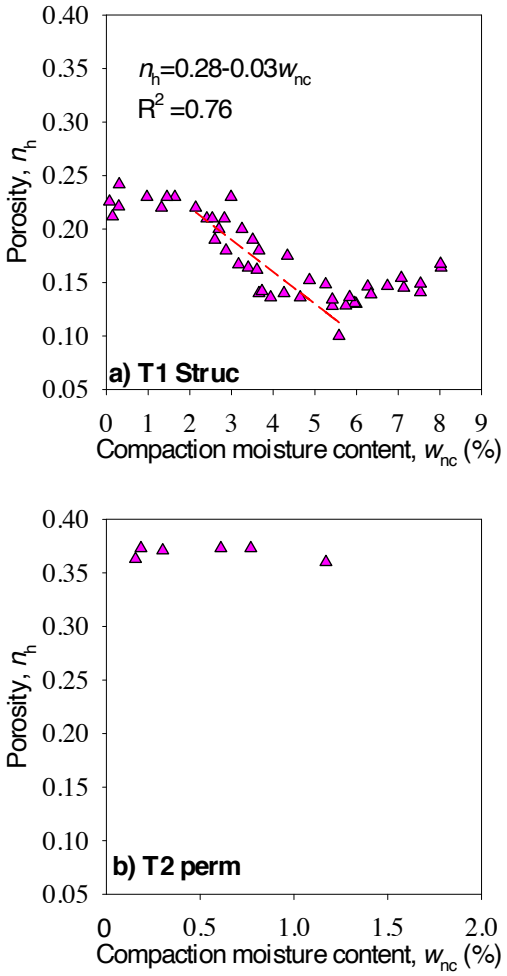

Figure 4.7. Variation in n_h and w_{nc} for (a) the T1 Struc and (b) T2 Perm granular fill materials.

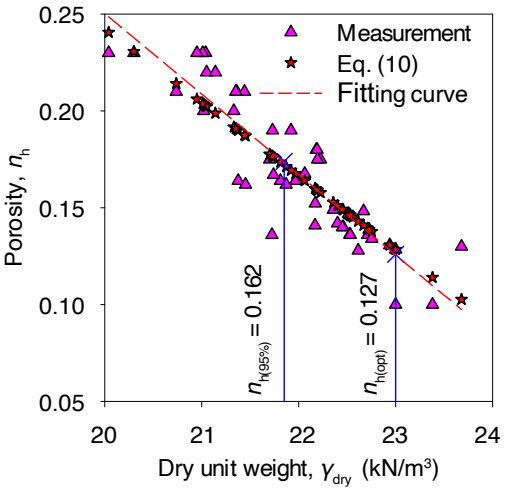

Figure 4.8. Relationship between n_h and γ_{dry} for T1 Struc.

For T2 Perm:

$$n_h = 0.37 \text{ when } w_{nc} \leq 1.4\% \quad (4.5)$$

4.1.5 Implications for practice

An important aspect of this study was to devise a method to determine k_{ah} values of granulated fill materials under compaction, including values for specified granulated fill materials in Ireland. There are no standards or regulations that describe the detailed design of SD systems in Ireland. Thus, selection of the permeable layer for an SD system is ideally based on the practical experience of the designer rather than on a scientific view. This study will enable engineers to select an appropriate w_{nc} value, and thus a k_{ah} value, for a compacted fill layer under footings or concrete floors.

In the field, the compaction degree of granulated fill material could be higher than the values reported in this study. This higher compaction degree might result in a lower k_{ah} and n_{ah} in comparison with those values presented in Table A2.2. Therefore, further investigation of the compaction degree of T1 Struc and T2 Perm is required using large-scale compactors, e.g. field compaction or large-scale tests.

4.1.6 Benchmarking of Spanish granular fill materials: experimental results

Figure 4.9 shows the particle size distribution curves for the Spanish granular fill materials tested. Based on the test results, garbancillo 4/12 and gravel 4/20 can be classified as poorly graded granular fill materials. The grading curves for T2 Perm and two British granular fill materials (i.e. 20-mm and 40-mm granular fill materials) described in BRE (1998) are also plotted for comparison. The particle size distribution curves for garbancillo 4/12 and gravel 4/20 are similar to those of T2 Perm and the British 20-mm and 40-mm materials. This finding suggests that characterisation of the Irish T2 Perm granular fill material could apply to the garbancillo 4/12 and Spanish gravel 4/12 granular fill materials and vice versa (Fuente *et al*., 2019a).

A comparison of the results from the permeability tests is presented in Figure 4.10 for the Spanish granular fill materials tested (uncompacted) and the British standards (i.e. 20-mm and 40-mm materials). Irish standards are not presented here because the test results are under compaction.

From Figure 4.10 it can be noted that the granular fill materials analysed show very similar trends, with similar gas permeability values of approximately 9×10^{-8} m^2. Considering the similarities between the Spanish granular fill materials and the Irish T2 Perm standard, it can be assumed that the results from Irish T2 Perm would be applicable to the Spanish standards analysed.

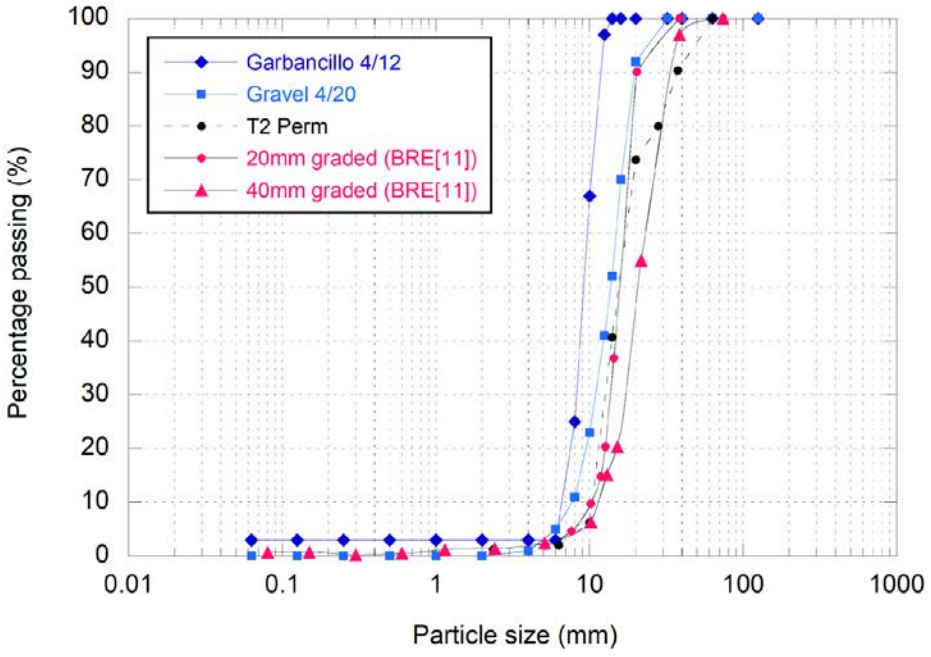

Figure 4.9. Particle size distribution for Spanish garbancillo 4/12 and gravel 4/12, Irish T2 Perm and British granular fill materials. The particle diameter for garbancillo 4/12 is the d_{50} = 9.1 mm and for gravel 4/20 is the d_{50} = 13.8 mm. The d_{50} is the particle size of the granular fill material at 50% passing.

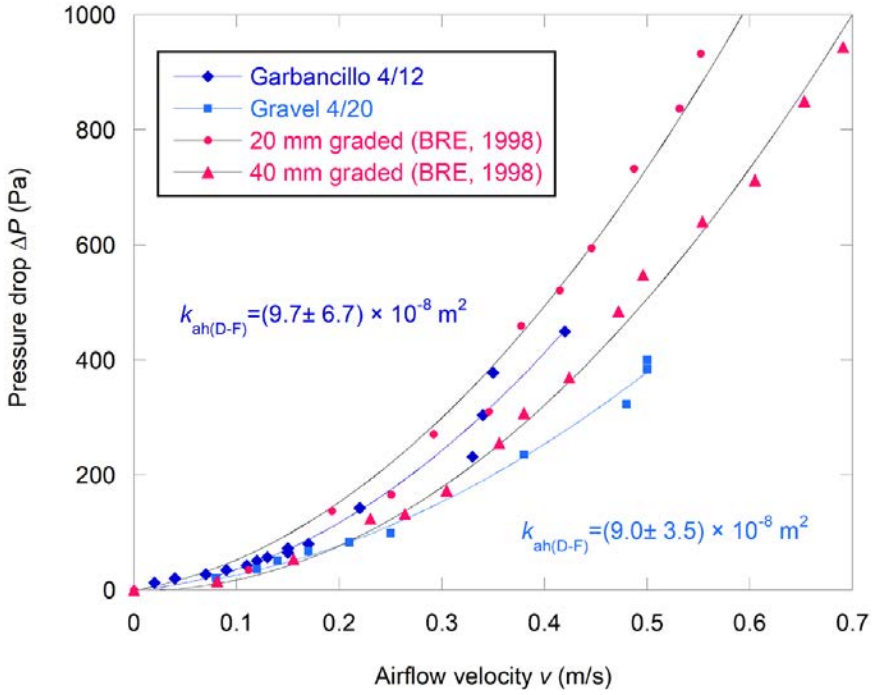

Figure 4.10. Relationship between pressure difference *ΔP* and airflow velocity for garbancillo 4/12 and Spanish gravel 4/20 samples and the British standards, taken from BRE (1998).

4.2 Phase 2: Experimental Test Results

4.2.1 Field compaction test results

Figure 4.11 provides examples of the field compaction test results. The results for T1−Layer #3, T1−Layer #5 and T1−Layer #6 for the T1 Struc, T2−H−Layer #7 for the Hybrid and T2−Layer #3 and T2−Layer #6 for the T2 Perm materials are presented. The results for other layers showed a similar trend and thus are not presented here. The compaction degree of the materials defined in the figures is the percentage of compaction from comparing the initial and compacted thicknesses.

Figure 4.11 shows that the compaction degree of the T1 Struc material varied between 25% and 30% of its initial thickness, whereas that of T2 Perm was observed to be 10–15% regardless of the initial thickness. These findings agree well with the conclusion drawn from the compaction test results reported in Hung *et al*. (2018a,b) using the small-scale compactor that the T1 Struc material has a higher compaction degree than the T2 Perm material. The reason for this is that T1 Struc is a well-graded material that contains a significant amount of fine particles mixed with coarse particles (see Figure 4.1a). In contrast, T2 Perm is a poorly graded material with particle sizes of between 4 mm and 40 mm (see Figure 4.1b). Furthermore, the field compactor induced a higher compaction degree for the T1 Struc and T2 Perm materials than the small-scale compactor, as expected (Figure 4.12).

4.2.2 Suction pressure measurement with active depressurisation

Suction pressure was generated using a speed-controllable electric fan (active depressurisation). The fan was connected at the outlet port (see Figures 3.7 and 3.10a) and the variation in Q_m was created by changing the fan speed. Each suction pressure measurement was recorded for approximately 500 s (Figure 4.13). The suction pressure increased gradually until the fan speed became constant. P_m used for the analyses is the average of the "steady state" part of the suction pressure versus time curve.

Figure 4.14 presents the effect of the different suction point types (see Figure 3.10 in terms of Q_m and P_m). Examinations were performed for Layer #2, Layer #3 and Layer #6 for the T2 Perm material, Layer #5 for the T1 Struc material and Layer #7 for the Hybrid material. P_m values presented in Figure 4.14 were obtained from pressure sensors placed immediately below the lid of the tank.

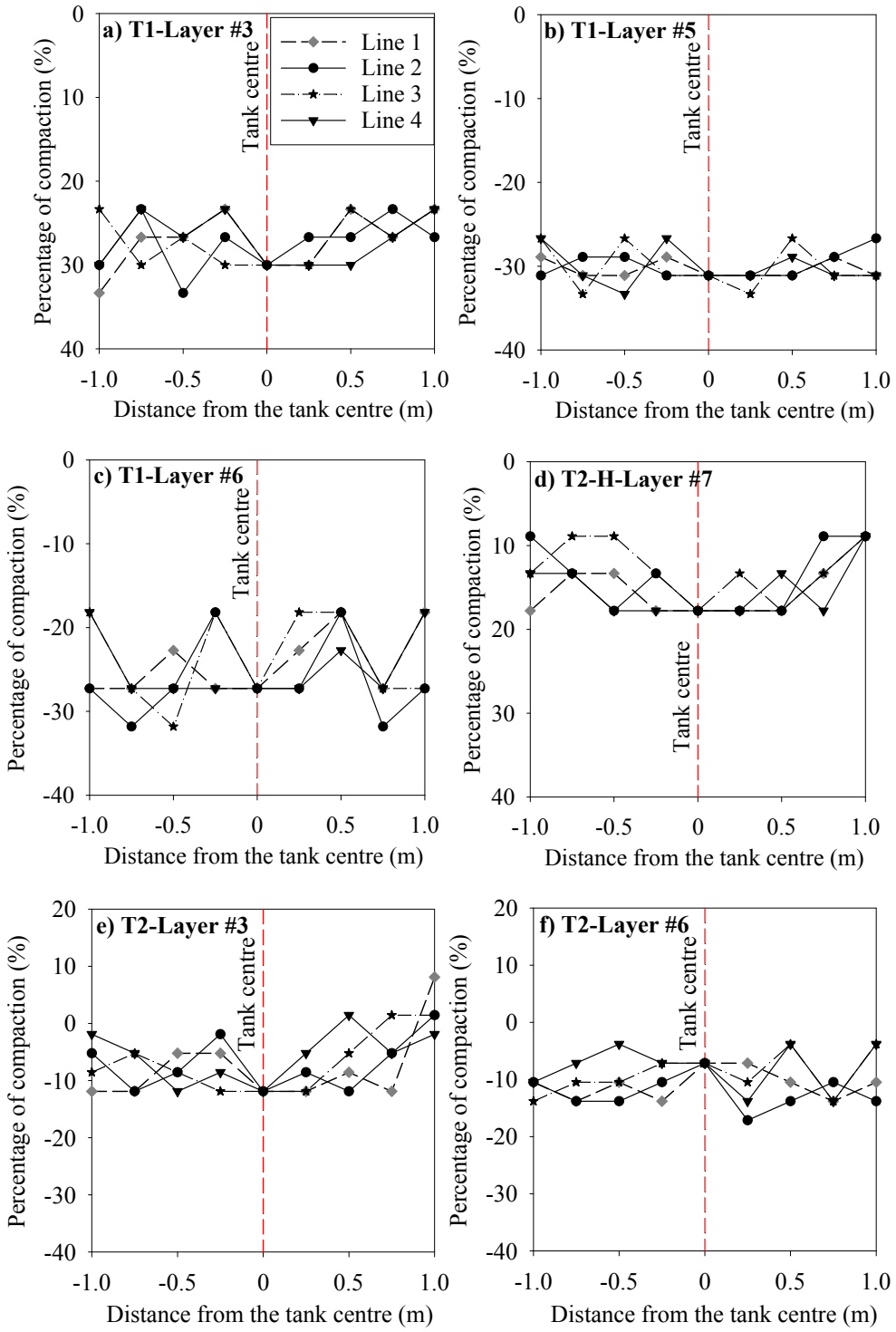

Figure 4.11. Field compaction test results for the T1 Struc, T2 Perm and Hybrid materials using a compactor with a compaction force of 39.1 kN/m². Other compacted layers showed a similar trend and thus are not presented here. Initial thicknesses (before compaction) were as follows: (a) 150 mm, (b) 225 mm, (c) 110 mm, (d) 225 mm, (e) and (f) 150 mm. The T2-H-Layer #7 in (d) is the T2 Perm layer compacted following Layer #6 of the T1 Struc material in (c).

The test results show that the type of suction point used did not significantly affect the suction pressure under the lid. This finding suggests that, in practice, the suction point embedded in the permeable layer of the SD system could be simply formed by an empty space. However, this examination was conducted with a perfectly sealed tank and this perfect airtightness does not exist in a practical situation. Furthermore,

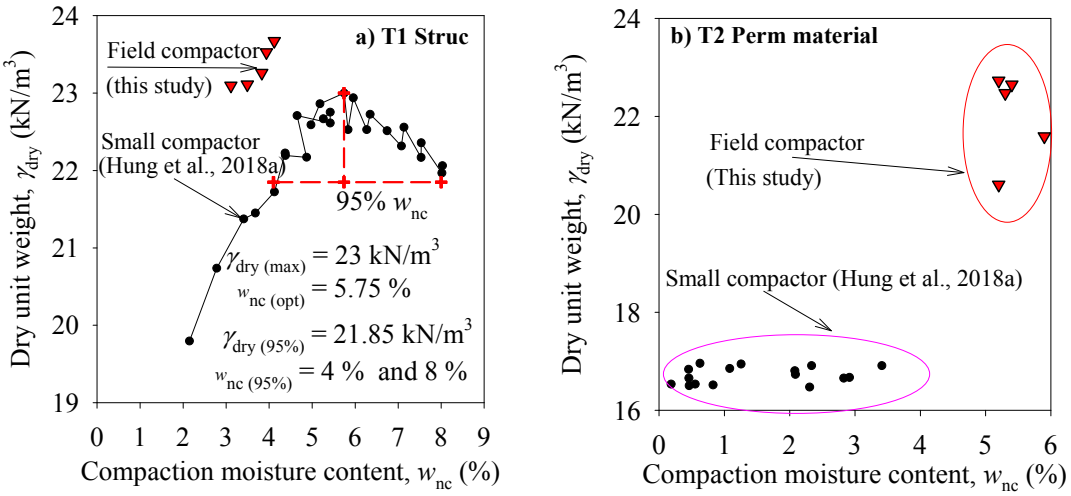

Figure 4.12. Relationship between γ_{dry} and w_{nc} for (a) the T1 Struc and (b) the T2 Perm granular fill materials.

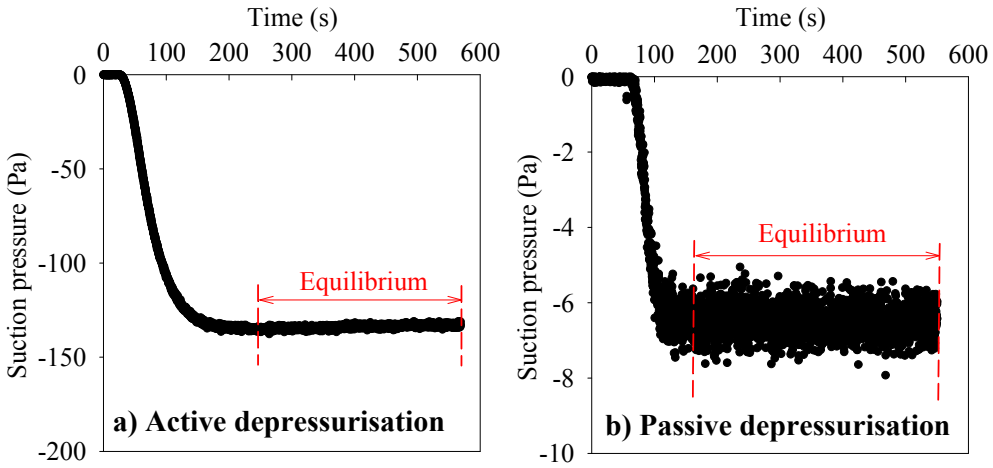

Figure 4.13. Example of suction pressure measurements over time: (a) using the electric fan; (b) using the cowl type a. Measurements for other suction pressure magnitudes showed a similar trend and thus are not presented here.

as the test tank was sealed perfectly, the pressure induced by these suction point types would be quickly transferred to the whole empty space below the lid of the tank and these suction point types might not show clear effects on the air connectivity.

Figure 4.15 compares the relationship between Q_m and P_m at different compacted thicknesses. The variation in Q_m for the T1 Struc and Hybrid materials with compacted thickness was insignificant (Figure 4.15a). However, the T2 Perm material exhibited a significant reduction in Q_m at the same P_m level when its compacted thickness increased (Figure 4.15b). For example, considering the tests for Layer #2 and Layer #6 at P_m = 200 Pa, the Q_m values were observed to be approximately 70 m^3/h and 30 m^3/h, respectively. This could be explained by the increase in the air movement resistance of the T2 Perm material when its compacted thickness increases, which is not observed in the T1 Struc material because of its fine content/grading.

Figure 4.16 shows the relationship between ΔP and Q_m at different compacted thicknesses. It has been previously discussed that ΔP depends only on the k_{ah} value of the material: the higher the ΔP value, the lower the k_{ah} value. The trend for ΔP was observed to be the same as that for P_m, presented in Figure 4.15. ΔP is an important factor because it affects the horizontal extension of suction pressure within the permeable granular fill layer in an SD system.

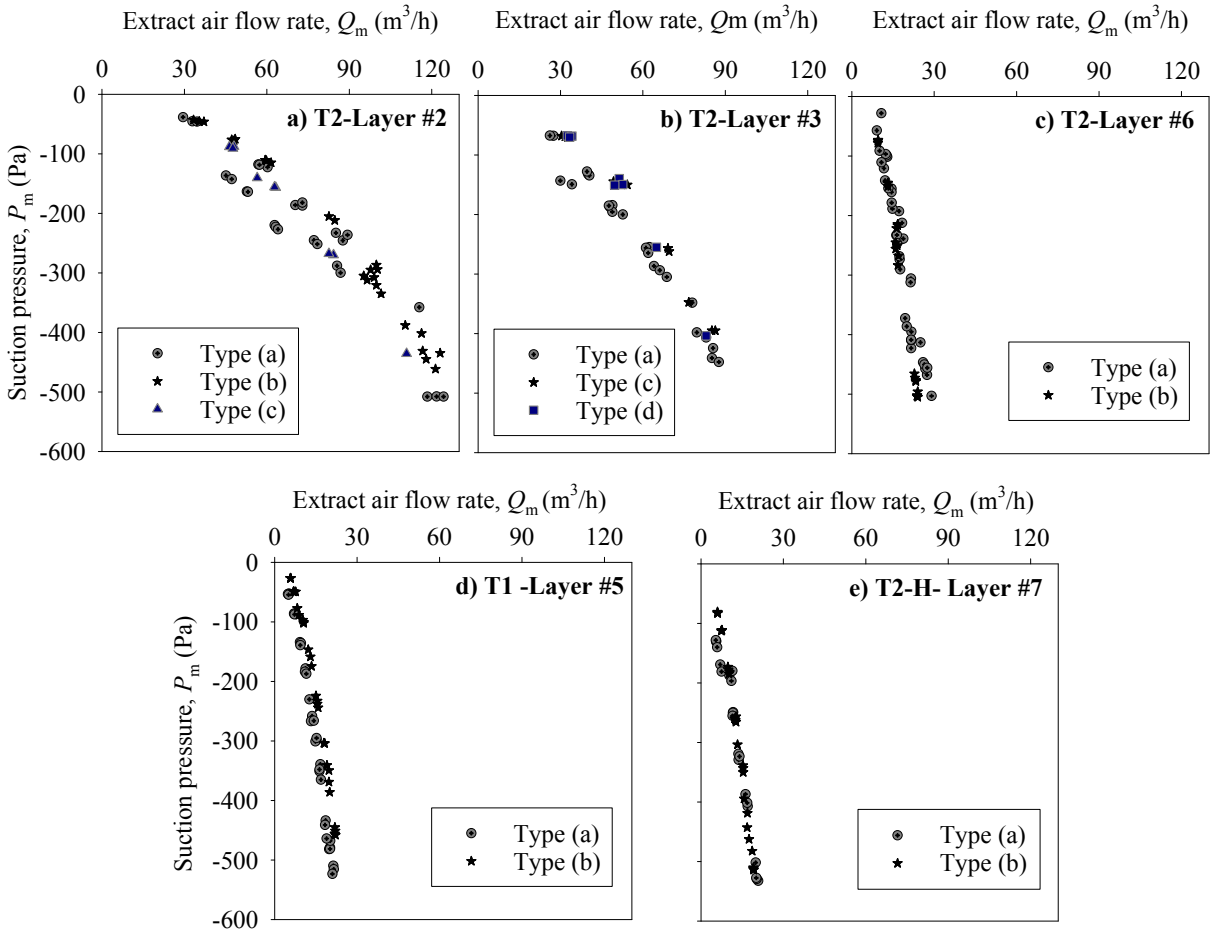

Figure 4.14. Effect of suction point types on the suction pressure developed below the lid of the tank at different compacted thicknesses of T1 Struc and T2 Perm materials.

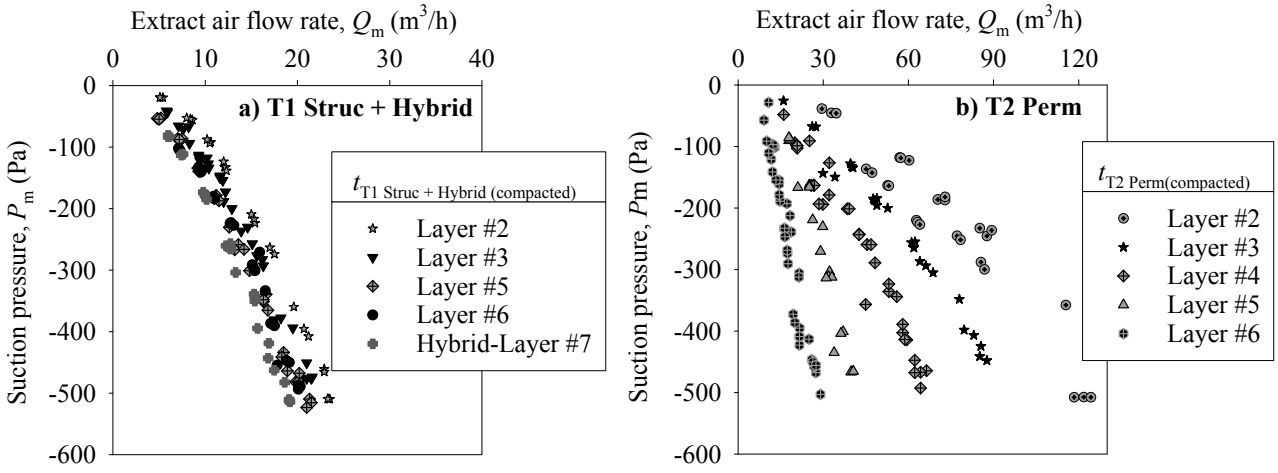

Figure 4.15. Suction pressure below the lid of the tank at different compacted thickness for (a) the T1 Struc and Hybrid materials and (b) the T2 Perm material.

A permeable granular material of an SD system is expected to have a low ΔP, i.e. ΔP tends to zero.

Based on the test results presented in Figure 4.16, the k_{ah} values of the T1 Struc and T2 Perm materials at different compacted thicknesses were calculated using equation 3.10. The overall trend of k_{ah} tended to decrease with the increase in compacted thickness, as expected (see Table A2.3).

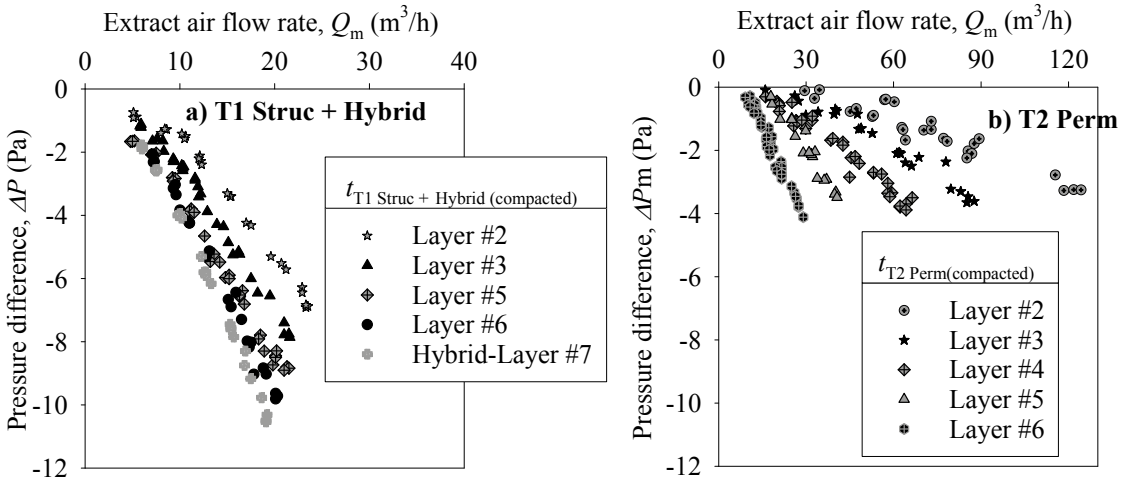

Figure 4.16. Variation in the suction pressure difference *ΔP* between the top and the bottom of the compacted granular material with extract airflow rate at different compacted thicknesses for (a) the T1 Struc and Hybrid materials and (b) the T2 Perm material.

4.2.3 Suction pressure measurement with passive depressurisation

This section presents the investigation of passive depressurisation using chimney cowls. Two types of cowls were used, rotating (types a and b) and static (types c–e), as shown in Figure 4.17. P_m was recorded using pressure sensors placed below the lid of the tank. The wind was generated using the controllable electric fan and a wind tunnel (Figure 4.18a). This wind tunnel was orientated directly towards the centre of the cowl.

Wind velocity was measured at three different locations around each cowl, i.e. at the front (Figure 4.18b), at the side (Figure 4.18c) and at the centre (Figure 4.18d) of the cowl. The final wind speed for each test was considered to be the average value of the wind speeds measured at these three locations. Examination was carried out with the T2−Layer #6 of the T2 Perm material.

Figure 4.19 shows the relationship between P_m and wind velocity for the different cowls. Observations indicated that, at the same wind speed, the rotating cowls (types a and b) induced the highest P_m, followed by the open-pipe cowl (type d), the common cap cowl (type c) and the black "mushroom" cowl (type e). In fact, the black "mushroom" cowl performed relatively poorly compared with the other cowl types, displaying a suction pressure that was at least 75% lower than that of any of the other cowls across a range of wind speeds (2−6 m/s). In general, the common cap cowl gives a slightly (approximately 10−12%) lower suction pressure than using only an open pipe with no cowl. As expected, the effectiveness of the rotating cowls increases with increase in wind speed.

4.2.4 Determination of the porosity of the compacted materials

As discussed previously, the n_h values were obtained using equation 3.2, using a specific gravity of $G_s = 2.73$ and 2.69 for the T1 Struc and T2 Perm materials, respectively.

For the T2 Perm material, the n_h values varied between 0.23 and 0.32, with an average n_h of 0.28. This average value is lower than the value of 0.37 reported in section 4.1. This is because the field compactor used in this study induced a higher compaction degree of the T2 Perm material than that induced by the small-scale compactor. For the T1 Struc material, the n_h values varied between 0.11 and 0.18, with an average n_h of 0.13.

4.2.5 Implications for practice

An important aspect of phase 2 was to validate the compaction degree, k_{ah} and n_h values for the Irish T1 Struc and T2 Perm materials reported in section 4.1 for phase 1. As the test results found in phase 1 were obtained with the small-scale test apparatus, it would be expected that the findings from phase 2 would more accurately reflect the behaviour of the T1 Struc and T2 Perm materials.

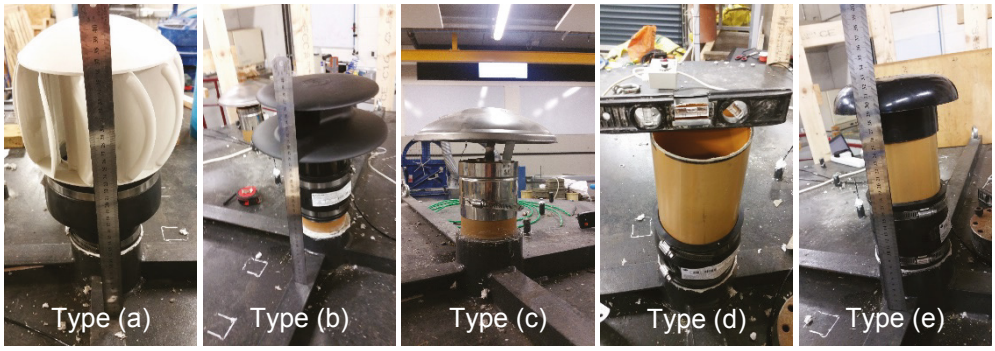

Figure 4.17. Rotating (types a and b) and static (types c–e) cowls examined in this study.

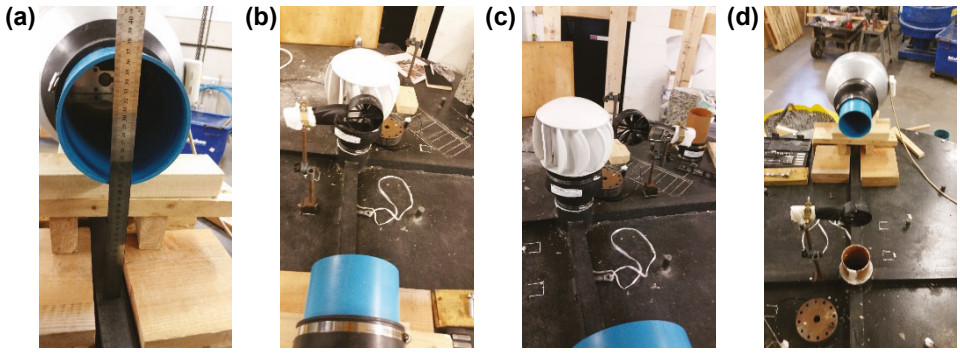

Figure 4.18. Example of the test set-up for cowl type a showing (a) the wind tunnel (blue pipe) and wind speed measurement (b) at the front, (c) besides and (d) at the centre of the cowl. This test set-up was applied for all cowl tests in this study.

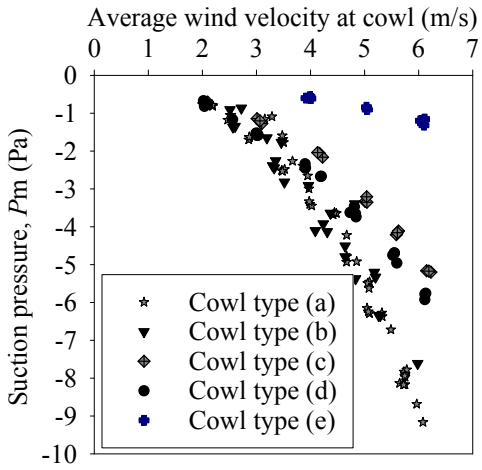

Figure 4.19. Relationship between suction pressure and wind velocity for the different cowls.

The k_{ah} and n_h values obtained in phase 2 for the T2 Perm material were lower than those obtained in phase 1. This is because, in phase 2, the T2 Perm material was compacted by a field compactor and thus it had a higher compaction degree than that in Phase 1. Therefore, it is suggested that the k_{ah} and n_h values determined in phase 2 of this study should be adopted for the design using T2 Perm materials.

The n_h value for the T1 Struc material in phase 2 was identical to that found in phase 1. However, its k_{ah} values were found to be higher. This could be explained by a number of factors, e.g. the thickness (length) of the test sample in phase 2 in comparison with the greater thickness of the sample tested in phase 1; the thickness of the test sample for T1 Struc compacted in this study varied between 300 mm and 750 mm, whereas it was 1500 mm in phase 1. Another issue was that a significant amount of water drained out of the T1 Struc in phase 2 before the test set-up was fully completed. The final moisture content of the T1 Struc material was measured after all tests were completed. This moisture content was found to vary between 1.27% and 1.74% at the top and the bottom of the material, respectively. This reduction in moisture content in comparison with the initial moisture content (i.e. 3–4%) could be a reason for the increase in the k_{ah} values for the T1 Struc material.

Passive depressurisations were carried out to examine the performance of the different chimney cowls. The test results obtained with the cowls might not reflect the actual relationships between the natural wind speed and suction pressure generated from each cowl type. Based on the test results, the rotating cowls were found to be the best, followed by the pipe with a cap cowl and the open-pipe cowl. The worst performance was observed for the "mushroom" cowl type.

Furthermore, experience has shown that the mechanical component in rotating cowls might physically degrade with time. Therefore, it is suggested that the open pipe with cap cowl (type c, Figure 4.17) could be a reliable cowl to apply in a passive SD system. The cap of the cowl can be optimised to increase its performance, e.g. by raising the height of the cap from the top of the pipe (E. Monahan, All Clear Radon Ltd, Wexford, Ireland, personal communication, 2018). Further investigation of this cowl is suggested.

It has been reported that a radon sump might have an influence over an area of 250 m^2 or a distance of 15 m from the sump (DEHLG, 2002). However, the results reported in this study were determined using a cylinder test tank that had a limited diameter of 2 m. Therefore, the influence area of the sump was not fully elucidated in this study. Moreover, the circular shape of the test tank developed in this study could not account for the effect of other factors in the performance of the granular fill material layer, e.g. the shape of the slab and foundation of the building, and obstruction of walls and foundations. Therefore, further investigations of prototype slabs of an SD system using the T1 Struc and T2 Perm materials are essential.

4.3 Computational Fluid Dynamics Simulation Results

4.3.1 Numerical model validation

The accuracy of the CFD simulations in this study was validated by comparing the CFD results with experimental test results from Gadgil *et al*. (1991) and BRE (1998) and experimental test results obtained in this study.

Figure 4.20 shows a typical numerical mesh for the air permeability test apparatus used in this study. The boundary conditions were specified based on the test set-up shown in Figures 3.4 and 3.7. An inlet boundary was set at the left end of the model, whereas the outlet is at the right end. The wall boundary was defined along the external wall of the apparatus. A hexahedral element type was applied for the meshing. An optimum mesh size of 0.01 m was determined so that the numerical mesh size does not affect the results. The residual convergence criterion for velocity was set at 10^{-4} and the scaled energy residual was set at 10^{-6}. These criteria were used to ensure that there were enough iterations to achieve a numerical converged solution.

As discussed, the k_{ah}, n_{ah} and d_{ef} parameters are required for CFD simulations. The d_{ef} value can be determined from the grading curve. The term d_{ef} is adopted to represent the inertial loss of flow through a granular specimen (Ergun, 1952). This inertial loss can be calculated according to the second term in the Ergun equation. The air used in CFD simulations has a density, ρ, of 1.225 kg/m^3 and a viscosity of 1.7894×10^{-5} kg/(m.s).

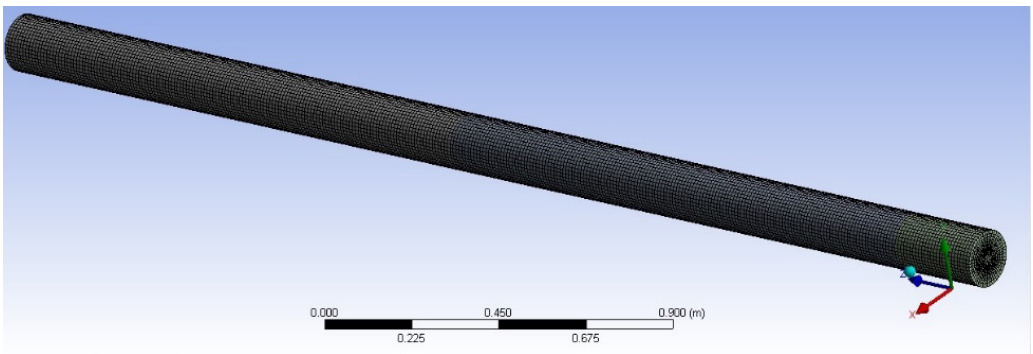

Figure 4.20. Typical numerical mesh for the test apparatus used in this study.

Gadgil et al. *(1991) laboratory test*

Gadgil *et al*. (1991) measured the air permeability of the ¾-inch (*c*.19-mm) rounded granular fill materials. The test apparatus was made of wood with the following dimensions: height 0.222 m × width 0.254 m × length 2.43 m. An average d_{ef} value was assumed to be 11 mm. The k_{ah} and n_h values were 1.3×10^{-7} m² and 0.4, respectively. The air pressure drop across the material with change in flow velocity was numerically simulated and compared with the test results. It was found that the CFD simulations simulate the test results correctly with an error of approximately ±2.5% (Figure 4.21a).

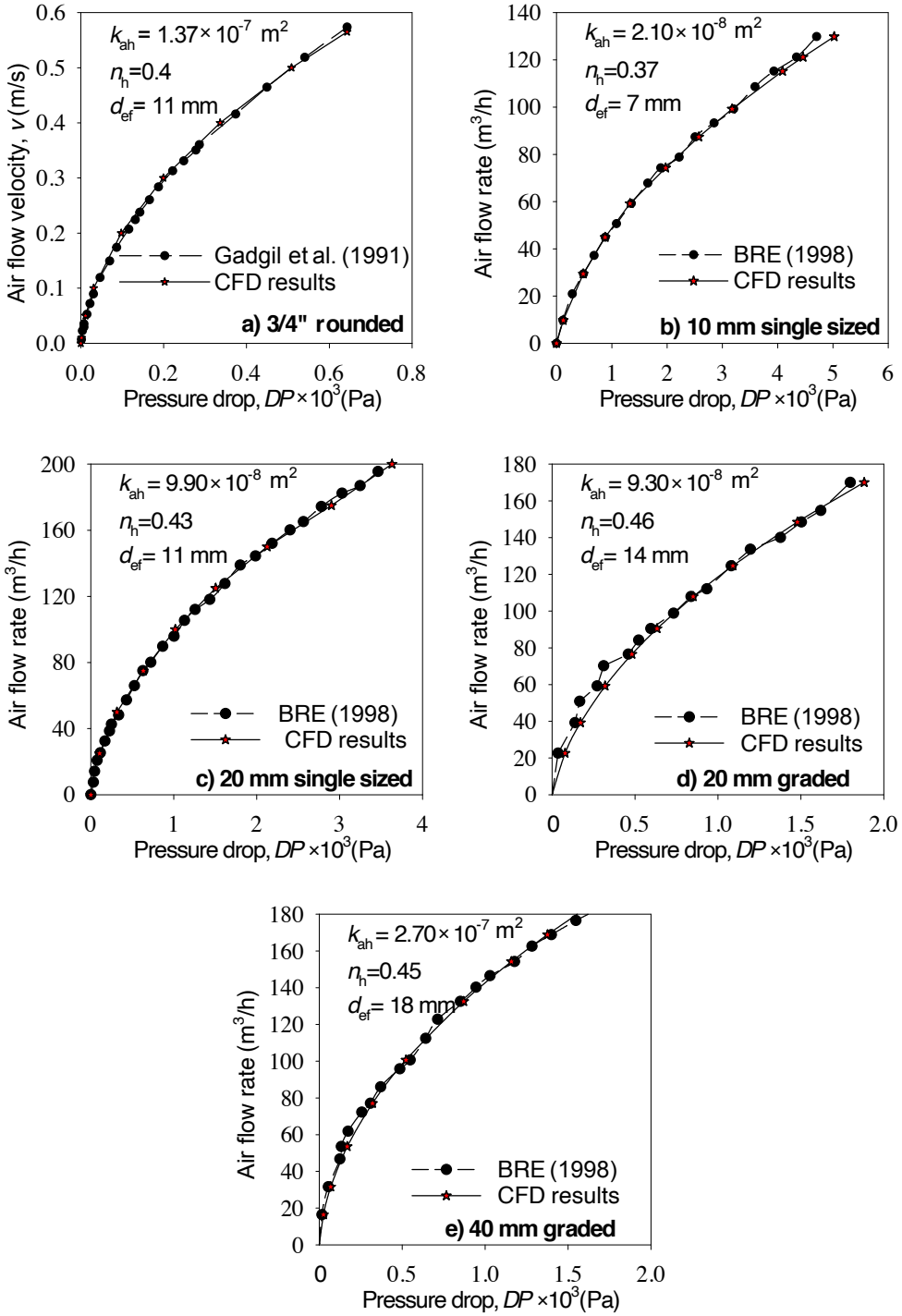

Figure 4.21. Comparison of CFD simulations and the experimental test results for poorly graded granular fill materials. Data adopted from Gadgil *et al*. (1991) and BRE (1998).

BRE (1998) laboratory test

BRE (1998) reported a series of laboratory tests to measure the k_{ah} of different types of well-graded and poorly graded granular fill materials used for SD systems in the UK. Poorly graded materials were 10-mm and 20-mm single sized materials and 20-mm and 40-mm graded materials; the well-graded material was MOT Type 1 sub-base. The test apparatus was the same as that reported in Gadgil *et al*. (1991). Measurements were performed for the uncompacted material only. The k_{ah} values obtained were between 2.1×10^{-8} m^2 and 2.7×10^{-7} m^2, whereas the n_h values varied between 0.32 and 0.46 according to material type. The d_{ef} was taken as the d_{50} on grading curves (the particle size of the granular fill material at 50% passing).

Values of k_{ah}, n_h and d_{ef} are presented in Figure 4.21b−e for the poorly graded materials and in Figure 4.22a and b for the well-graded materials. The CFD results are in good agreement with the test results for the 10-mm and 20-mm single-sized materials and the 20-mm and 40-mm graded materials, with an error of between 2% and 4% (Figure 4.21b−e). However, the CFD simulations for the MOT Type 1 sub-base (Figure 4.22a) failed to yield the test results accurately. This is because the d_{50} value on the grading curve of the MOT Type 1 material does not reflect well the d_{ef} of this material. Therefore, additional simulations were performed to find the correct d_{ef} value for MOT Type 1. It was found that a d_{ef} of 6.5 mm gives excellent agreement between the CFD simulation and the test results, with an error of approximately 2.5% (Figure 4.22b).

Spanish pilot house measurements

Suction pressure measurements were conducted in the pilot house in Spain (Vazquez *et al*., 2011). The SD system in the house consists of a 1 m × 1 m sump, with 15 cm of granular fill material and 10 cm of concrete slab material. The sump is placed at the centre of the house. The area of the slab is 25 m^2, as shown in Figure 4.23a. A k_{ah} value of 9×10^{-8} m^2 for the granular fill material was obtained in the laboratory. To generate the sump pressure, a 30-W electric fan was connected to the pipe that comes from the sump centre, as shown in Figure 4.23c. A highly accurate pressure sensor with an accuracy of ±0.25% (Honeywell TruStability) was used to measure the suction pressure.

Suction pressure measurements were performed at seven different holes drilled through the concrete slab at various distances from the sump centre (sections #1 and #2 in Figure 4.23a). The interval distance between each hole is 0.5 m. The maximum fan speed was activated and an average sump pressure of approximately −20.5 Pa was recorded. The suction pressures obtained are shown in Figure 4.24a. Each measurement was conducted at least three

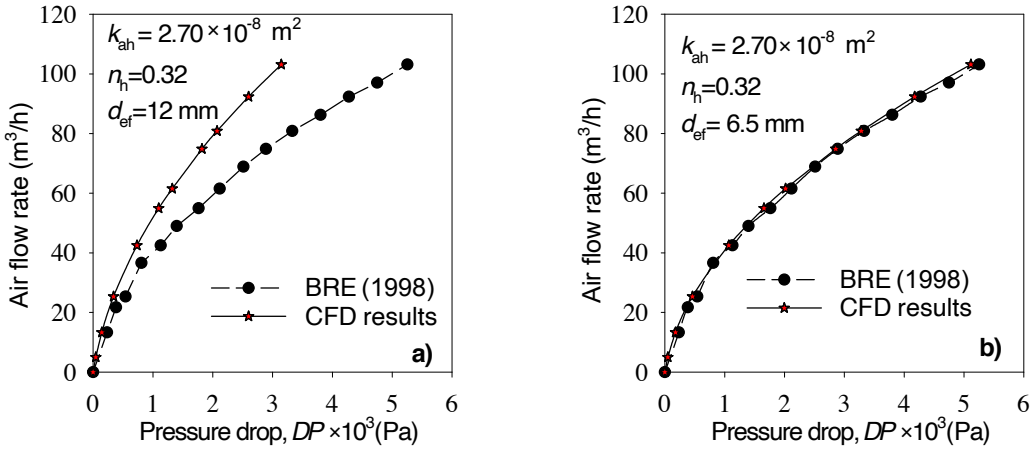

Figure 4.22. Comparison of CFD simulations and the experimental test results for well-graded MOT Type 1. Using a d_{ef} of 12 mm (a), the CFD simulation does not simulate the test results well; using a d_{ef} of 6.5 mm (b), the CFD simulation simulates the test results with an error of approximately ±2.5%. Data adopted from BRE (1998).

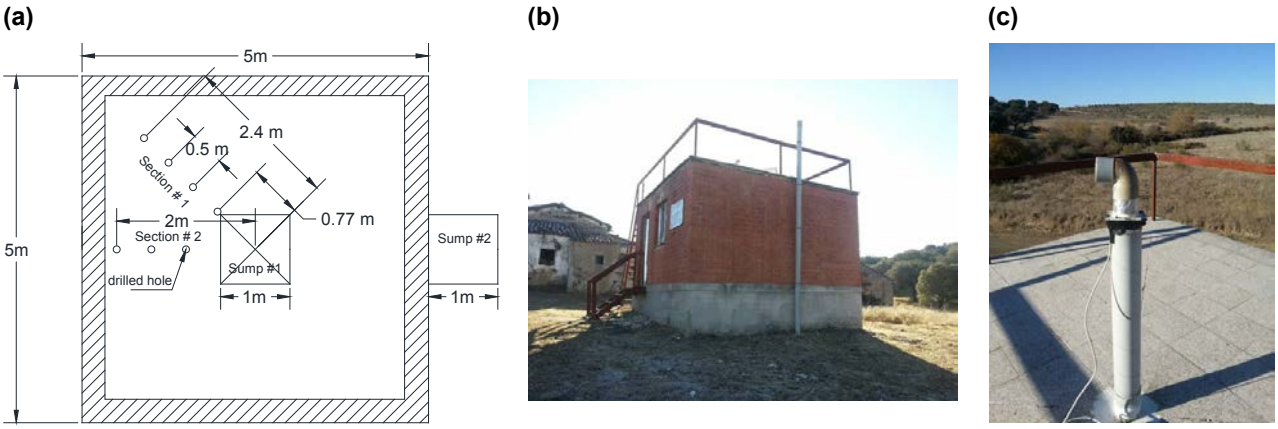

Figure 4.23. Test configuration and photographs of the pilot house in Spain (not to scale): (a) test hole locations; (b) photograph of the house; (c) electric fan on the pipe coming from the sump.

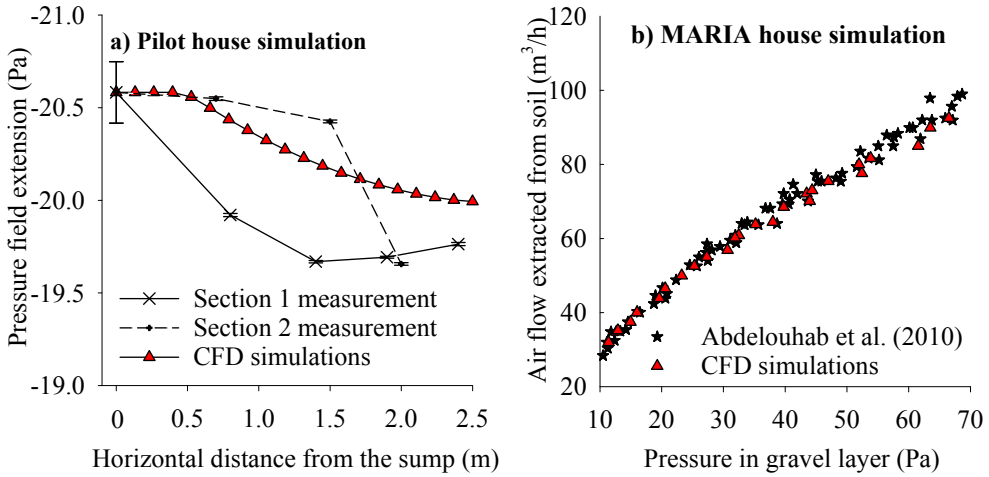

Figure 4.24. Comparison of suction pressure between the experimental measurements and the CFD simulations. MARIA, Mechanized house for Advanced Research on Indoor Air.

times (approx. 1 hour per measurement). As shown in Figure 4.24a, the suction pressures are homogeneous, with pressures varying between 19.5 Pa and 20.5 Pa. This finding suggests that the slab of the pilot house was well treated to minimise the development of cracks in the slab, together with a sufficient permeable layer built under the slab.

To validate the CFD simulations with the measurements from the Spanish pilot house, two-dimensional CFD simulations were conducted. The boundary conditions and configurations were defined as discussed above. The air permeability of the soil, k_{as}, was set at 10^{-12} m^2 (Vazquez, 2017). Comparisons between the CFD simulation results and the measurements from the pilot house are presented in Figure 4.24a. The CFD simulations agreed with the test data, with an average error of ±2%.

French MARIA (Mechanized house for Advanced Research on Indoor Air) house

Abdelouhab *et al*. (2010) and Abdelouhab (2011) reported experimental measurements for the PFE in the MARIA house in France. This house had a floor area of 81 m^2, with a 40-cm-thick gravel layer. Diallo *et al*. (2015) reported that this gravel had a k_{ah} value of 10^{-7} m^2 and the soil beneath the house had a k_{as} value of 2.61×10^{-13} m^2. All boundary conditions for CFD simulations were defined following Abdelouhab *et al*. (2010) and Abdelouhab (2011). The comparison between CFD simulation results and the test results is shown in Figure 4.24b. An average error of ±5.6% was found between the CFD simulations and the test measurements.

Based on the above comparisons, it can be concluded that the CFD simulations are reliable. Therefore, the

CFD simulations could be used to analyse the PFE behaviour of an SD system.

Numerical simulation of small-scale experimental tests in this study

As detailed above, the d_{ef} value for the well-graded T1 Struc granular fill material could not be obtained as the d_{50} from the grading curve. Therefore, the d_{ef} value for T1 Struc needed to be confirmed. The d_{ef} value for T2 Perm was obtained as a d_{50} of 16.2 mm from the grading curve (Figure 4.1b). Approximately 300 CFD simulations were performed to match the CFD results with the measurements for T1 Struc and T2 Perm. This step enabled the d_{ef} value to be obtained for T1 Struc. The k_{ah} and n_h values were taken from Table A2.2.

Figure 4.25 shows the results from the CFD simulation of the pressure difference contour developed along the length of the test apparatus for the T1 Struc granular fill material (T1#1-1), with an inlet airflow rate, Q_{in}, of 2.51×10^{-4} m³/s. The inlet airflow was numerically pressurised with air entering the air inlet chamber (Figure 4.25). The pressure difference was defined as the absolute pressure, $P_{(CFD)}$, at the point of interest along the length of the sample relative to the absolute pressure at the outlet air chamber, $P_{2(CFD)}$. Figure 4.26 shows the pressure differences along the length of the test apparatus for the two samples T2#1-1 and T1#1-1

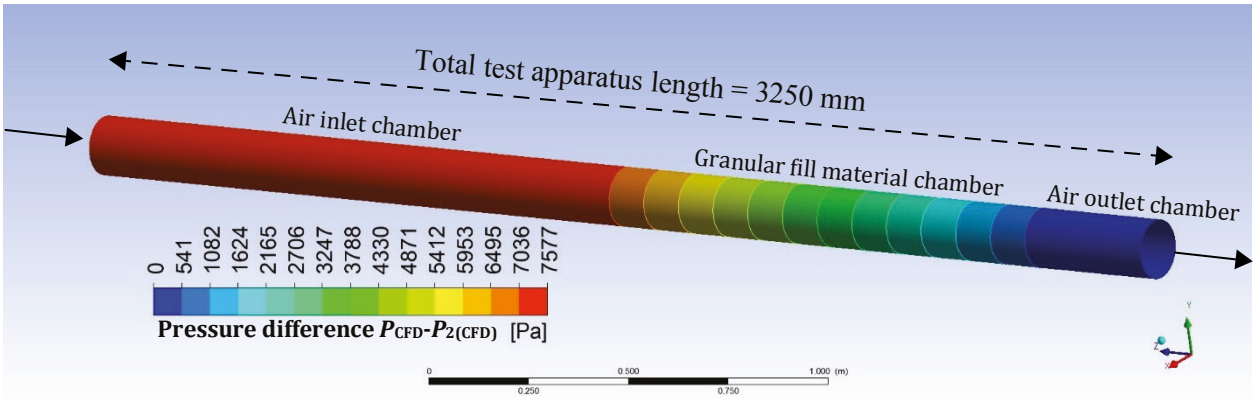

Figure 4.25. CFD simulation of the pressure difference ($P_{CFD} - P_{2(CFD)}$) contour that develops along the length of the test apparatus in the compacted T1 Struc granular fill material (T1#1-1) for $Q_{in} = 2.51 \times 10^{-4}$ m³/s. The pressure difference is relative to the absolute pressure at the outlet air chamber, $P_{2(CFD)}$.

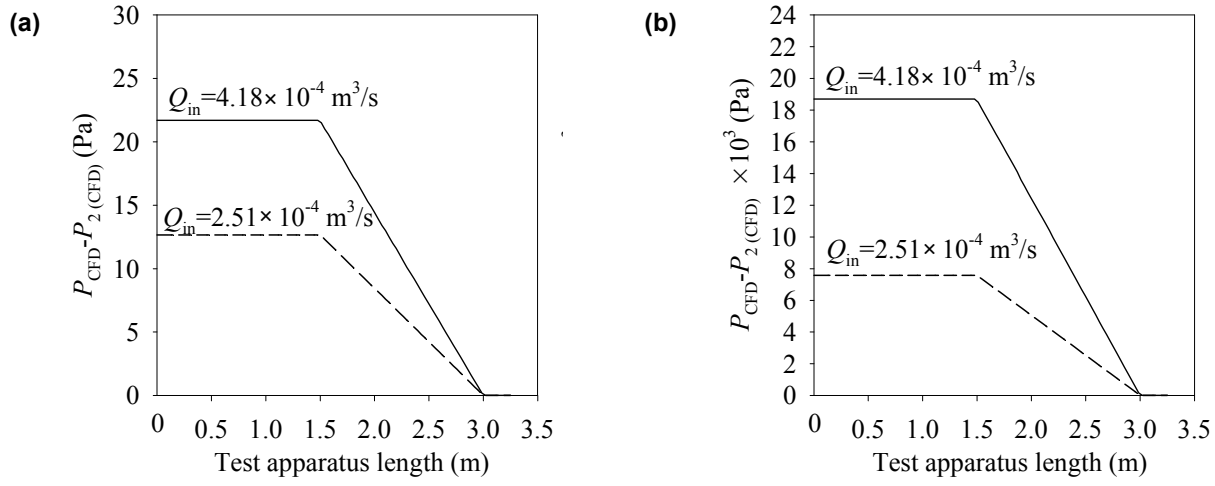

Figure 4.26. CFD simulation of the pressure difference ($P_{CFD} - P_{2(CFD)}$) that develops along the length of the test apparatus in (a) compacted T1 Perm (T2#1-1 sample) and (b) compacted T2 Struc (T1#1-1 sample). At the same inlet airflow rate, Q_{in}, the T1 Struc material induces a much higher pressure difference than the T2 Perm material, suggesting that the ability of T2 Perm to extract air is much better than that of T1 Struc.

at Q_{in} values of 2.51×10^{-4} m³/s and 4.18×10^{-4} m³/s. The pressure difference decreases linearly along the length of the test apparatus. In addition, the pressure developed in the T2 Perm material is significantly lower than that in the T1 Struc material. This is because the T2 Perm material has a much higher k_{ah} value than that for the T1 Struc material. This suggests that the ability of T2 Perm to extract air is much better than that of T1 Struc.

Figure 4.27 compares the CFD simulations and test results for T1 Struc and T2 Perm. The CFD simulations agree well with the experimental test results. The d_{ef} values were determined by back-calculating the test results using the CFD simulations. Variation in the d_{ef} value with w_{nc} for T1 Struc is shown in Figure 4.28. The d_{ef} value decreases significantly with the increase in w_{nc} until $w_{nc} \approx 3.5\%$. The effect of d_{ef} on the k_{ah} value of the T1 Struc material is evident, as the k_{ah} value increases linearly with the increase in d_{ef} (Figure 4.29).

Based on the CFD results, a simple equation that can be used to evaluate the d_{ef} value is proposed (equation 4.6). Alternatively, d_{ef} values can be used to interpolate k_{ah}, as shown in equation 4.7.

The equations are expressed as a function of the compaction moisture content w_{nc}.

$$d_{ef} = 1.56e^{-0.83w_{nc}} \text{ for } 1\% < w_{nc} \leq 4.5\% \quad (4.6)$$

$$k_{ah} = 6.51 d_{ef} \text{ for } 1\% \leq w_{nc} \leq 4.5\% \quad (4.7)$$

From the validation, it can be concluded that the CFD simulation is reliable and could be used to analyse

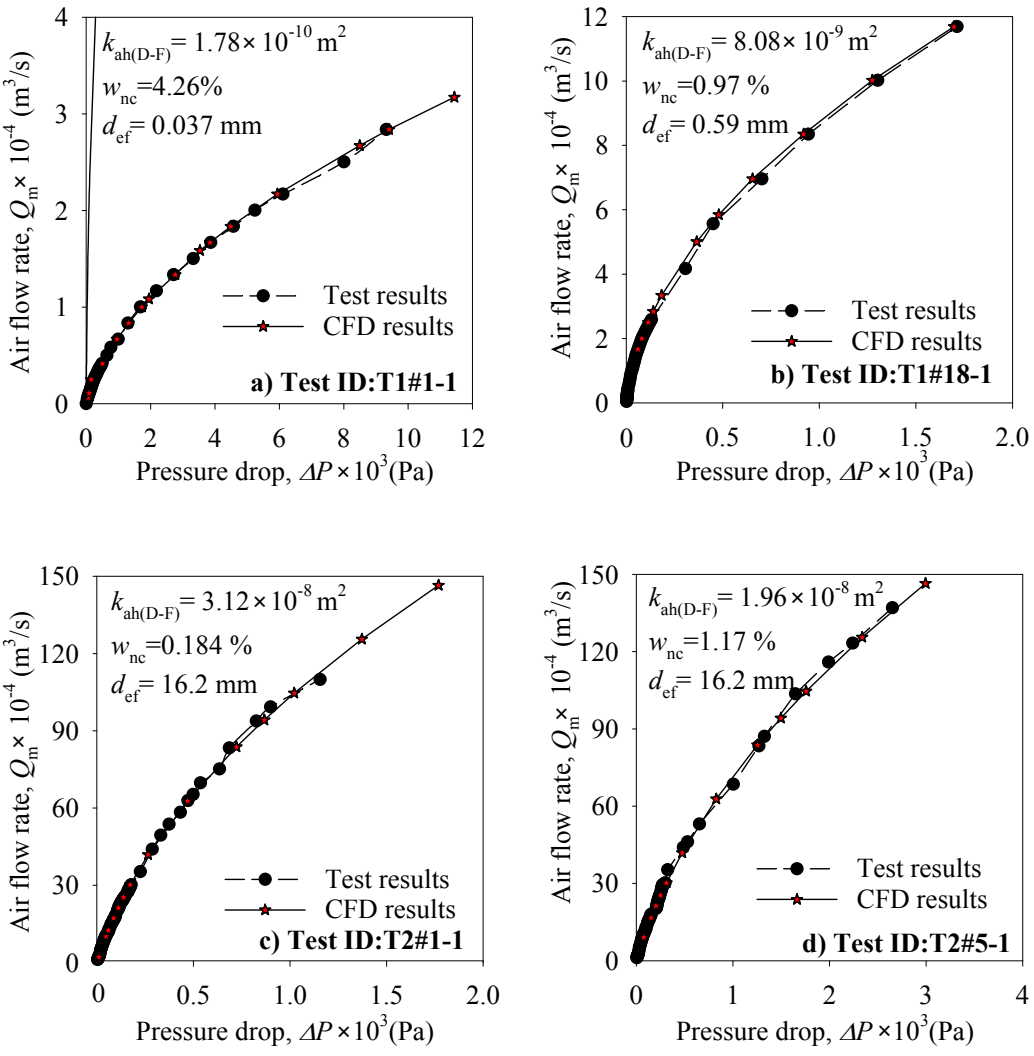

Figure 4.27. Comparison of the CFD simulations and the test results for T1 Struc and T2 Perm. The test results were selected randomly. Test results for other samples show similar trends and thus are not presented here.

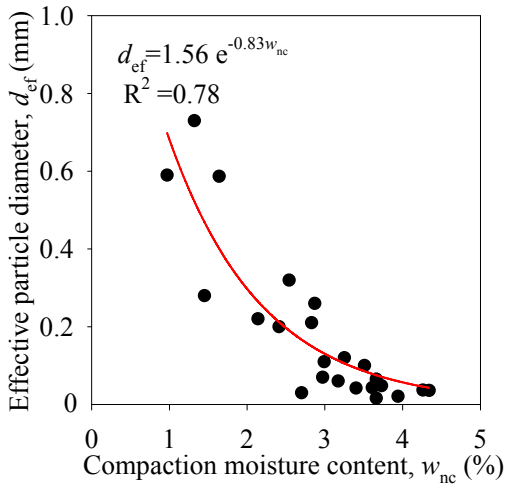

Figure 4.28. Variation in d_{ef} with w_{nc} for T1 Struc.

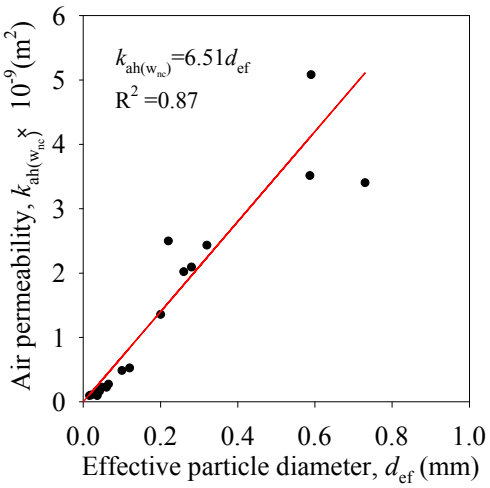

Figure 4.29. Relationship between d_{ef} and $k_{ah(w_{nc})}$ for T1 Struc.

the airflow behaviour of the granular fill materials. In addition, the d_{ef} value for poorly graded material can be taken to be the d_{50} value from the grading curve. The d_{50} value taken from the grading curve does not reflect the d_{ef} value for the well-graded material.

4.3.2 Numerical simulation of large-scale soil depressurisation systems

Parametric study and material properties

Three types of granular fill materials for forming the permeable layer of SD systems were investigated: the T1 Struc, T2 Perm and Hybrid materials, as defined in Irish standard IS 888:2016 (NSAI, 2016a) and shown in Figure 3.9. The Hybrid material is made by layering the T1 Struc and the T2 Perm materials. The thickness, *t*, of the granular fill layers was varied in this study and will be described in the following sections. Irish standard IS 888:2016 states that the maximum thickness of a permeable layer in an SD system should be 90 cm. The footing dimensions were simulated at a width of 50 cm and at a depth of 90 cm from the ground surface.

Wall cracks and the airtightness of the concrete slab of a house significantly affect the effectiveness of its SD system. A wall crack might develop along the joint of a wall and a slab. In this study, the width of the wall crack (w_{crack}) was assumed to vary as follows: 0 mm, 0.5 mm, 1 mm, 1.5 mm, 2 mm, 3 mm, 5 mm, 7.5 mm, 10 mm and 20 mm. The airtightness degree could be defined as perfectly and imperfectly sealed slabs.

A perfect seal could exist in a newly built house if good-quality construction methods are used at the interface between the concrete slab and the wall. For example, a perfect seal could be formed by using proper radon membranes under the slab and following good construction practices. This perfect seal could prevent soil gas from entering the house through the slab. However, a perfectly sealed slab might not last for the full lifetime of the building. For example, cracks might develop on the surface of an old slab and radon membranes can deteriorate over time, allowing soil gas to pass through. In this case, an imperfectly sealed slab is expected.

Figure 4.30 shows two typical radon sumps that have been widely used in Ireland for SD systems. These sumps either have perforated sides (sump type 1, Figure 4.30a) or are completely open at the bottom (sump type 2, Figure 4.30b). Based on the manufacturer specifications, each sump has a cross-sectional area of 0.072 m^2, with a sump depth (d_{sump}) of 0.124 m, as indicated in Figure 4.30b. For simplicity, in the numerical simulations a square sump with a sump width (w_{sump}) of 0.27 m (and therefore an equivalent sump area) and a d_{sump} of 0.124 mm was utilised, unless stated otherwise. The suction pressure at the sump (P_{sump}) was set at −100 Pa for all cases. The sub-slab pressures (P) were normalised by this P_{sump} and thus the final results are not affected by P_{sump}. This assumption was also confirmed by performing initial simulations at different values of P_{sump}. P_{sump} was applied simultaneously at the bottom and the side of the sump, unless stated otherwise.

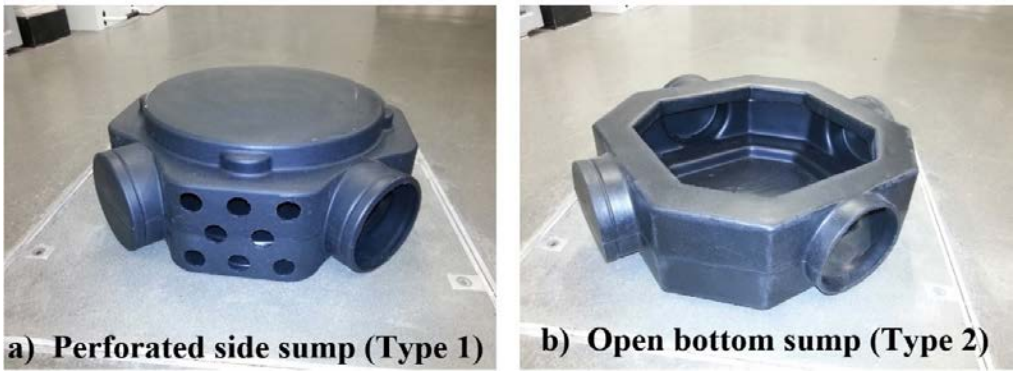

Figure 4.30. Example of two common sump types used in SD systems in Ireland.

It has been previously reported that k_{ah}, n_h and d_{ef} are three key parameters of granular materials that are required for the design of an SD system. Ergun (1952) found that the pressure loss of fluid flow through a column of granular material is mainly governed by the kinetic and viscous energy losses, which are directly related to these three parameters. Ergun (1952) suggested the following equations to represent the pressure loss:

$$\frac{\Delta P}{L} = \frac{\mu \times V}{k_{ah}} + \frac{C \times G \times V}{2} \tag{4.8}$$

$$\frac{1}{k_{ah}} = 150 \times \frac{\left(1 - n_h\right)^2}{n_h^3 \times d_{ef}^2} \tag{4.9}$$

$$C = \frac{3.5 \times \left(1 - n_h\right)}{n_h^3 \times d_{ef}} \tag{4.10}$$

where ΔP is the pressure drop; L is the flow length (m); μ is the dynamic viscosity of air; G is the mass flow rate; V is the airflow velocity; and C is the inertial loss coefficient (1/m) (a parameter required for the CFD simulations in this study).

The properties of the T1 Struc and T2 Perm materials used in this study were adopted from experimental tests carried out in phase 1. The test results for the particle size distributions and compaction tests of these materials are shown in Figures 4.1 and 4.2. Previous studies have shown that the permeable layer of an SD system should be formed from a poorly graded granular material (US EPA, 1993; BRE, 1998). Therefore, it would be expected that a T1 Struc fill layer would induce a poor suction pressure in an SD system in comparison with that formed by the T2 Perm material.

The following equations were applied to determine the input parameters for the T1 Struc material:

$$ka_{h(T1Struc)} = 20 \times 10^{-9} e^{-1.25 w_{nc}} \text{ for } 1\% \le w_{nc} \le 4.5\% \tag{4.11}$$

The w_{nc} value for T1 Struc was varied at 1.0%, 1.5%, 2.0%, 2.5%, 3.0%, 3.5%, 4.0% and 4.5%. The w_{nc} value of the T2 Perm material was not considered in this study as the trend in its compaction degree is unclear (see Figure 4.2).

$$n_{h(T1Struc)} = 0.23 \text{ when } w_{nc} \le 2\% \tag{4.12a}$$

$$n_{h(T1Struc)} = 0.28 - 0.03 w_{nc} \text{ when } 2\% \le w_{nc} \le 6\% \tag{4.12b}$$

$$d_{ef(T1Struc)} = 1.56 e^{-0.83 w_{nc}} \text{ when } 1\% \le w_{nc} \le 4.5\% \tag{4.13}$$

The air permeability of the T2 Perm granular fill material, $k_{ah(T2Perm)}$, and the porosity of the T2 Perm granular fill material, $n_{h(T2Perm)}$, were fixed at 22.5×10^{-9} m^2 and 0.37, respectively, for all simulations, whereas its $d_{ef(T2Perm)}$ value was taken to be the d_{50} value on its grading curve (see Figure 4.1b). The air permeability of soil (k_{as}) was set at $10^{-4} \times k_{ah(T2Perm)}$ for all simulations, unless stated otherwise. The porosity of soil was fixed at 0.3. The air used in CFD simulations has a density of 1.225 kg/m^3 and a viscosity of 1.7894×10^{-5} kg/(m.s).

Abbas *et al*. (1999) found that the air permeability of 28-day aged concrete could vary from 0.2×10^{-16} m^2 to 0.8×10^{-16} m^2. Diallo *et al*. (2015) reported a measurement for the air permeability of the concrete slab from the MARIA house in France. They found that the effective air permeability of the concrete slab

was 1.69×10^{-10} m^2. Therefore, the air permeability of the concrete slab was set at 0.5×10^{-16} m^2 and 1.69×10^{-10} m^2 for perfectly and imperfectly sealed slabs, respectively.

Effects of a wall crack on the suction pressure

This section presents the effect of a wall crack on the suction pressure of the SD systems. The results presented in this section were investigated at different w_{crack} values, as mentioned previously. T2 Perm and Hybrid granular materials for forming the permeable fill layers of SD systems were considered. The thicknesses of these fill layers were set in accordance with standard IS 888: 2016 (NSAI, 2016a). For the T2 Perm fill layer, the thickness, *t*, was set at two different values, i.e. $t_{T2Perm} = 0.2$ m and 0.9 m, whereas for the Hybrid fill layer the thicknesses of the sub-layers were set at $t_{T2Perm} = 0.2$ m and $t_{T1Struc} = 0.7$ m for the T2 Perm and the T1 Struc materials, respectively.

Soil depressurisation system with T2 Perm material fill layer

Figure 4.31 presents the suction pressures for SD systems using the T2 Perm granular fill material with thicknesses of $t_{T2Perm} = 0.2$ m (Figure 4.31a and b) and 0.9 m (Figure 4.31c and d) for the case of a perfectly sealed slab. For $t_{T2Perm} = 0.2$ m, the suction pressure decreases dramatically when w_{crack} is varied from 0.5 mm to 1.5 mm, and the differential rate of the normalised pressure (P/P_{sump}) reduces at $w_{crack} > 1.5$ mm. For example, at a horizontal distance of 4 m from the sump centre, $P/P_{sump} = 1$ for $w_{crack} = 0$ mm and $P/P_{sump} = 0.6$ for $w_{crack} = 1.0$ mm, as shown in Figure 4.31a. For $t_{T2Perm} = 0.9$ m, this differential rate is

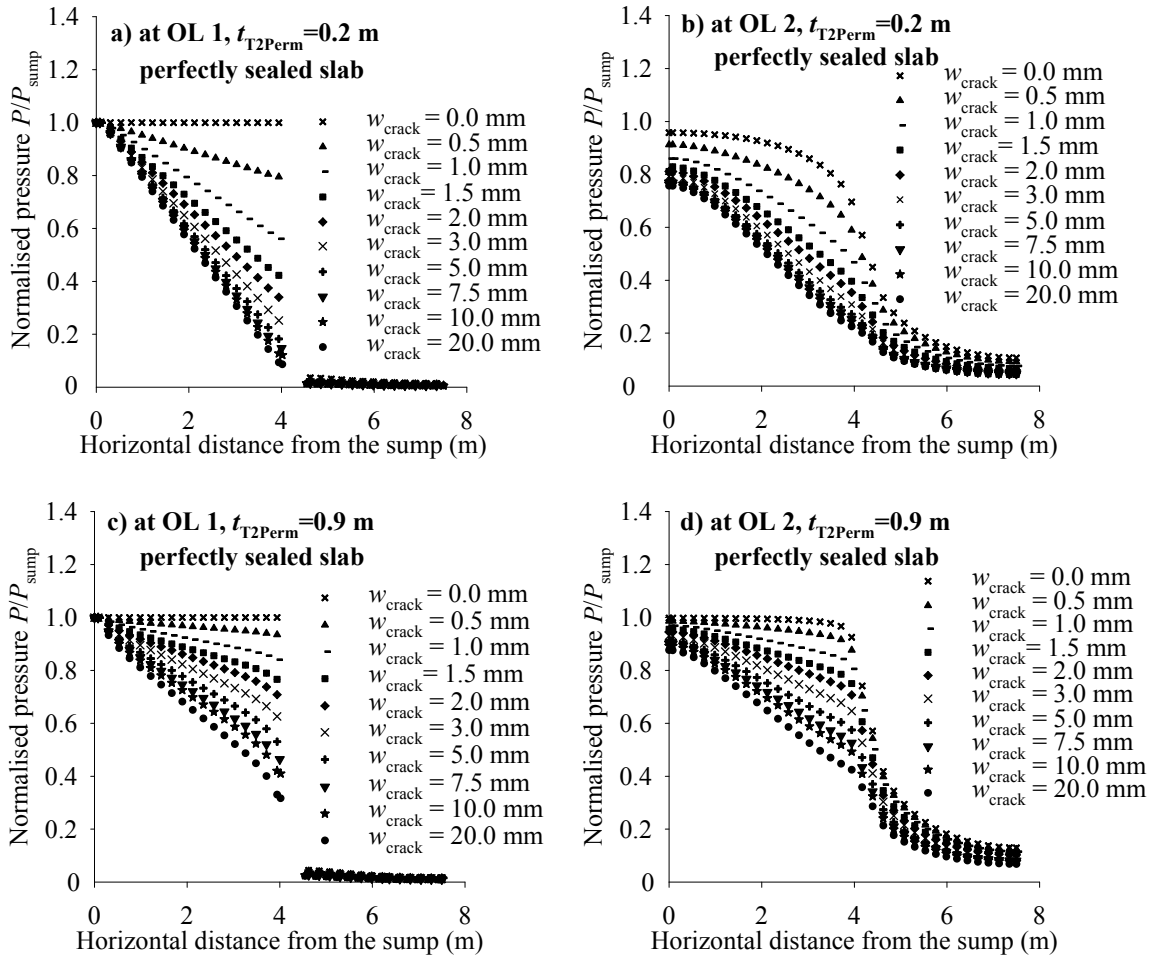

Figure 4.31. Effect of a wall crack on the sub-slab PFE for the T2 Perm granular fill material layer (perfectly sealed slab) at observation lines OL1 (at the sump level) (a and c) and OL2 (at the footing level) (b and d) for two thicknesses of T2 Perm, i.e. $t_{T2Perm} = 0.2$ m (a and b) and 0.9 m (c and d).

smaller, as shown in Figure 4.31c and d. The reduction in suction pressure occurs because the airflow resistance decreases through the wall crack when the crack becomes wider, i.e. a larger amount of air enters the granular fill layer, thus reducing the pressure from the crack side to the sump side, as shown in Figure 4.32. Figures 4.33 and 4.34 show the suction pressures for the case of a imperfectly sealed slab. A similar explanation can be applied as discussed above. The pressures for the imperfectly sealed slab are smaller than those for the perfectly sealed slab, as expected. In addition, as can be seen from these figures, the SD system with a t_{T2Perm} of 0.9 m induces a higher suction pressure than the SD system with a t_{T2Perm} of 0.2 m. This finding suggests that the thicker the T2 Perm layer, the better the suction pressure.

Soil depressurisation system with Hybrid granular material

Figure 4.35 shows the suction pressure development in an SD system with Hybrid granular fill layers (t_{T2Perm} = 0.2 m and $t_{T1Struc}$ = 0.7 m) for perfectly and imperfectly sealed slabs. The properties of T1 Struc were obtained using equations 4.10 and 4.11. The compaction moisture content, w_{nc}, was considered to be 4%. As shown in Figure 4.35, similar findings were observed for the Hybrid material as for the case of t_{T2Perm} = 0.2 m, presented in Figure 4.31. This similarity could be a result of the low degree of permeability of the T1 Struc material, as it does not provide a good suction pressure at its low k_{ah} value at w_{nc} = 4%.

Effects of the w_{nc} value of the T1 Struc material on suction pressure

The effects of the w_{nc} value of the T1 Struc material on the sub-slab PFEs were investigated for the SD systems with the Hybrid granular fill layer and the T1 Struc granular fill layer alone. The w_{nc} was varied at 1.0%, 1.5%, 2.0%, 2.5%, 3.0%, 3.5%, 4.0% and 4.5%, and the w_{crack} value was fixed at 1.5 mm for all simulations. For the SD system with the Hybrid granular fill layer, t_{T2Perm} and $t_{T1Struc}$ were set at 0.2 m and 0.7 m, respectively. For the T1 Struc layer alone, $t_{T1Struc}$ was fixed at 0.9 m. Both perfectly and imperfectly sealed slabs were considered. Simulation results for the Hybrid fill layer are shown in Figure 4.36. The pressures decrease slightly with increase in w_{nc} for both the perfectly sealed and the imperfectly sealed slabs, as the pressure is trapped inside the T2 Perm fill layer because of the low air permeability of the T1 Struc granular fill material, $k_{ah(T1Struc)}$, and k_{as}. This is in contrast to the results for the T1 Struc fill layer, as

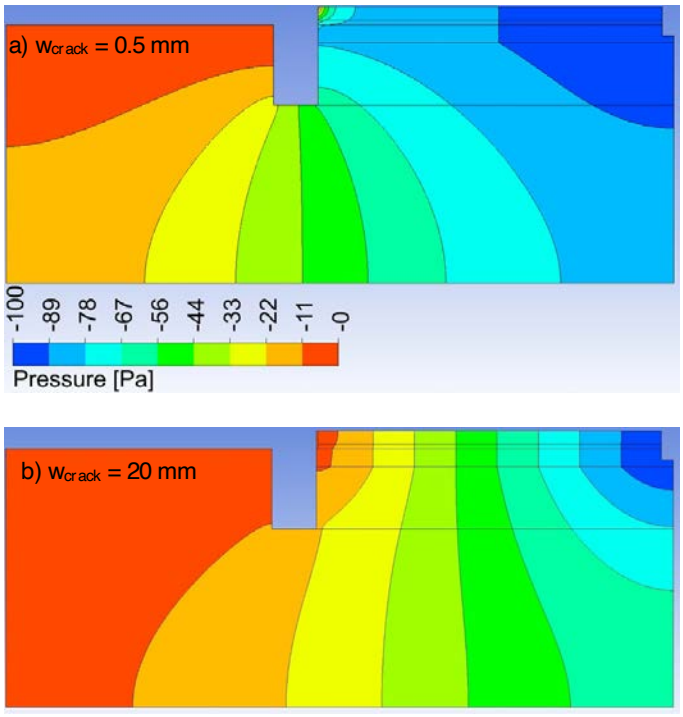

Figure 4.32. Example of the sub-slab PFE contours for the T2 Perm granular fill material layer (t_{T2Perm} = 0.2 m) for the case of a perfectly sealed slab.

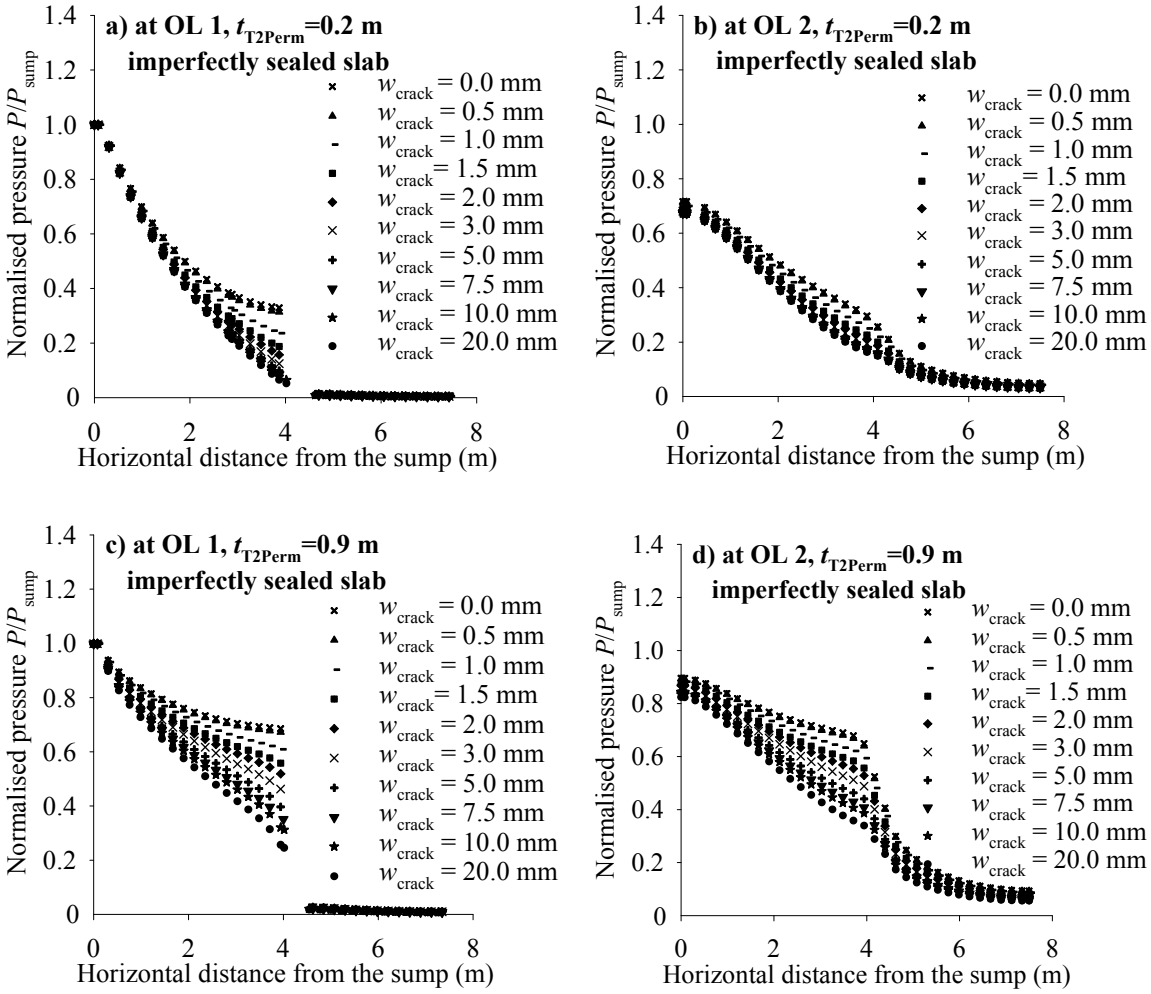

Figure 4.33. Effect of a wall crack on the sub-slab PFE for the T2 Perm granular fill material layer (imperfectly sealed slab) at observation lines OL1 (at the sump level) (a and c) and OL2 (at the footing level) (b and d) for two thicknesses of T2 Perm, i.e. t_{T2Perm} = 0.2 m (a and b) and 0.9 m (c and d).

shown in Figure 4.37. The suction pressures decrease significantly when w_{nc} increases. For example, at a distance of 4 m from the sump centre, a normalised pressure of 0.62 was obtained when w_{nc} = 1% [high $k_{ah(T1Struc)}$], whereas a pressure of 0.1 was obtained when w_{nc} = 4.5% [low $k_{ah(T1Struc)}$].

Therefore, in order to have a high suction pressure, the w_{nc} value should be low enough, e.g. $w_{nc} \leq 3\%$, with relatively good airtightness of the slab. An example of the pressure contours for w_{nc} = 4% for the imperfectly sealed slab are shown in Figure 4.38. As can be seen, the suction pressure decreases rapidly from the sump centre. These findings suggest that the T1 Struc material is not an optimum material to form a permeable layer for an SD system. It is also evident that an imperfectly sealed slab will result in a significant reduction in suction pressure.

Effects of the k_{as} value on suction pressure

An important factor in the design of the foundation for a house is to characterise the properties of the native soil. This characterisation allows designers to accurately define the type of foundation that should be used to support the house. In addition, if an SD system is required for the house, the k_{as} value is a key parameter. Practically, k_{as} is expected to affect the effectiveness of an SD system. For example, a significant pressure loss in the system would occur if the native soil had a relatively high k_{as} because of significant airflow entering the system from the ground surface outside the house.

In this section, the effects of the k_{as} values were investigated. Only a perfectly sealed ground-bearing slab was considered to minimise the effects of pressure loss through the slab. SD systems with the

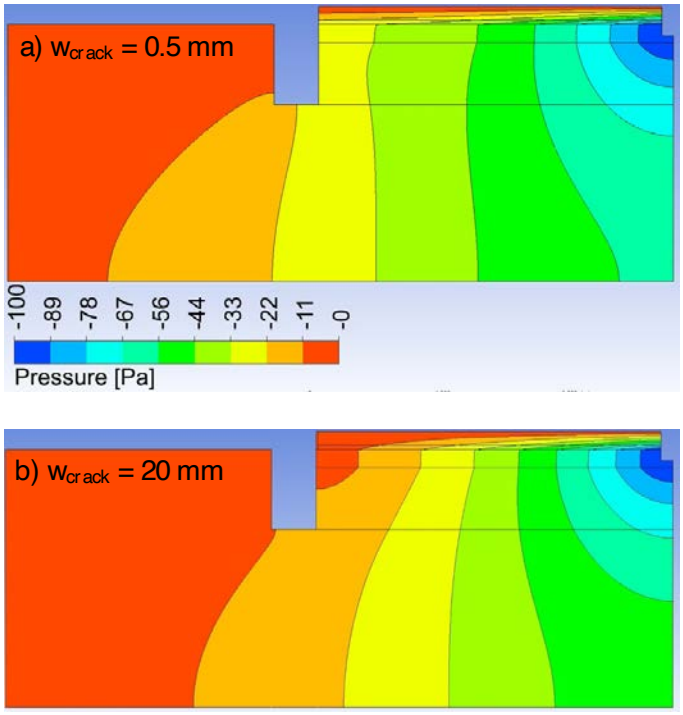

Figure 4.34. Example of the sub-slab PFE contours for the T2 Perm granular fill material layer (t_{T2Perm} = 0.2 m) for the case of an imperfectly sealed slab.

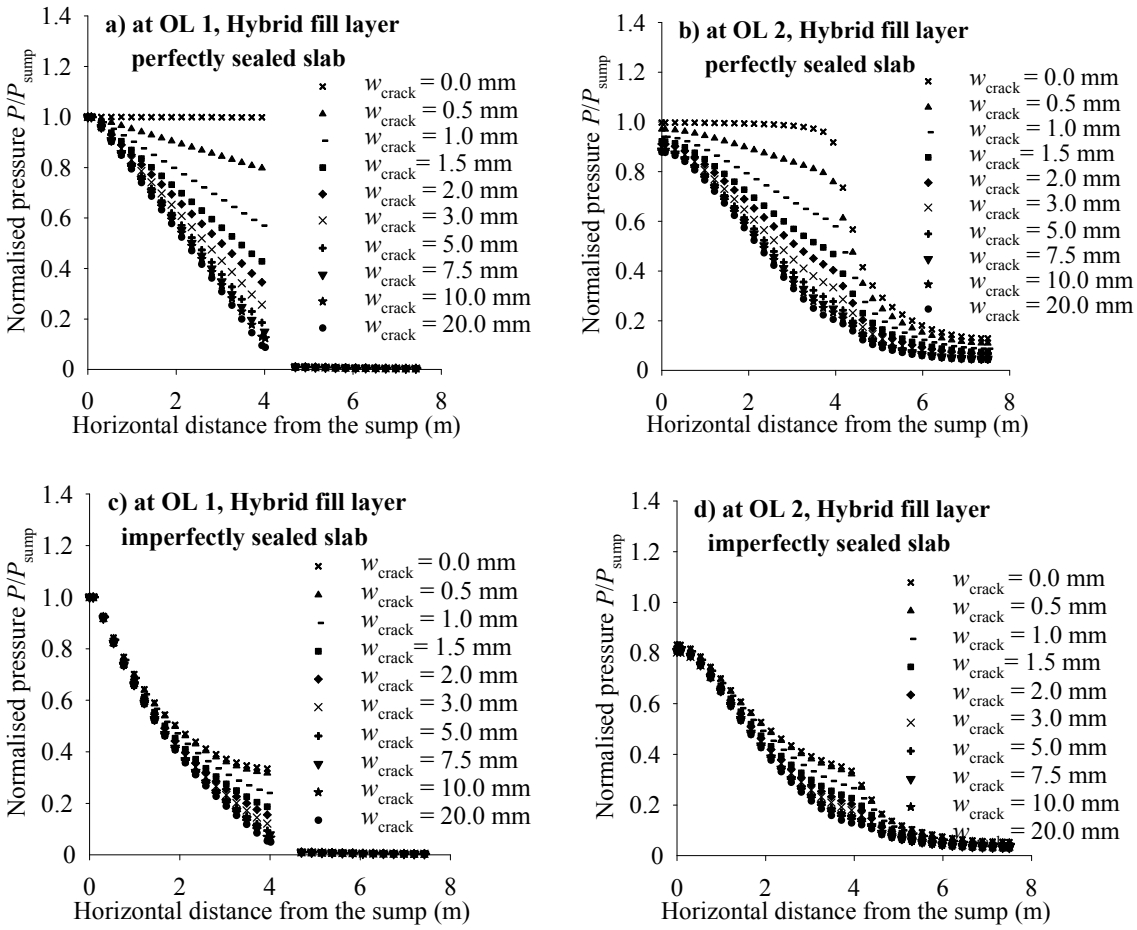

Figure 4.35. Effect of a wall crack on the sub-slab PFE for the Hybrid granular fill material layer (i.e. 0.2-m T2 Perm over 0.7-m T1 Struc) at observation lines OL1 (at the sump level) (a and c) and OL2 (at the footing level) (b and d) for a perfectly sealed slab (a and b) and an imperfectly sealed slab (c and d).

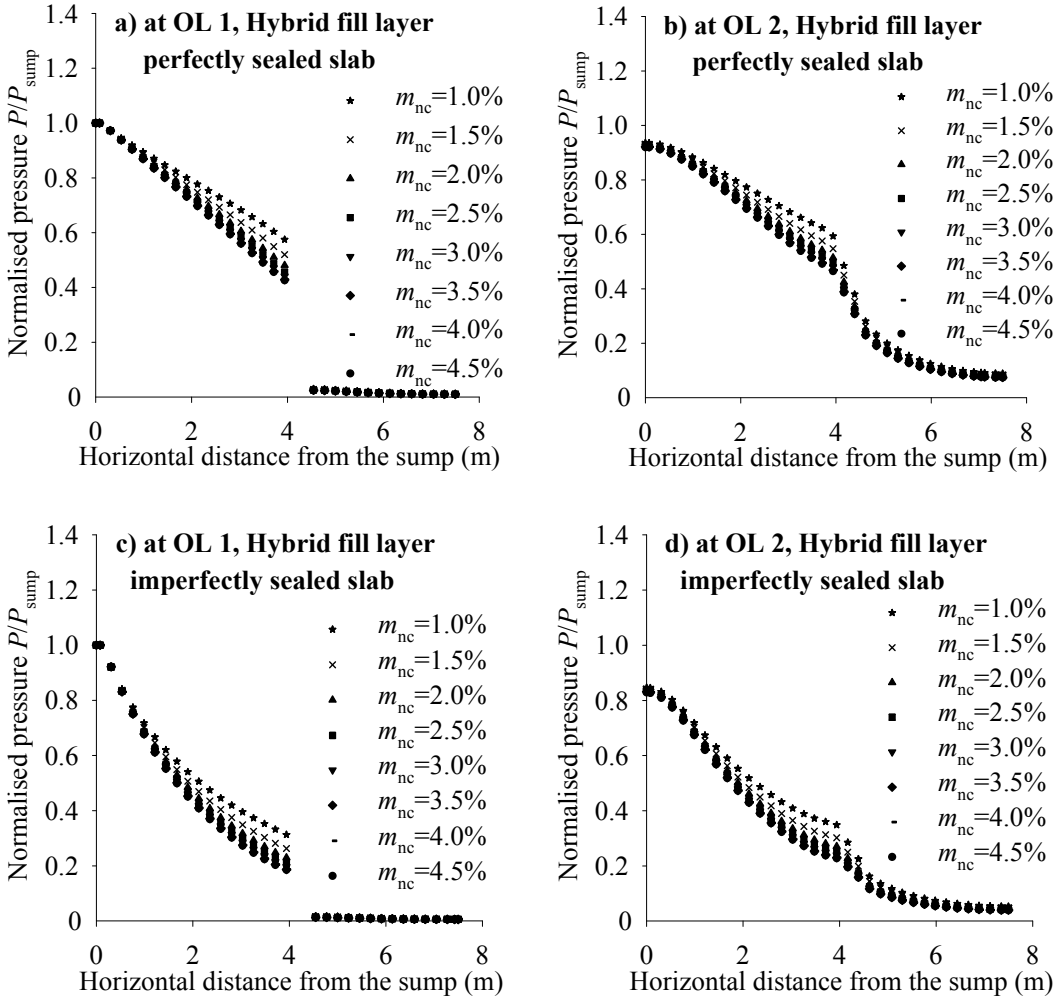

Figure 4.36. Effect of w_{nc} values of the T1 Struc granular fill material on the sub-slab PFE for the Hybrid granular fill layer at observation lines OL1 (at the sump level) (a and c) and OL2 (at the footing level) (b and d) for a perfectly sealed slab (a and b) and an imperfectly sealed slab (c and d).

Hybrid and T2 Perm granular fill material layers were examined. For the Hybrid case, $t_{T1Struc}$ and t_{T2Perm} were fixed at 0.7 m and 0.2 m, respectively. The w_{nc} value of T1 Struc was set at 4%, as it is expected to be in practice. Five k_{as} values were assigned for the soil with the ratio of $k_{ah(T2Perm)}/k_{as}$: 1, 10, 100, 1000 and 10,000. The wall crack was specified as w_{crack} = 1.5 mm.

The suction pressures developed at different k_{as} values are shown in Figure 4.39. For the SD system with the T2 Perm granular fill layer, the pressures were similar at $k_{ah(T2Perm)}/k_{as} \geq 100$ at the same horizontal distance along the two observations lines (i.e. at the sump and foundation levels). However, a significant reduction in pressure was observed at $k_{ah(T2Perm)}/k_{as} < 100$ for all cases. For example, at a horizontal distance of 4m from the sump centre, when $k_{ah(T2Perm)}/k_{as}$ = 100, the ratio P/P_{sump} was 0.75; this ratio reduced to 0.65 and 0.34 at $k_{ah(T2Perm)}/k_{as}$ = 10 and 1, respectively.

This significant reduction in suction pressure can be explained by a significant amount of airflow entering the granular fill layer from the ground surface outside the house when k_{as} is high, thus reducing the air resistance of the system (Figure 4.40b).

However, an insignificant reduction in pressure is obtained in the SD system with the Hybrid fill layer at the sump level (OL1) (Figure 4.39c), with a significant pressure loss found at the foundation level (OL2) (Figure 4.39d), at $k_{ah(T2Perm)}/k_{as} \leq 100$. These findings are supported by monitoring the airflow paths, as shown in Figure 4.40. For the T2 Perm fill layer with $k_{ah(T2Perm)}/k_{as}$ = 10,000, the airflow paths occur predominantly in the granular fill layer, whereas when $k_{ah(T2Perm)}/k_{as}$ = 1 these occur predominantly in both the fill layer and the granular soil. For the Hybrid fill layer with $k_{ah(T2Perm)}/k_{as}$ = 1, the airflow paths occur in both the soil and the fill layers, and a significant pressure loss

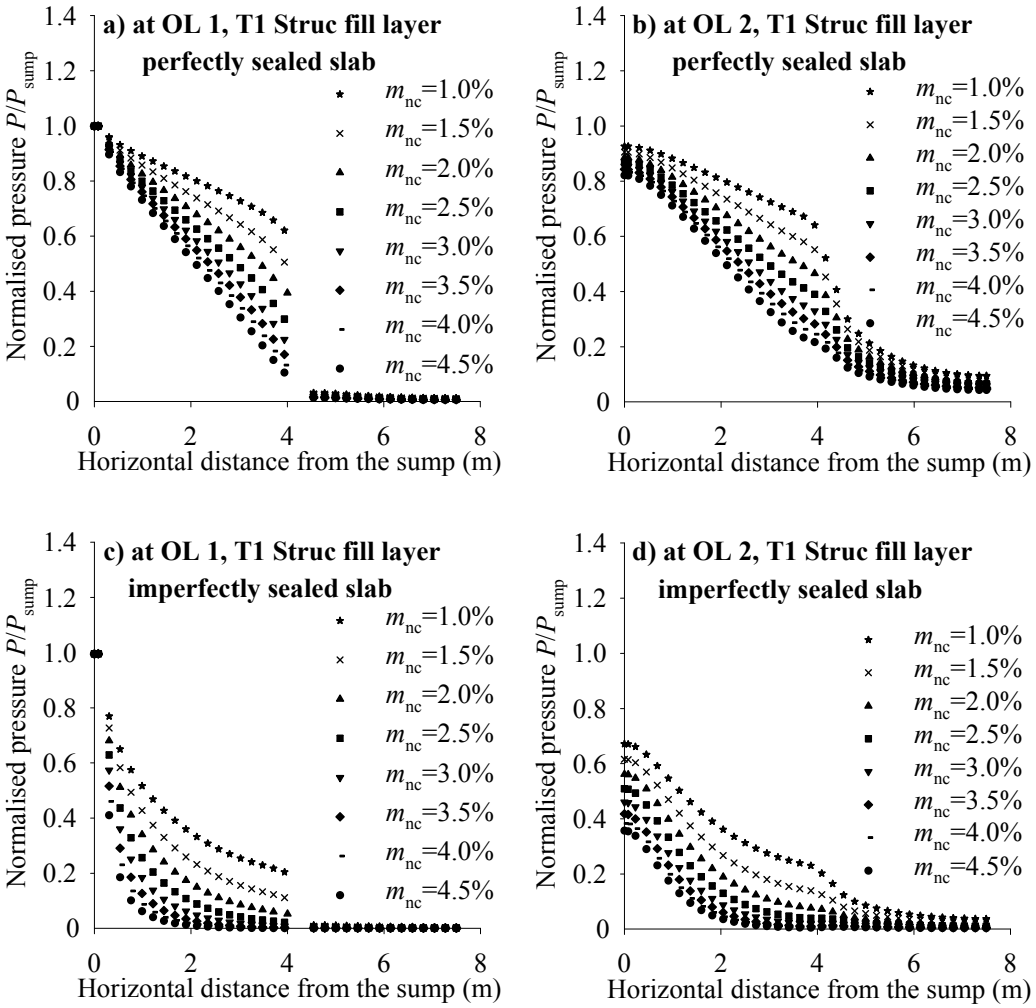

Figure 4.37. Effect of w_{nc} values of the T1 Struc granular fill material on the sub-slab PFE for the T1 Struc granular fill layer at observation lines OL1 (at the sump level) (a and c) and OL2 (at the footing level) (b and d) for a perfectly sealed slab (a and b) and an imperfectly sealed slab (c and d).

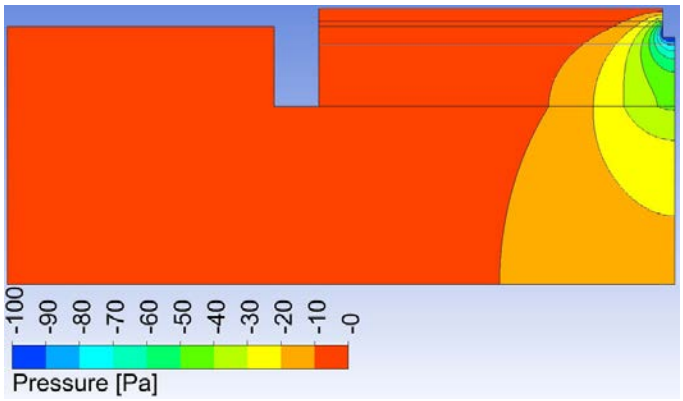

Figure 4.38. Example of the sub-slab PFE contours for $t_{T1Struc}$ = 0.9 m (w_{nc} = 4%) for an imperfectly sealed slab.

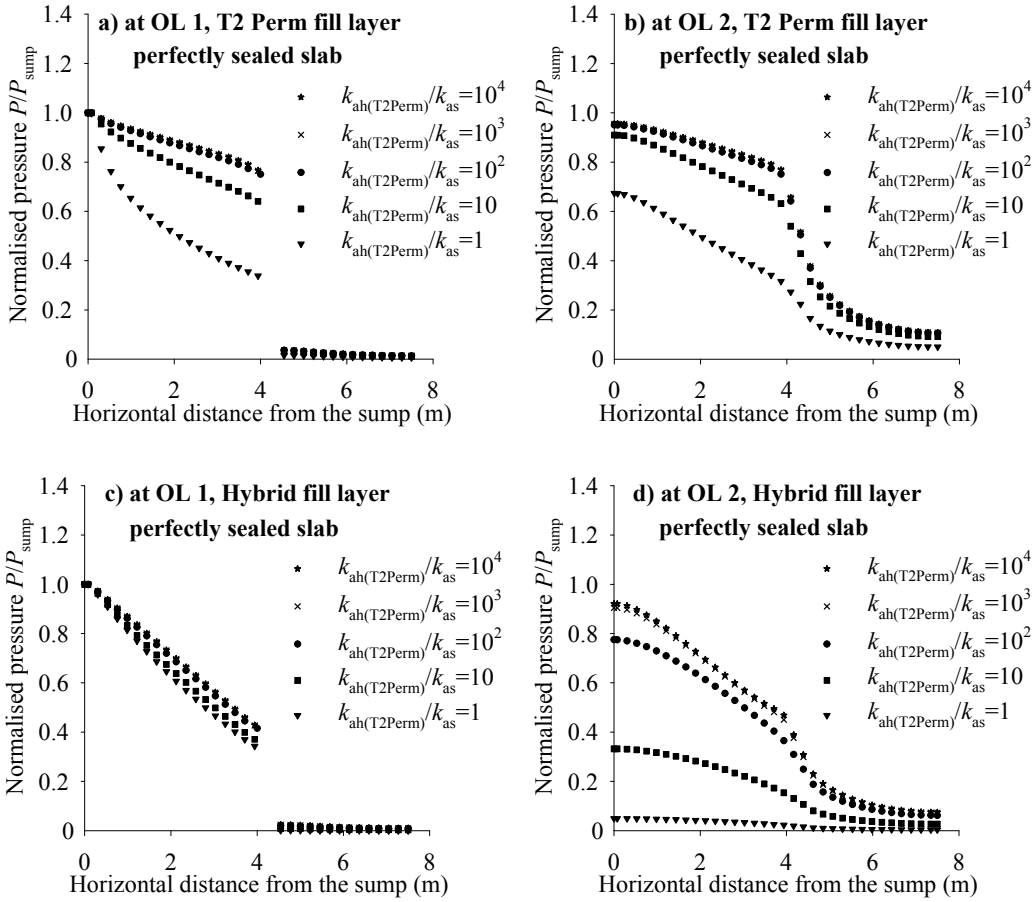

Figure 4.39. Effect of the air permeability of the soil on the sub-slab PFE at observation lines OL1 (at the sump level) (a and c) and OL2 (at the footing level) (b and d) for a perfectly sealed slab over the T2 Perm granular fill material (a and b) and the Hybrid granular fill material (c and d).

is observed in the soil, whereas good sub-slab PFE is maintained in the fill layer.

Thus, it is inferred that T1 Struc could work as a barrier layer to minimise pressure loss in the granular fill layer of a system because of the high k_{as}. Therefore, the Hybrid granular fill material might be preferred and the T1 Struc sub-layer should be well compacted at a high compaction degree (e.g. $w_{nc} \geq 4\%$) below the T2 Perm sub-layer, especially if the native soil has a high permeability degree in comparison with that of the T2 Perm material.

Effects of the variation in t_{T2Perm} and $t_{T1Struc}$

As discussed previously, the Hybrid granular fill layer might be preferred in some cases, for example when k_{as} is high or when soil improvement is required because of the presence of soft soil. Moreover, a greater thickness of the T2 Perm layer (t_{T2Perm}) induces better PFE when the granular fill layer is formed by the T2 Perm material, as discussed previously. Hence, it is expected that the same principle could be applied to the Hybrid granular fill layer.

According to Irish standard IS 888:2016 (NSAI, 2016a), the t_{T2Perm} value can vary from 0.2 m to 0.9 m. The selection of the t_{T2Perm} value will depend on the characteristics of the native soil and the requirements of the SD system. In this section, t_{T2Perm} was varied at 0 m, 0.2 m, 0.4 m, 0.6 m and 0.9 m, while maintaining the total thickness of the Hybrid granular layer ($t_{T2Perm} + t_{T1Struc}$) at 0.9 m. Both perfectly and imperfectly sealed slabs were examined. The w_{crack} value was set at 1.5 mm for all cases.

The simulation results are shown in Figure 4.41. The best suction pressure development was obtained for $t_{T2Perm} = 0.9$ m; $t_{T1Struc} = 0.9$ m induced the worst suction pressure as the T2 Perm material has a much higher k_{ah} than the T1 Struc material. In addition, as t_{T2Perm} becomes larger, this will allow the pressure gradient to develop deeper and wider in the fill layer. The pressure

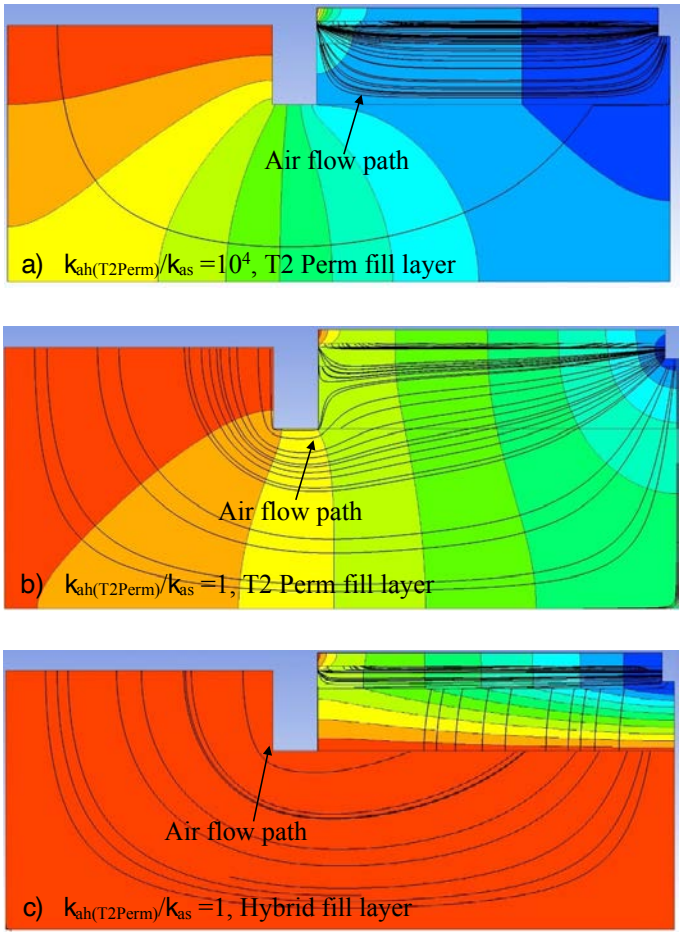

Figure 4.40. Examples of the airflow paths that develop in the granular fill layers at different air permeability values.

also increases significantly when t_{T2Perm} increases from 0.2 m to 0.4 m for all cases. Figure 4.41 suggests that the optimum thickness of the T2 Perm material is between 0.2 m and 0.6 m, depending on the actual design conditions, e.g. the foundation soil condition and the airtightness of the house. In addition, these results reconfirm that T1Struc is not an optimum material for the permeable layer of an SD system.

Effect of sump type and sump size

The suitability of different sump types has not been well documented. Furthermore, the sump size might also affect suction pressure development. Previous studies have used sumps of different sizes. For example, Abdelouhab (2011) used a sump made from a concrete block of approximately 0.5 m × 0.5 m × 0.5 m, with circular holes on each side of the block, whereas Vazquez *et al*. (2011) built a relatively large sump of conventional perforated bricks with dimensions of 1 m × 1 m × 0.5 m. In Ireland, plastic sumps with an octangular shape (see Figure 4.30) (effective area of 72,000 mm^2 and height of 124 mm) have been widely used. Therefore, it is also important to examine the effect of sump size.

Figure 4.42 shows the effects of the two types of sumps shown in Figure 4.20 on suction pressure development. A Hybrid granular fill layer with t_{T2Perm} = 0.2 m and $t_{T1Struc}$ = 0.7 m was considered, as this would allow any improvement in suction pressure from the sump to be monitored most easily. The w_{crack} value was set at 1.5 mm and both perfectly and imperfectly sealed slabs were investigated. As shown in Figure 4.42, the suction pressure is practically identical for both sump types. This means that both sump types on the Irish market are suitable for use in SD systems.

Figure 4.43 shows the effect of sump size on suction pressure development. The w_{sump} and d_{sump} values were investigated separately. To investigate the effect of sump width, the w_{sump} values were varied at 0.14 m,

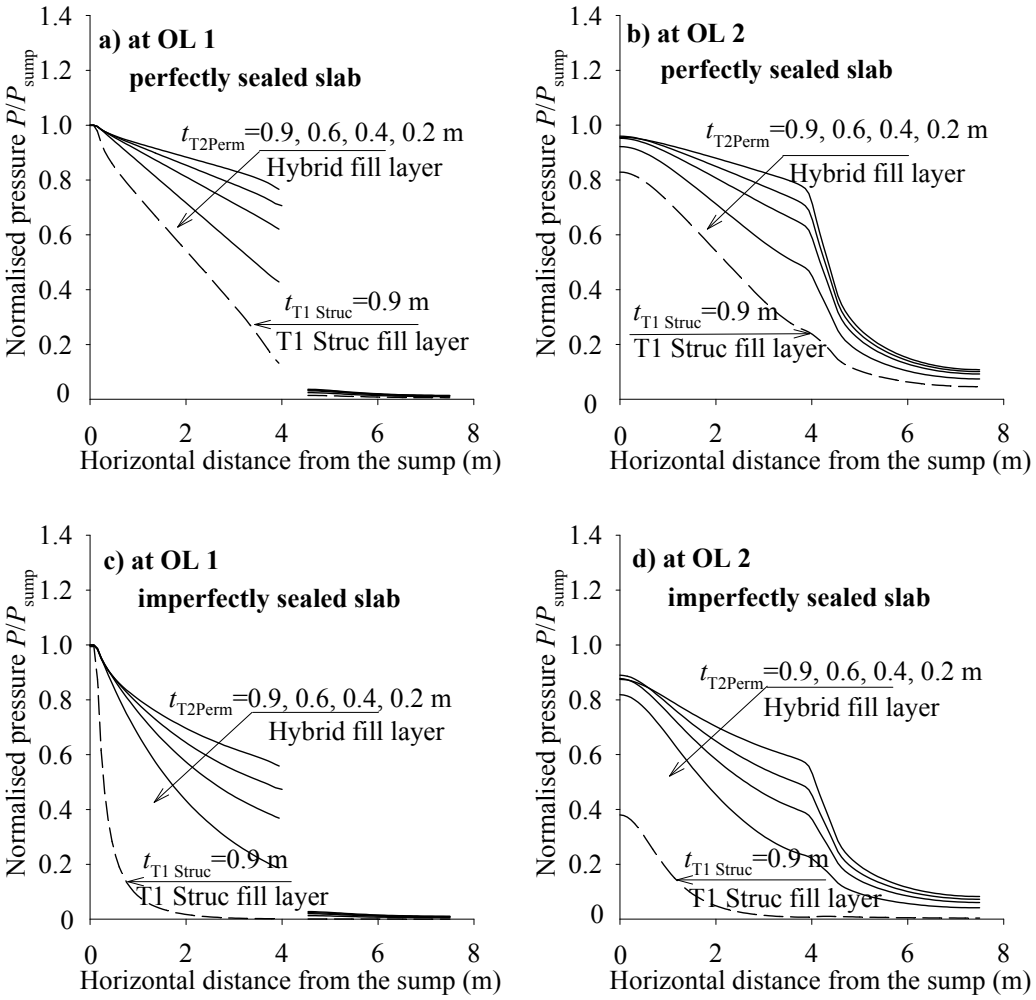

Figure 4.41. Variation in the sub-slab PFE at various values of t_{T2Perm} and $t_{T2Struc}$ at observation lines OL1 (at the sump level) (a and c) and OL2 (at the footing level) (b and d) for a perfectly sealed slab (a and b) and an imperfectly sealed slab (c and d).

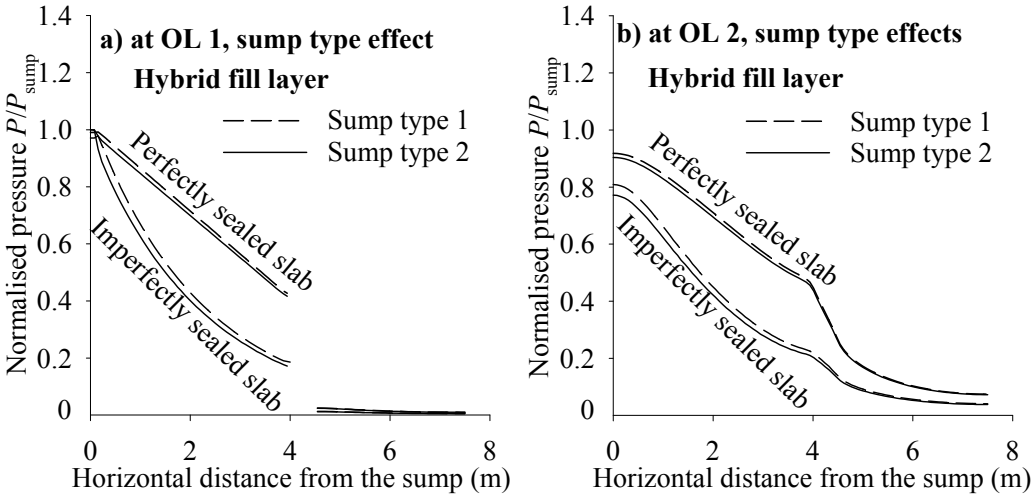

Figure 4.42. Effect of sump type on the sub-slab PFE at observation lines OL1 (at the sump level) (a) and OL2 (at the footing level) (b) for a perfectly sealed slab and an imperfectly sealed slab.

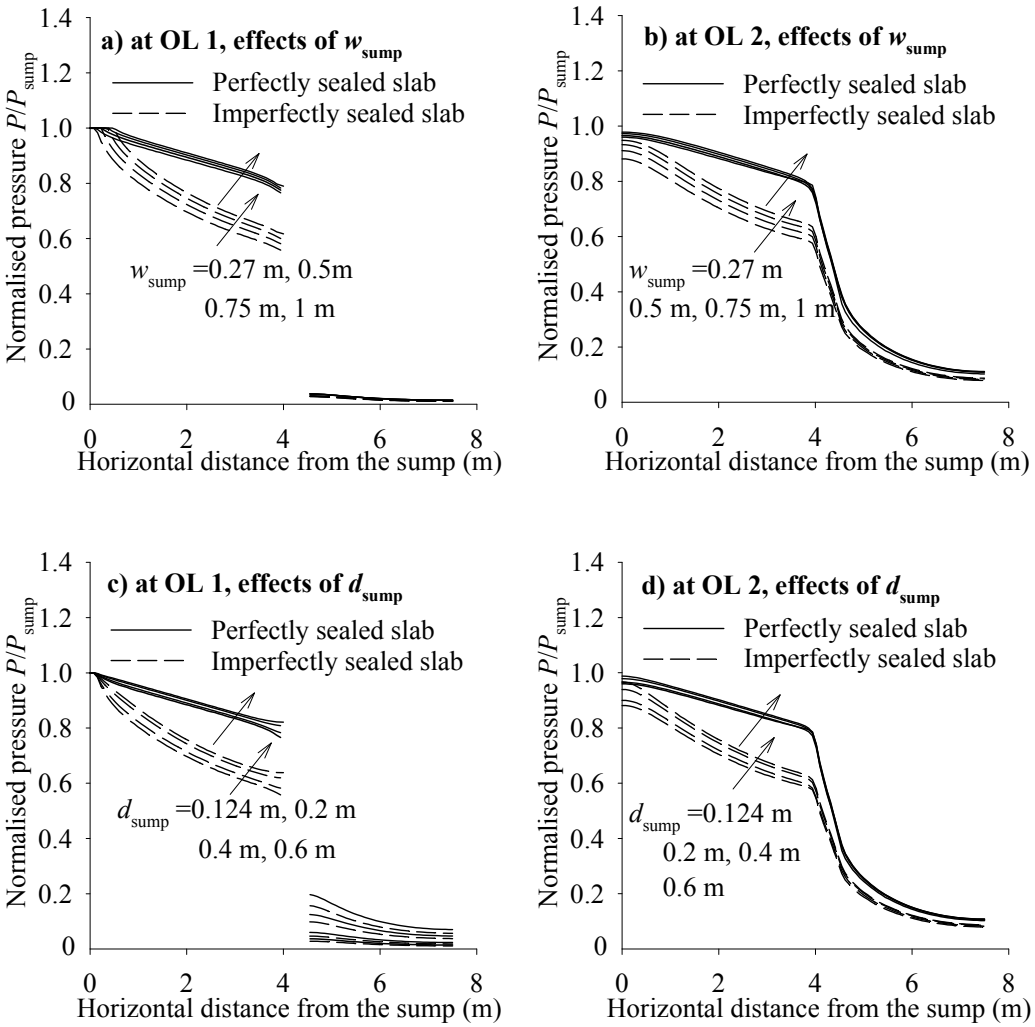

Figure 4.43. Effect of sump size on the sub-slab PFE for the T2 Perm granular fill material layer (t_{T2Perm} = 0.9 m) at observation lines OL1 (at the sump level) (a and c) and OL2 (at the footing level) (b and d).

0.27 m, 0.5 m, 0.75 m and 1 m, while maintaining d_{sump} at 0.124 m. Similarly, to investigate the effect of sump depth, the d_{sump} values were varied at 0.124 m, 0.2 m, 0.4 m and 0.6 m, while maintaining w_{sump} at 0.27 m. The suction pressure was found to slightly increase with an increase in w_{sump} and d_{sump}. This finding suggests that, at a specific sump pressure, the sump size does not affect the PFE significantly.

Effect of strip footing shape and dimension

In practice, different shapes of strip footings can be used, which might affect the suction pressure development of an SD system. The footing can be either partially embedded, with the top of the footing on the ground surface (Figure 4.44a), or fully embedded (Figure 4.44b). This section discusses the effects of footing shape and dimensions on the sub-slab PFE for four different cases:

Case 1 – partially embedded footing. The footing width and embedment depth are set at 0.5 m and 0.9 m, respectively, which are the same values as those analysed in the previous sections.

Case 2 – partially embedded footing. The footing width and embedment depth are set at 0.5 m and 0.4 m, respectively.

Case 3 – fully embedded footing. The footing width and embedment depth are set at 0.65 m and 0.4 m, respectively.

Case 4 – fully embedded footing. The footing width and embedment depth are set at 0.4 m and 0.4 m, respectively.

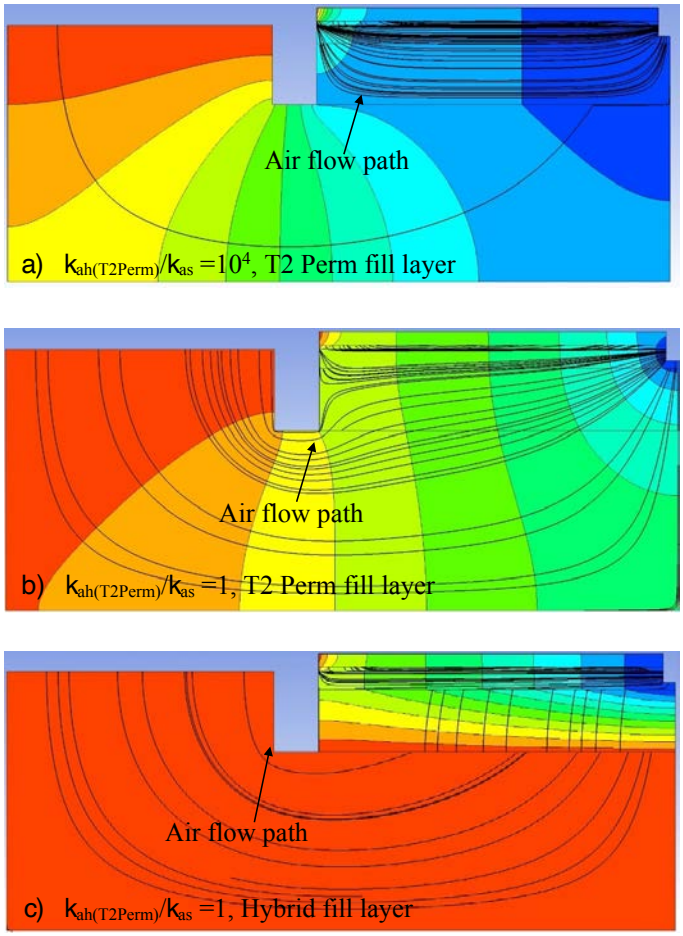

Figure 4.44. Pressure contour development for two strip footings with different shapes and dimensions. (a) Case 2: partially embedded footing with a footing width of 0.5 m and an embedment depth of 0.4 m. The footing for case 1 has the same shape and width but the embedment depth is 0.9 m. (b) Case 3: fully embedded footing with a footing width of 0.65 m and an embedment depth of 0.4 m. The footing for case 4 has the same shape and embedment depth but a width of 0.4 m. The pressure contours for cases 1 and 4 show a similar trend and thus are not presented here.

The footing thickness was fixed at 200 mm for cases 3 and 4 (DEHLG, 2012). The granular fill layer was formed with T2 Perm, with t_{T2Perm} = 0.4 m. A perfectly sealed slab and a w_{crack} of 1.5 mm were considered for all cases. Pressure contours obtained from cases 2 and 3 are presented in Figure 4.44 and the sub-slab PFE obtained at observation lines OL1 and OL2 are shown in Figure 4.45. As shown in the figures, the sub-slab PFE is similar within the slab area for all cases. For these cases, the shape and dimension of a strip footing do not have a significant influence on the effectiveness of an SD system.

4.3.3 Discussion

The CFD results presented in this section address the effect of different factors on the suction pressure development of an SD system. The impact level of each factor will depend on an actual practical situation. Previous studies have confirmed that the main entry mechanism of radon gas into buildings is convection, which is related to the pressure difference between the indoor air and the soil/granular fill layers beneath the floor slab (Collignan, 2018). In addition, the design of an SD system should focus mainly on decreasing the pressure in the permeable granular fill layers beneath the floor slab of buildings (Jiránek, 2014). Therefore, the air extraction ability of the permeable layer and the airtightness of the slab are two key issues.

The air extraction ability of a permeable granular fill layer is greatly influenced by its k_{ah}, n_h and d_{ef} values, whereas the airtightness of the slab strongly

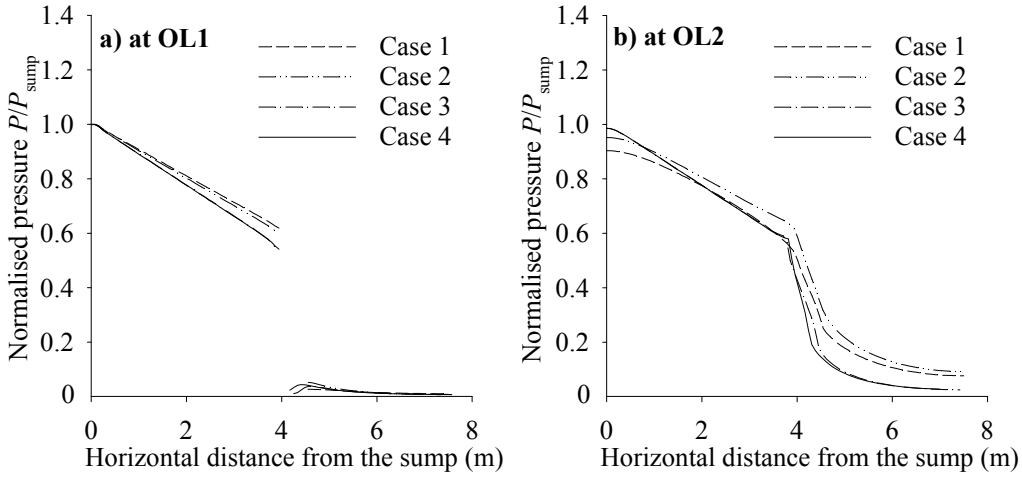

Figure 4.45. Pressure development for strip footings with different shapes and dimensions.

depends on the development of cracks and the air permeability of the native soil. Bonnefous *et al*. (1992) experimentally proved that, by carefully sealing the crack along the wall of a house, the sub-slab PFE in the permeable layer increased significantly. A similar observation was reported by Jiránek and Svoboda (2007), and Jiránek (2014). They showed that high suction pressure development was obtained in houses with good airtightness of the sub-slab. In addition, Jiránek and Svoboda (2007) also found that the ratio of k_{ah}/k_{as} is an important factor, with higher k_{ah}/k_{as} ratios inducing higher suction pressure development.

In buildings, the bearing layer beneath the foundation and the floor should be designed appropriately. This should include a good compaction process and the layer should be of a sufficient thickness to ensure that the bearing capacity and serviceability criteria are met; the granular fill material layers should also have a good degree of permeability beneath the floor and foundation. Therefore, the thickness of the granular layer is an important factor that should be addressed before any further action required in the design of the footing and the SD system for a building is taken.

This study investigated suction pressure development in specified granular fill materials incorporating a sump-based SD system only. Previous research has shown that suction pressure in an SD system can be generated using perforated drainage pipes instead of a radon sump (Jiránek and Svoboda, 2007; Jiránek, 2014). Further investigation is required to assess the performance of perforated pipe-based SD systems.

4.4 Results of the Monitoring Study at the Spanish Pilot House

4.4.1 Radon concentration behaviour in the pilot house

A long-term record of radon concentration fluctuations in the experimental house measured during the different testing phases is available. To understand the natural behaviour of the radon concentration inside the house, the closed testing periods, when no mitigation measures were in operation and the house remained closed with the exhaust pipes of the SD systems capped, were analysed.

Indoor radon levels in the experimental house depend on the radon source, the entry rate and the air exchange between the building and the outdoor air, all of which depend on many other variables and, especially, atmospheric conditions. The radon source is made up of the soil beneath and surrounding the house, which contains high radium levels. Therefore, it is expected that higher radon levels would be found in the basement, which is partially below-grade and in direct contact with the soil, than on the ground floor. An overview of the radon levels recorded is presented in Figure 4.46.

For the closed house conditions, average radon concentrations of 55 kBq/m^3 and 26 kBq/m^3 were found in the basement and on the ground floor, respectively. The average radon concentration values from the initial study conducted in 2006 were 40 kBq/m^3 for the basement and 7 kBq/m^3 for the ground floor. These values were obtained from a 3-month measurement period (January–April) in which the experimental

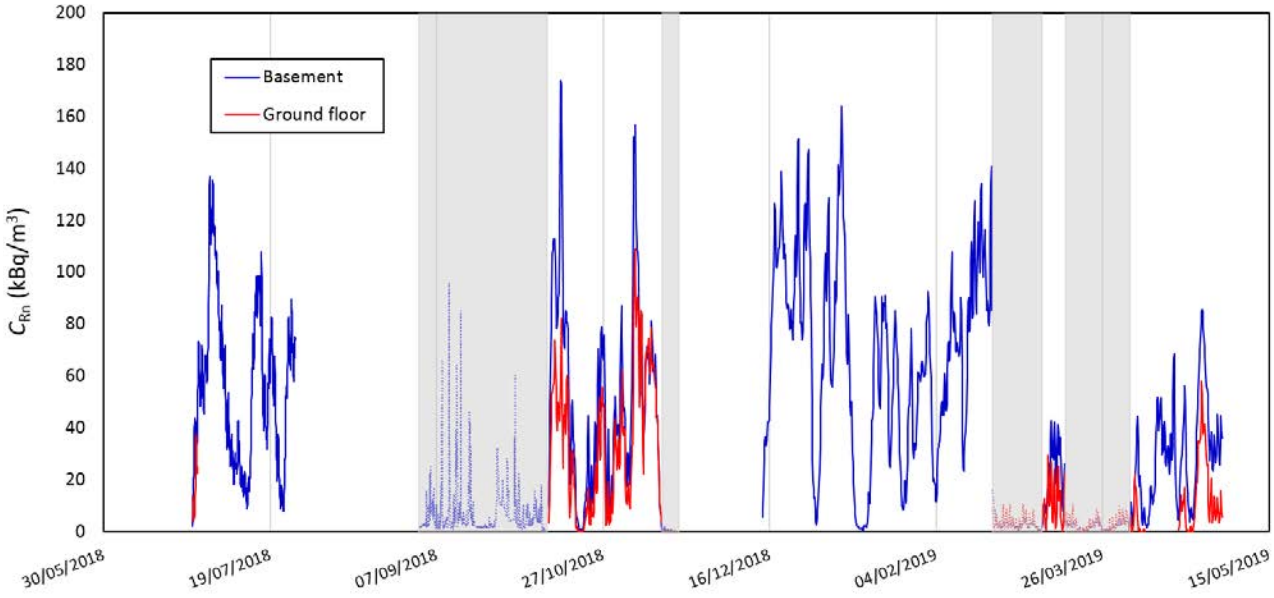

Figure 4.46. Radon concentrations recorded in the basement and on the ground floor of the pilot house. The solid lines indicate the closed testing periods and the dashed lines (shaded areas) indicate the periods of SD performance.

house remained closed, before the installation of any mitigation measures (Vazquez *et al.*, 2011). The difference in concentrations may be related to the deterioration of the basement slab associated with thermal dilation or other analogous phenomena, therefore leading to the formation of new cracks or radon pathways.

The concentration ratio between the floors found for the closed house testing configuration is approximately 2, which means that the concentration recorded in the basement is approximately double the concentration recorded on the ground floor. This result is as expected, as the basement is in direct contact with the soil and the main radon gas entry route is through gaps or cracks in the foundation; the radon on the ground floor comes from the radon in the basement. Infiltration through the main door and the windows could be considered as a source of radon gas, but the outdoor air radon concentration at the site is much lower, at approximately 300 Bq/m^3. Assuming that radon on the ground floor comes only from the basement, the lower radon concentration on the ground floor is explained by radioactive decay and the exchange of outdoor air through infiltration.

Radon behaviour and atmospheric parameters

Fluctuations in radon concentrations are daily and seasonal and are related to atmospheric conditions and air exchange between the building and the outdoor air. There is also a seasonal component related to outdoor temperature changes and the associated atmospheric pressure variations that directly affects radon entry into the building (Nero *et al.*, 1990; Scivyer and Jaggs, 1998). The air exchange rate in the experimental house reached its minimum value during the closed testing periods, as there is no ventilation mechanism. The radon levels in the house depend on the atmospheric conditions, which determine the soil gas pressure-driven flow from the ground into the building.

Multiple atmospheric conditions influence radon concentrations and it is possible to find correlations between the trends in radon concentrations and atmospheric variables (Schubert *et al.*, 2018; Garcia-Tobar, 2019). The radon concentration trends as a function of the different atmospheric parameters recorded were analysed for the closed testing periods. Selected measurement periods when statistically significant correlations were found between the atmospheric variables and radon levels in the pilot house are presented in Figure 4.47.

According to theory, pressure variation inside a dwelling is almost simultaneous with atmospheric pressure changes, but pressure changes in the soil pores beneath the building reach the atmospheric pressure values with a time delay that depends on

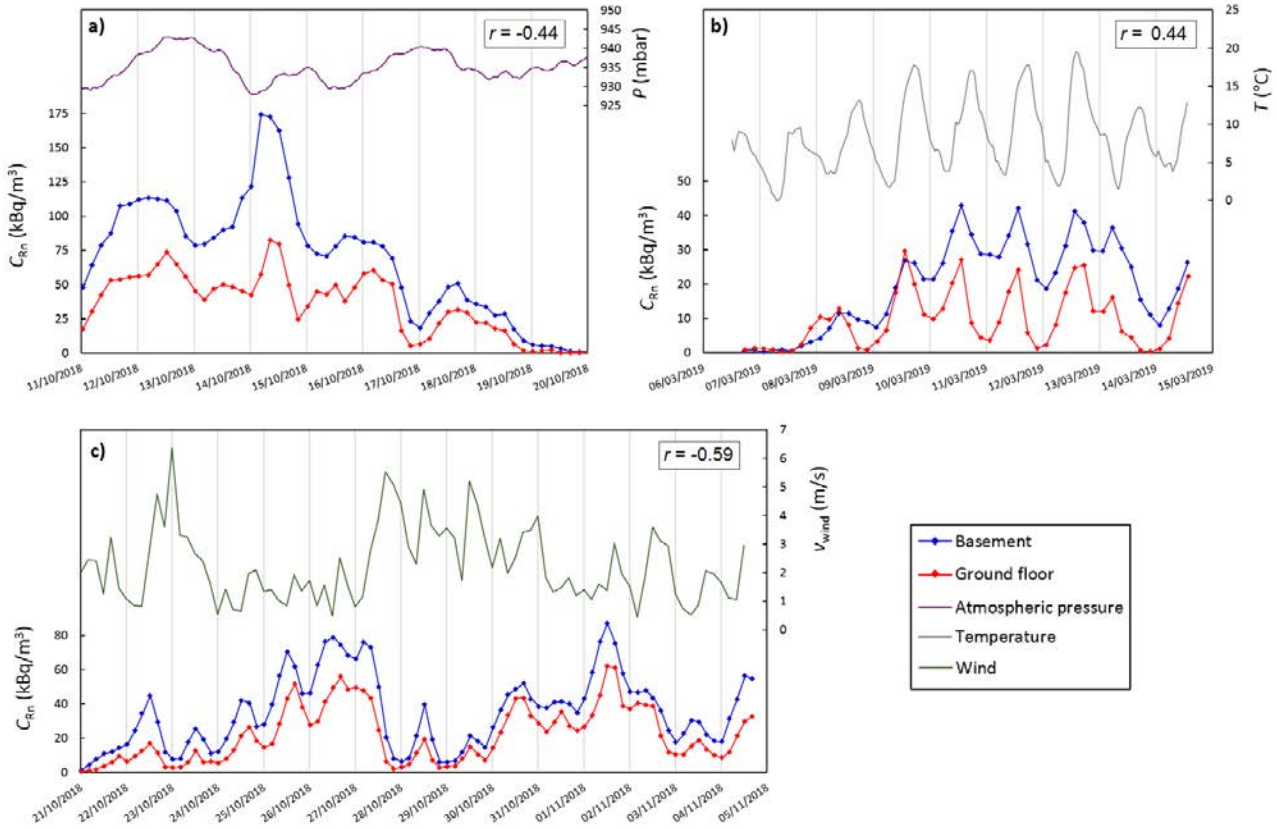

Figure 4.47. Radon concentrations recorded in the basement and on the ground floor of the pilot house and (a) atmospheric pressure, (b) outdoor temperature and (c) wind velocity for different time periods when the house was closed. Pearson's correlation coefficients between the radon concentration in the basement and the corresponding atmospheric variable are indicated.

the soil characteristics (e.g. porosity). Therefore, a pressure gradient is generated between the soil and the inside of the building that leads to an increase in soil gas airflow into the building (Frutos, 2009). From the analysis of the experimental data recorded, a negative correlation was found between the atmospheric pressure and radon levels, which is consistent with results from other investigations (Mentes and Eper-Papao, 2015). Figure 4.47a depicts the radon concentration decreasing with a time delay with the increase in atmospheric pressure. The Pearson's correlation coefficient for this case was $r = -0.44$ at a 95% confidence level.

A positive correlation between outdoor temperature and radon concentration was found only at a daily scale, agreeing with the results of previous studies (Mentes and Eper-Papao, 2015; Schubert *et al*., 2018). A Pearson's correlation coefficient of $r = 0.44$ at a 95% confidence level was obtained. A negative correlation between the radon concentration and wind velocity was found – as wind velocity increases, the radon level decreases – as observed in Figure 4.47c. For this case, the Pearson's correlation coefficient was $r = -0.59$ at a 95% confidence level. This result is also consistent with the previously published results (Riley *et al*., 1996; Schubert *et al*., 2018). No significant correlation with radon levels was found for the other two atmospheric parameters monitored in the study: relative humidity percentage and accumulated rain.

Looking at diurnal radon fluctuations, apart from the difference in the radon concentrations between the basement and the ground floor, it was found that radon concentration records in the basement and ground floor are temporally shifted from one to the other in some cases. An example can be seen in Figure 4.47c, where the peaks are slightly shifted in both radon concentration curves. Considering the concentration in the basement as a reference, this can be explained by the fact that the radon in the ground floor comes from the basement and the exchange between floors takes a few hours, causing a time delay in changes in the radon concentration.

4.4.2 Soil depressurisation effectiveness analysis

Pressure field extension

The pressure distribution under the pilot house was studied for different depressurisations induced at the central sump of the SD system, by both active and passive performance of the system. Prior to the depressurisation analysis, it was found that the pressure difference between the indoor air and the measurement points under the slab fluctuates around 0 Pa for the closed testing periods when no SD is in operation. During the passive SD testing period, the pressure induced under the slab as a consequence of the wind force reached levels of −20 Pa; an example of the passive depressurisation in relation to the wind velocity is shown in Figure 4.48.

The analysis of the pressure data recorded under the slab for the different testing phases at distances (*d*) of 1, 2 and 2.4 m from the suction point, using the centre of the sump as the reference, enabled the rate of pressure drop with distance across the slab to be determined, which is also related to the depressurisation generated (Figure 4.49).

Figure 4.49 shows that the pressure drop with distance is consistent for measurements recorded at distances (*d*) of 1, 2 and 2.4 m from the suction point. The trend in pressure drop with distance has a linear dependence on the depressurisation under the slab; therefore, the lower the pressure induced under the slab, the higher the pressure drop with distance. However, a quite homogeneous PFE was found, which did not exceed a 1 Pa/m pressure drop rate with distance for the highest depressurisation tested, induced by the highest extraction airflow rate permitted by the fan during the active SD operation.

The results for pressure induced under the slab are presented in Figure 4.50 as a function of the extraction velocity in the exhaust pipe (for the active SD operation, generated by means of the mechanical fan; Figure 4.50a), and the wind velocity (for the passive SD operation, generated by means of a rotating cowl; Figure 4.50b).

Results from the passive SD operation show a lower depressurisation induced at the sump by the wind velocity than the depressurisation generated as a result of the active SD operation using a mechanical fan. The highest depressurisation under the slab recorded during the passive SD operation, induced by the wind force using a rotating cowl, was −22 Pa, corresponding to wind velocities of up to 8 m/s. However, the highest depressurisation recorded under

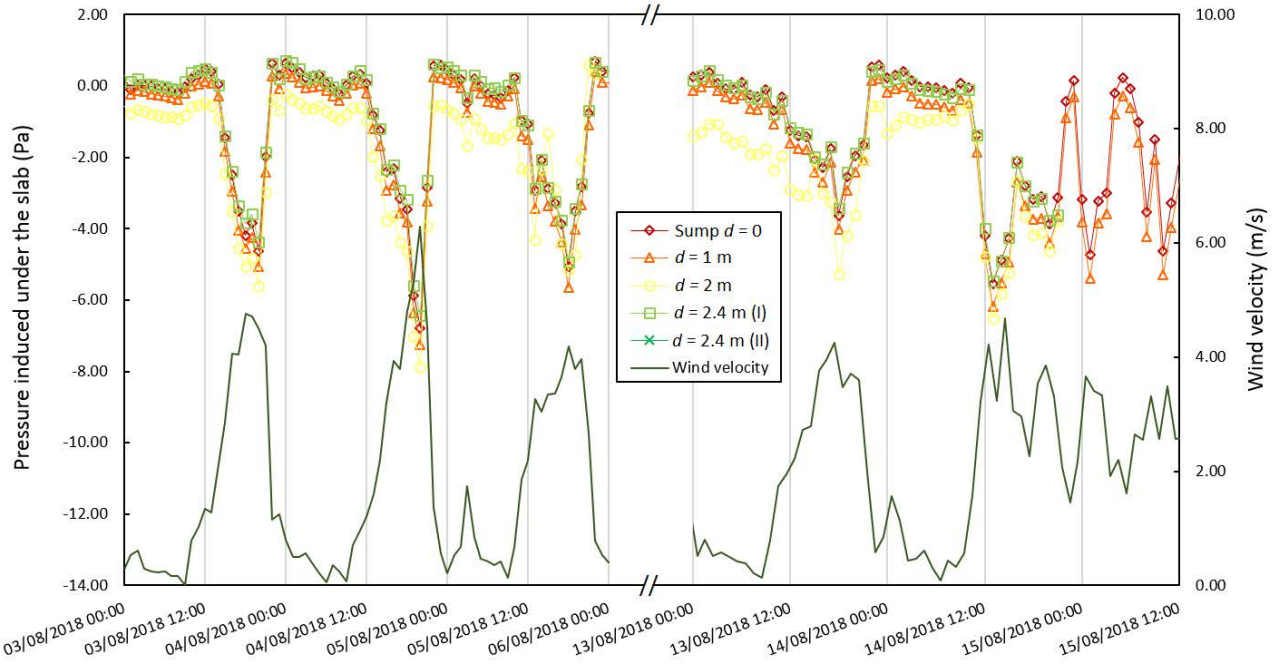

Figure 4.48. Hourly averaged pressure induced under the slab at the sump and the different measurement points, with distances indicated from the central pipe, and the hourly averaged wind velocity recorded at the site.

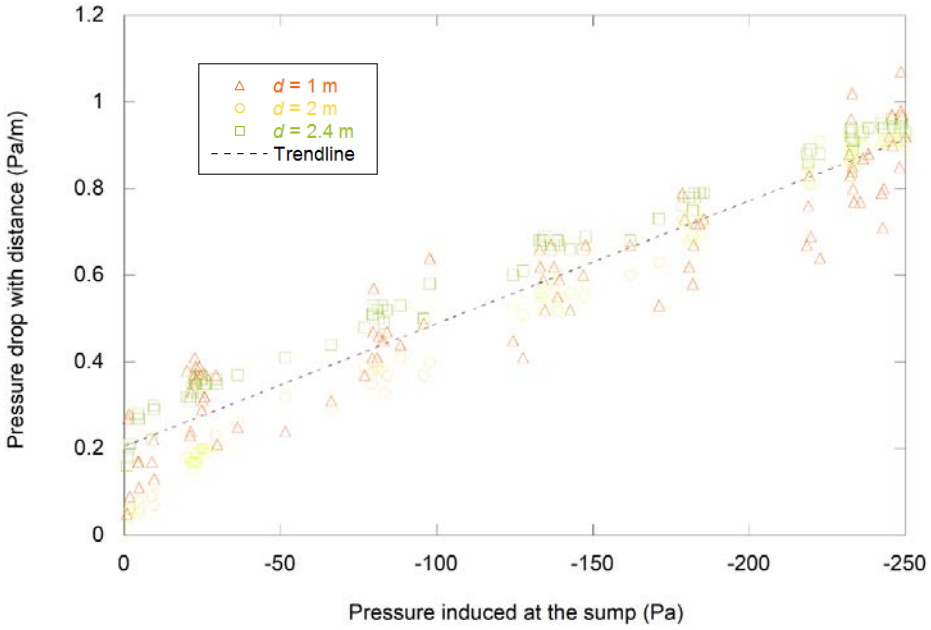

Figure 4.49. Pressure drop with distance plotted against pressure induced at the sump. The experimental data obtained from pressure records at distances (*d*) of 1, 2 and 2.4 m from the sump are shown, both for the active and the passive SD testing phases. The dashed line is the linear trend obtained from all of the experimental data, with a coefficient of determination (R^2) of 0.95.

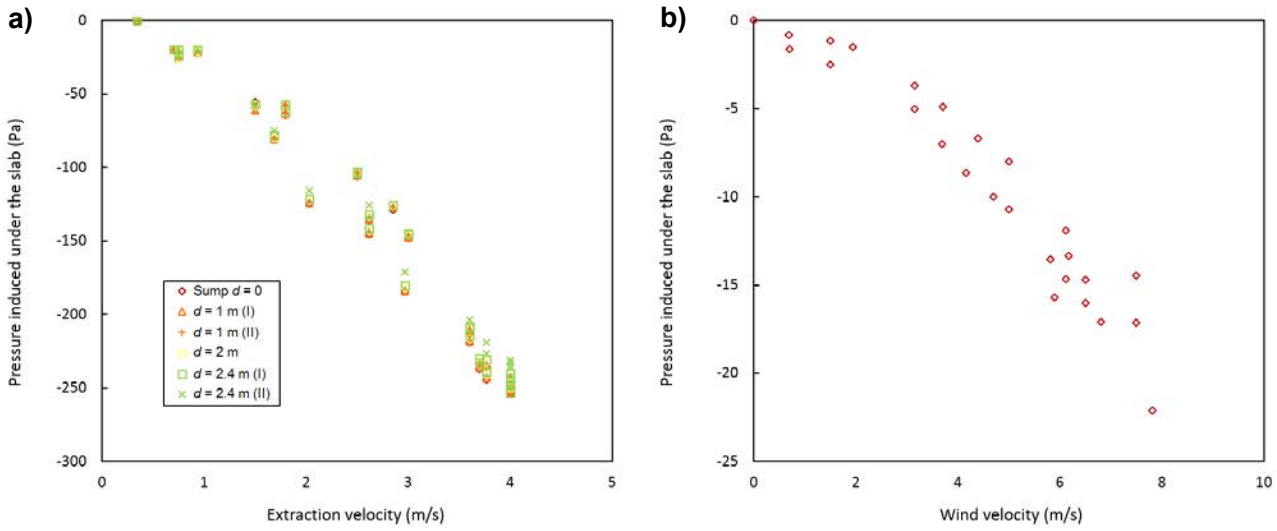

Figure 4.50. (a) Pressure induced under the slab plotted against the extraction velocity of the mechanical fan measured at different distances from the suction point. (b) Pressure induced at the sump under the slab plotted against wind velocity.

the slab during the active SD operation was around −250 Pa, induced by the highest extraction airflow rate of the mechanical fan, equivalent to 4 m/s.

As mentioned previously, Abdelouhab *et al*. (2010) conducted a similar study in France at the MARIA experimental house, built with a 40-cm-thick aggregate layer beneath the slab and two sumps, one centred and another decentred, placed on the aggregate layer. They deduced two behaviour laws to relate the extraction airflow, *Q*, to the pressure difference, *ΔP*, induced between the aggregate layer and the inhabited volume for the natural and mechanical extraction (Figure 4.51). A similar behaviour law can be obtained from the active SD experimental data from the monitoring study at the pilot house (Figure 4.51), but in this case it is clear that the extraction airflow

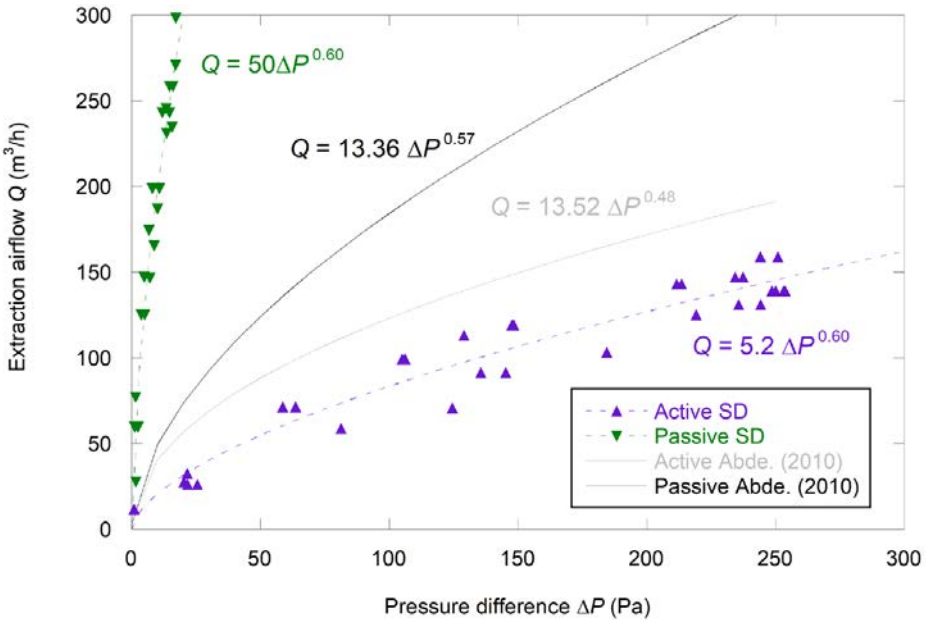

Figure 4.51. Extraction airflow through the central exhaust pipe as a function of the pressure difference *ΔP* generated between the aggregate layer under the slab and the inhabited volume of the basement. Triangles represent the experimental data for the active SD (purple) and passive SD (green) operations, the dashed lines are the trends obtained from the experimental data and the solid lines represent the laws relating extraction airflow to depressurisation for active and passive SD from Abdelouhab *et al.* (2010).

needed to generate the same pressure difference is lower than in the MARIA house.

Figure 4.51 shows that the behaviour law differs for the active and passive SD operations in Abdelouhab *et al*. (2010), which agrees with the experimental results found here, although, in the pilot house, the behaviour of active SD and the behaviour of passive SD are significantly different.

According to the results, the permeability characterisation of the aggregate layer under the slab is different for active and passive SD. However, it should be taken into account that the extraction airflow rate during active SD was measured in the exhaust pipe right under the mechanical fan with a hot wire anemometer, whereas, for passive SD, the wind velocity was recorded by a weather station on the experimental house rooftop and it can differ from the effective extraction airflow at the exhaust pipe.

A comparison between the experimental results from the monitoring study at the pilot house and the results from phase 2 is shown in Figure 4.52. The results presented are for T2 Perm, as the evidence from the characterisation of the Spanish granular fill materials is that standard Spanish granular fill materials are similar to the Irish T2 Perm material. For extraction airflow rates below 100 m³/h, the experimental data for passive SD testing at the pilot house match the results from phase 2 (Figure 4.16b).This means that the permeability characterisation of the aggregate layer under the slab in the pilot house, based on the passive SD testing results, is similar to that of a layer of 30–60 cm of Irish T2 Perm aggregate material. This result also agrees with the outcomes from the phase 1 benchmarking of granular fill materials in the European context.

Radon reductions

The radon reductions obtained for the different testing phases are summarised in Table A2.6 relative to the average radon concentration in the basement and on the ground floor calculated during the closed testing phases. It should be emphasised that the outdoor radon concentration in the area surrounding the pilot house is very high, at approximately 300 Bq/m³, whereas the average outdoor radon concentration globally is between 5 and 15 Bq/m³ (WHO, 2016).

In all cases the radon reductions obtained were over 85%, with the highest reduction found for testing

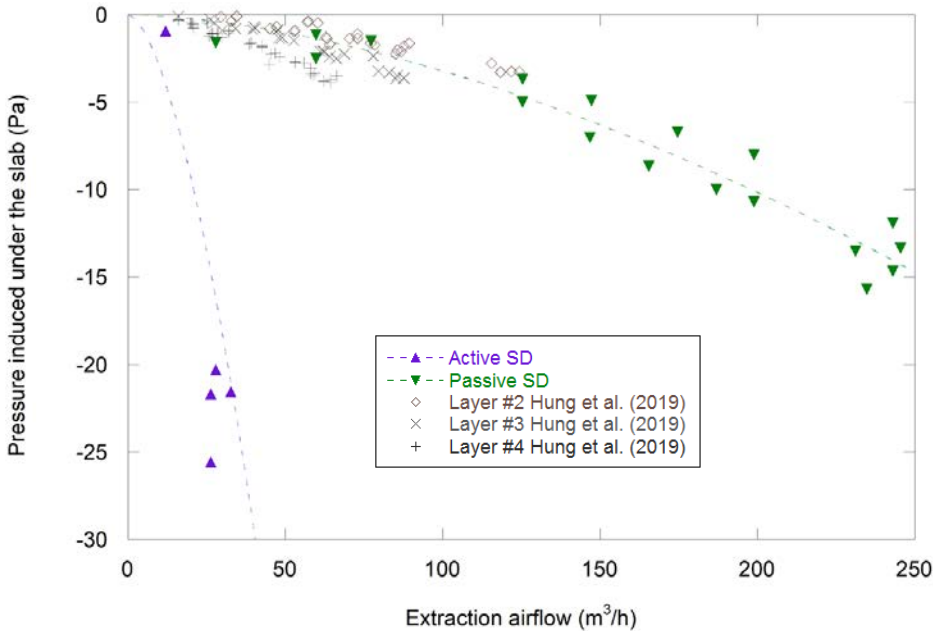

Figure 4.52. Pressure induced under the slab plotted against the extraction airflow through the central exhaust pipe, and the results from phase 2 for the pressure difference obtained through different layers of T2 Perm aggregate material as a function of the extraction airflow (Figure 4.16b). Triangles represent the experimental data for active SD (purple) and passive SD (green); the results from phase 2 are indicated in grey. The dashed lines are the trends obtained for the experimental data.

phase 4, in which the radon concentration on the ground floor was 328 Bq/m^3, which is comparable to the outdoor radon concentration at the site, and the radon concentration in the basement was 662 Bq/m^3. The mechanical fan was tested during phase 4, with the extraction airflow varied up to the highest power permitted (80 W).

From the phase 6 experimental results it can be highlighted that a 30-W mechanical fan, which is equivalent to the power used for the extraction airflow during testing in phase 6, is sufficient to produce radon reductions of up to 94% in the basement and 86% on the ground floor in a house of these permeability characteristics. In terms of pressure induced under the slab, the average value at the sump recorded for testing phase 6 was −55 Pa.

Although it depends on the atmospheric conditions (mainly wind and temperature) and occupant behaviour, the typical pressure difference found between the indoors and the soil in a dwelling oscillates between 0 and 5 Pa. Therefore, the depressurisation system should be designed to induce a pressure of at least −6 Pa in every point of the slab area (Fowler *et al.*, 1991; Broadhead, 2018; Dumais, 2018). Looking at Figure 4.50a, it can be observed that such a pressure is obtained for extraction velocities below 1 m/s, which corresponds to the speed at which the mechanical fan is operating at 20-W power. Therefore, a 20-W mechanical fan is sufficient to achieve an optimum SD providing radon reductions above 85% for dwellings with similar permeability characteristics to those of the experimental house studied here.

5 Conclusions

The main findings of this study, based on the results of the experimental tests and numerical simulations, are summarised in the following sections.

5.1 Main Findings from Phase 1

- According to the sieve analysis results, the T1 Struc and T2 Perm materials can be classified as well-graded and poorly graded granular fill materials, respectively. The effective particle diameter d_{ef} required for CFD simulations can be taken from the grading curve as the d_{50} for T2 Perm. However, the d_{ef} of T1 Struc varies according to the compaction degree. In addition, compaction test results showed that T1 Struc is relatively easier to compact than T2 Perm. The optimum w_{nc} value of T1 Struc is approximately 5.75%, whereas that of T2 Perm is unclear.
- A test apparatus was developed to measure the k_{ah} and n_h values of the granular fill materials under compaction. It was observed that the k_{ah} and n_h values of T1 Struc decrease with increase in w_{nc}, whereas those of T2 Perm are relatively independent.
- The investigation procedures developed in this study can be adopted to characterise other granular fill materials. The results presented in this study apply to the conditions considered in this study only. However, the results might apply to other granular fill materials that have similar characteristics to those of T1 Struc and T2 Perm.
- From the benchmark study of the Spanish granular fill materials, it was found that garbancillo 4/12 and gravel 4/20 can be classified as poorly graded granular fill materials, similar to the Irish T2 Perm material. The Spanish granular fill materials studied have a similar particle size distribution to those of the Irish T2 Perm and the British standard 20-mm graded and 40-mm graded materials. In addition, in the gas permeability tests (uncompacted), similar trends were found for the Spanish samples and the British (i.e. 20-mm graded and 40-mm graded) granular fill materials, with similar gas permeability values of approximately 9×10^{-8} m^2. Considering the similarities between the Spanish granular fill materials tested and the Irish T2 Perm standard, it can be assumed that the results for Irish T2 Perm are applicable to the Spanish standards analysed.

5.2 Main Findings from Phase 2

- A series of large-scale experimental tests was performed in this study to examine and validate the field compaction degree and design parameters (i.e. k_{ah} and n_h) of the T1 Struc and T2 Perm granular materials for SD systems used in Ireland.
- A large-scale test tank was developed to measure the field compaction degree and k_{ah} and n_h values of the materials. The compaction degree of the materials was observed to be higher when using the field compactor than when using the standardised small-scale compactor.
- The k_{ah} values of the materials decreased with increase in their compacted thickness. The n_h values were observed to be similar for all compacted layers. In addition, the n_h values of T2 Perm were found to be smaller than those reported by Hung *et al*. (2018a,b) in phase 1, whereas those of the T1 Struc material were similar.
- Test results showed that the rotating cowls performed better than the static cowls. However, the pipe with a cap cowl might be considered to be a reliable cowl for a passive SD system because of the absence of mechanical parts that could degrade over time.

5.3 Main Findings from the Computational Fluid Dynamics Simulations

- The k_{ah}, n_h and d_{ef} values were confirmed to be the three key parameters of the granular fill material for the CFD simulations. CFD simulations with transient analysis obeying the RANS realisable k–ω turbulence model are reliable in the design of SD systems with T1 Struc and T2 Perm granular fill materials. These parameters can be determined using the graphs, proposed equations or data (see Table A2.2) reported in this study.

- A series of transient CFD simulations was conducted to investigate the behaviour of the PFE of SD systems for radon mitigation. The results showed that the wall crack and airtightness of the concrete slab of the house affected the sub-slab PFE significantly. Good sub-slab PFEs were observed if the granular fill layers were formed from the T2 Perm material.
- The T1 Struc fill layer induces poor sub-slab PFEs. This suggests that the T1 Struc material is not optimal for use as the permeable layer of an SD system. The compaction moisture content (w_{nc}) of the T1 Struc material does not affect the sub-slab PFEs of the Hybrid granular fill layer, which contains T2 Perm on top of T1 Struc, and the T1 Struc sub-layer might work as a barrier layer to prevent pressure loss of the system.
- The thickness of the T2 Perm layer (t_{T2Perm}) plays an important role in the sub-slab PFE. The pressures increase with increase in the t_{T2Perm}. In addition, soil with a high air permeability (k_{as}) will induce a poor sub-slab PFE for an SD system. In this case, a design approach might be considered by using the Hybrid granular fill layers with a T1 Struc material having a high compaction moisture content, e.g. $w_{nc} \geq 4\%$, to improve the sub-slab PFE.
- At a specified pump suction pressure (P_{sump}), the sump type and sump size do not significantly affect the sub-slab PFE of the SD system. However, selection of sump types might be based on practical experience, as well as on the individual design conditions.
- The results presented in this study apply to the conditions considered in the study, i.e. they are based on the design parameters for the T1 Struc and T2 Perm granular materials in Ireland. However, the results might be adopted to analyse the sub-slab PFE of SD systems formed with different permeable granular materials. For a proper design, it is suggested that a suitable k_{ah}/k_{as} ratio should vary between 10^2 and 10^4, and the air permeability of the permeable layer should fall in the range from 10^{-8} to 10^{-9} m^2.
- Finally, the results reported in this study were obtained from two-dimensional CFD simulations, which did not consider a number of complexities, e.g. the effects of slab shape, wall corners, sump shape, the limited area of the house and the limited granular material types analysed.

5.4 Main Findings from the Monitoring Study at the Spanish Pilot House

- The radon concentration behaviour at the Spanish pilot house was analysed under closed, no SD operation conditions. An average radon concentration of 55 kBq/m^3 was found in the basement, whereas the ground floor had an average radon concentration of 26 kBq/m^3. The influence of atmospheric variables on the radon behaviour in the house was also studied, with significant negative correlations found between atmospheric pressure and wind velocity and the radon concentration in the house, and a positive correlation found with temperature.
- The analysis of the pressure distribution under the slab showed that the pressure drop with distance from the suction point of the SD system varies linearly with the depressurisation generated under the slab. It was found that the distribution of the pressure under the slab in the pilot house is relatively homogeneous and does not exceed a 1 Pa/m pressure drop with distance for the highest depressurisation generated under the slab by active SD.
- Results from passive SD show a lower depressurisation induced at the sump by wind velocity than the depressurisation generated by active SD using a mechanical fan. However, based on the analysis of passive SD, it was found that the permeability characterisation of the pilot house agrees with previous studies on the characterisation of granular fill materials for radon SD systems across Europe.
- Radon reductions in excess of 85% were achieved for the different testing phases in all cases. Based on the radon reduction results associated with the depressurisation generated under the slab as a function of the extraction airflow for the active SD conditions considered, it was found that a 20-W mechanical fan is sufficient to achieve SD resulting in radon reductions of more than 85%.
- To summarise, the monitoring study at the Spanish pilot house contributes to the specification of the optimum SD system performance and the findings can be applied to similar types of dwellings with comparable aggregate layer permeability characteristics within the European context.

6 Recommendations for Further Research

- In practice, the compaction degree of a granular fill material may be higher than those reported in this study. This higher compaction degree might result in a lower k_{ah} and n_{ah} than the values presented in this report. Therefore, further investigation of the compaction degree of T1 Struc and T2 Perm is required at the field scale, e.g. using field-scale slabs for buildings.
- It has been reported that a radon sump might have an influence over an area of 250 m^2 or over a distance of 15 m from the sump (BRE, 1992; EHLG, 2004). However, the results reported in this study were determined using a small-scale test apparatus and a cylinder test tank that had limited diameters of 0.15 m and 2 m, respectively. Moreover, the circular shape of the small-scale test apparatus and the test tank developed in this study could not account for the effect of other factors on the performance of the granular fill material layer, e.g. the shape of the slab and foundation of the building, and obstruction of the walls and foundations. In addition, the measurements taken in the pilot house in Spain have shown that homogeneous suction pressure is developed under the slab if an SD system is built with a highly permeable granular fill material. However, the pilot house had an area of 25 m^2 only and, therefore, the influence area of the sump could not be fully determined in this study. Further investigations using prototype slabs of an SD system incorporating the T1 Struc and T2 Perm materials are essential.
- This study found that the open-pipe cowl and the pipe with a large mushroom cap cowl could reliably be used as passive cowls for an SD system. Further investigations should be performed to find the optimum design for these cowls.
- Pressure loss was found to increase with an increase in the number of bends in the pipework of an SD system. Therefore, additional experimental investigations are recommended to examine the effect of bends and the length of the pipework in both active and passive SD systems.

References

Abbas, A., Carcasses, M. and Ollivier, J.P., 1999. Gas permeability of concrete in relation to its degree of saturation. *Materials and Structures* 32: 3–8.

Abdelouhab, M., 2011. Contribution à l'étude du transfert des polluants gazeux entre le sol et les environnements intérieurs des bâtiments. Autre. University of La Rochelle, La Rochelle, France.

Abdelouhab, M., Collignan, B. and Allard, F., 2010. Experimental study on passive soil depressurization system to prevent soil gaseous pollutants into the building. *Building and Environment* 45: 2400−2406.

Andersen, C.E., 2001. Numerical modelling of radon-222 entry into houses: an outline of techniques and results. *Science of the Total Environment* 272: 33–42.

Ansys Inc., 2013. *Ansys FLUENT 15.0 User's Guide.* Ansys Inc., Canonsburg, PA.

Ansys Inc., 2014. *Introduction to Ansys Fluent*. Ansys Inc., Canonsburg, PA.

ASTM International, 2013. *D6539 − Standard Test Method for Measurement of the Permeability of Unsaturated Porous Materials by Flowing Air*. ASTM International, West Conshohocken, PA.

AWWA (American Water Works Association), 2014. *Manual of Water Supply Practices-Groundwater (4th Edition)*. AWWA, Denver, CO.

Baeza, A., García-Paniagua, J., Guillen, J. and Montalban, B., 2018. Influence of architectural style on indoor radon concentration in a radon prone area: a case study. *Science of the Total Environment* 610–611: 258–266.

Ball, B.C. and Schjonning, P., 2002. Air permeability. In Dane, J.H. and Topp, G.C. (eds), *Methods of Soil Analysis*. Part 4. SSA, Madison, AL, pp. 1141–1158.

Bonnefous, Y.Y., Gadgil, A.J., Fisk, W.J., Prill, R.J. and Nematollahi, A., 1992. Field study and numerical simulation of subslab ventilation systems. *Environmental Science and Technology* 26: 1752−1759.

BRE, 1998. *Modeling and Measurement of Soil Gas Flow*. IHS BRE Press, Bracknell, UK.

Broadhead, B., 2018. Radon mitigation in the US. WPB-Radon Inc. ROOMS (Radon Outcomes on Mitigation Solutions) Conference, Lugano, Switzerland, 27–28 September 2018.

BSI (British Standards Institution), 1990a. *BS 1377 − Methods of Test for Soils for Civil Engineering Purposes. Part 2: Classification Tests*. BSI, London.

BSI (British Standards Institution), 1990b. *BS 1377 − Methods of Test for Soils for Civil Engineering Purposes. Part 4: Compaction-related Tests*. BSI, London.

Budhu, M., 2010. *Soil Mechanics and Foundations*, 3rd edn. John Wiley & Sons, Hoboken, NJ.

Collignan, B., 2018. Radon management in buildings: applied research results on building characterization and protection. IAEA webinar, 25 April 2018.

Darby, S., Hill, D., Auvinen, A., Barros-Dios, J.M., Baysson, H., Bochicchio, F., Deo, H., Falk, R., Forastiere, F., Hakama, M., Heid, I., Kreienbrock, L., Kreuzer, M., Lagarde, F., Mäkeläinen, I., Muirhead, C., Oberaigner, W., Pershagen, G., Ruano-Ravina, A., Ruosteenoja, E., Rosario, A.S., Tirmarche, M., Tomásek, L., Whitley, E., Wichmann, H.E. and Doll, R., 2005. Radon in homes and risk of lung cancer: collaborative analysis of individual data from 13 European case–control studies. *BMJ* 330: 223. https://doi.org/10.1136/bmj.38308.477650.63.

Darcy, H., 1856. *Les Fontaines Publiques de la Ville de Dijon*. Dalmont, Paris.

DEHLG (Department of Environment, Heritage and Local Government), 1997. *Building Regulations 1997. Technical Guidance Document C*. Stationery Office, Dublin.

DEHLG (Department of Environment, Heritage and Local Government), 2002. *Radon in Existing Buildings – Corrective Options*. Stationery Office, Dublin.

DEHLG (Department of Environment, Heritage and Local Government), 2012. *Building Regulation*. Government Publications, Mayo, Ireland.

Detmer, D.M., 1995. Permeability porosity, and grain-size distribution of selected Pliocene and Quaternary sediments in the Albuquerque Basin. *New Mexico Geology*: 79–87.

DETR (Department of the Environment, Transport and the Regions), 1997a. *Passive Venting of Soil Gases beneath Buildings*: *Guide for Design*. Vol. 1, DETR Partners In Technology Research, London.

DETR (Department of the Environment, Transport and the Regions), 1997b. *Passive Venting of Soil Gases beneath Buildings: Guide for Design*. Vol. 2, DETR Partners In Technology Research, London.

Diallo, T.M.O., 2013. Impact des polluants gazeux du sol sur la qualité de l'air intesrieur des bâtiments. Genie civil. Université de La Rochelle, La Rochelle, France.

Diallo, T.M.O., Collignan, B. and Allard, F., 2015. Air flow models for sub-slab depressurization systems design. *Building and Environment* 87: 327−341.

Diallo, T.M.O., Collignan, B. and Allard, F., 2018. Analytical quantification of the impact of sub-slab gravel layer on the airflow from soil into building substructures. *Building Simulation* 11(1): 155–163.

Dumais, C., 2018. The Canadian approach to radon mitigation and design. Radonwest Inc. ROOMS (Radon Outcomes on Mitigation Solutions) Conference, Lugano, Switzerland, 27–28 September 2018.

Ergun, S., 1952. Fluid flow through packed columns. *Chemical Engineering Progress* 48: 89−94.

EU (European Union), 2014. Council Directive 2013/59/Euratom of 5 December 2013 laying down basic safety standards for protection against the dangers arising from exposure to ionising radiation, and repealing Directives 89/618/Euratom, 90/641/Euratom, 96/29/Euratom, 97/43/Euratom and 2003/122/Euratom. OJ L 13, 17.1.2014, p. 1–73.

Fetter, C.W., 2001. *Applied Hydrogeology (4th Edition)*. Pearson, Upper Saddle River, NJ.

Fowler, C.S., Williamson, A.D., Pyle, B.E., Belzer, F.E. and Coker, R.N., 1991. *Handbook: Sub-slab Depressurization for Low-permeability Fill Material. Design & Installation of a Home Radon Reduction System*. US Environmental Protection Agency, Washington, DC.

Fredlund, D.G. and Rahardjo, H., 1993. *Soil Mechanics for Unsaturated Soils*. John Wiley, Hoboken, NJ.

Freeze, R.A. and Cherry, J.A., 1979. *Groundwater*. Prentice Hall, Upper Saddle River, NJ.

Frutos, B., 2009. *Estudio experimental sobre la efectividad y la viabilidad de distintas soluciones constructivas para reducir la concentración de gas radón en edificaciones.* Universidad Politécnica de Madrid, Madrid.

Forchheimer, P., 1901. Wasserbewegung durch Boden. *Zeitschrift des Vereines Deutscher Ingenieure* 45: 1782–1788.

Fuente, M., Rabago, D., Herrera, S., Quindos, L., Fuente, I., Foley, M. and Sainz, C., 2018. Performance of radon monitors in a purpose-built radon chamber. *Journal of Radiological Protection* 38: 1111–1127. https://doi.org/10.1088/1361–6498/aad969

Fuente, M., Muñoz, E., Sicilia, I., Goggins, J., Hung, L.C., Frutos, B. and Foley, M., 2019. Investigation of gas flow through soils and granular fill materials for the optimisation of radon soil depressurisation system. *Journal of Environmental Radioactivity* 198: 200–209. https://doi.org/10.1016/j.jenvrad.2018.12.024

Fuente, M., Rabago, D., Goggins, J., Fuente, I., Sainz, C. and Foley, M., 2019. Radon mitigation by soil depressurisation case study: radon concentration and pressure field extension monitoring in a pilot house in Spain. *Science of the Total Environment* 695: 133746. https://doi.org/10.1016/j.scitotenv.2019.133746

Fuente, M., Long, S., Fenton, D., Hung, L.C., Goggins, J. and Foley, M., 2020. Review of recent radon research in Ireland, OPTI-SDS project and its impact on the National Radon Control Strategy. *Applied Radiation and Isotopes* 163: 109210. https://doi.org/10.1016/j.apradiso.2020.109210

Gadgil, A.J., Bonnefous, Y.C., Fisk, W.J., Prill, R.J. and Nematollahi, A., 1991. *Influence of Subslab Aggregate Permeability on SSV Performance*. Report no. LBL−31160, Ernest Orlando Lawrence Berkeley National Laboratory, Berkeley, CA.

Gadgil, A.J., Bonnefous, Y.C. and Fisk, W.J., 1994. Relative effectiveness of sub-slab pressurization and depressurization systems for indoor radon mitigation: studies with an experimentally verified numerical model. *Indoor Air* 4: 265−275.

Garcia-Tobar, J., 2019. Weather-dependent modelling of the indoor radon concentration in two dwellings using CONTAM. *Indoor and Built Environment* 28: 1341–1349. https://doi.org/10.1177/1420326X19841119

Gunning, G.A., Pollard, D. and Finch, E.C., 2014. An outdoor radon survey and minimizing the uncertainties in low-level measurements using CR−39 detectors. *Journal of Radiological Protection* 34: 457−467.

Hung, L.C., Goggins, J., Fuente, M. and Foley, M., 2018a. Characterisation of specified granular fill materials for radon mitigation by soil depressurisation systems. *Construction and Building Materials* 176: 213–227.

Hung, L.C., Goggins, J., Fuente, M. and Foley, M., 2018b. Investigation of sub-slab pressure field extension in specified granular fill materials incorporating a sump-based soil depressurisation system for radon mitigation. *Science of the Total Environment* 637–638: 1081–1097.

Hung, L.C., Goggins, J., Croxford, C. and Foley, M. 2019. Large−scale experimental investigations of specified granular fill materials for radon mitigation by active and passive soil depressurisations. *Journal of Environmental Radioactivity* 207: 27–36. https://doi.org/10.1016/j.jenvrad.2019.05.018

ICRP (International Commission on Radiological Protection), 2010. Lung cancer risk from radon and progeny and statement on radon. ICRP Publication 115. *Annuals of the ICRP* 40(1).

Jelle, B.P., 2012. Development of a model for radon concentration in indoor air. *Science of the Total Environment* 416: 343–350.

Jiránek, M., 2014. Sub-slab depressurisation systems used in the Czech Republic and verification of their efficiency. *Radio Protection Dosimetry* 162: 63–67.

Jiránek, M. and Svoboda, Z., 2007. Numerical modelling as a tool for optimisation of sub-slab depressurisation system design. *Building and Environment* 42: 1994–2003.

Lopez-Abente, G., Nunez, O., Fernandez-Navarro, P., Barros-Dios, J.M., Martín-Méndez, I., Bel-Lan, A., Locutura, J., Quindos, L., Sainz, C. and Ruano-Ravina, A., 2018. Residential radon and cancer mortality in Galicia, Spain. *Science of the Total Environment* 610–611: 1125–1132.

Long, S., Fenton, D., Cremin, M. and Morgan, A., 2013. The effectiveness of radon preventive and remedial measures in Irish homes. *Journal of Radiological Protection* 33(1): 141.

Lu, N. and Likos, W.J., 2004. *Unsaturated Soil Mechanics*. John Wiley, Hoboken, NJ.

McWhorter, D.B. and Sunada, D.K., 1977. *Groundwater Hydrology and Hydraylics*. Water Resources Publications, Highlands Ranch, CO.

Mentes, G. and Eper-Papao, I., 2015. Investigation of temperature and barometric pressure variation effects on radon concentration in the Sopronbanfalva Geodynamic Observatory, Hungary. *Journal of Environmental Radioactivity* 149: 64–72. https://doi.org/10.1016/j.jenvrad.2015.07.015.

Nagtegaal, P.J.C., 1978. Sandstone-framework instability as a function of burial diagenesis. *Journal of the Geological Society* 135: 101–105.

Nero, A.V., Gadgil, A.J., Nazaroff, W.W. and Revzan, K.L., 1990. *Indoor Radon and its Decay Products: Concentrations, Causes and Control Strategies*. Technical report. Lawrence Berkeley National Laboratory, University of California, Berkeley, CA.

NSAI (National Standards Authority of Ireland), 2016a. *IS 888:2016 Code of Practice for the Procurement and Use of Unbound Granular Fill Hardcore Material for Use under Concrete Floors*. NSAI, Dublin.

NSAI (National Standards Authority of Ireland), 2016b. *S.R. 21:2014+A1:2016. Guidance on the Use of I.S. EN 13242:2002 +A1:2007 – Aggregates for Unbound and Hydraulically Bound Materials for Use in Civil Engineering Work and Road Construction*. NSAI, Dublin.

Reddy, T.A., Gadsby, K.J., Black, H.E., Harrje, D.T. and Sextro, R.G., 1991. Modelling air flow dynamics in radon mitigation system: a simplified approach. *Journal of Air & Waste Management Association* 41: 1476–1482. https://doi.org/10.1080/10473289.1991.10466946

Riley, W.J., Gadgil, A.J., Bonnefous, Y.C. and Nazaroff, W., 1996. The effect of steady winds on radon-222 entry from soil into houses. *Atmospheric Environment* 30: 1167–1176. https://doi.org/10.1016/1352-2310(95)00248-0

Schubert, M., Mussolff, A. and Weiss, H., 2018. Influences of meteorological parameters on indoor radon concentrations (^{222}Rn) excluding the effects of forced ventilation and radon exhalation from soil and building materials. *Journal of Environmental Radioactivity* 198: 81–85.

Scivyer, C.R. and Jaggs, M.P.R., 1998. *A BRE Guide to Radon Remedial Measures in Existing Dwellings. Dwellings with Cellars and Basements*. IHS BREPress, Bracknell, UK.

Shukla, M., 2014. *Soil Physics: An Introduction*. CRC Press, Boca Raton, FL.

Springer, D.S., Loaiciga, H.A., Cullen, S.J. and Lorne, G.E., 1998. Air permeability of porous material under controlled laboratory conditions. *Groundwater* 36: 558–565.

Terzaghi, K., Peck, R.B. and Mesri, G., 1996. *Soil Mechanics in Engineering Practice*, 3rd edn. John Wiley, Hoboken, NJ.

US EPA (US Environmental Protection Agency), 1993. *Radon Reduction Techniques for Existing Detached Houses. Technical Guidance (Third Edition) for Active Soil Depressurization Systems*. EPA/625/R-90/011. US EPA, Washington, DC.

Vazquez, B.F., 2017. The Spanish experience: approaches, optimisation, and singularities concerning to energy saving. International IAEA Workshop 'Radon for building professionals', Ciudad Rodrigo, Salamanca, Spain, 13–17 November.

Vazquez, B.F., Adan, M.O., Poncela, L.S.Q., Fernandez, C.S. and Merino, I.F., 2011. Experimental study of the effectiveness of four radon mitigation solutions, based on underground depressurization, tested in prototype housing built in a high radon area in Spain. *Journal of Environmental Radioactivity* 102: 378−385.

Vogeltanz-Holm, N. and Schwartz, G.G., 2018. Radon and lung cancer: what does the public really know? *Journal of Environmental Radioactivity* 192: 26–31.

WHO (World Health Organization), 2009. *WHO Handbook on Indoor Radon: A Public Health Perspective*. WHO Press, Geneva.

WHO (World Health Organization), 2016. Radon and health. Available online: http://www.who.int/mediacentre/factsheets/fs291/en/ (accessed 4 September 2017).

Abbreviations

ΔP	Pressure difference
BS	British Standard
CFD	Computational fluid dynamics
d_{50}	Particle size of the granular fill material at 50% passing (mm)
d_{ef}	Effective particle size of the granular fill material (m)
DETR	Department of the Environment, Transport and the Regions
D–F	Darcy–Forchheimer
d_{sump}	Sump depth (m)
EPA	Environmental Protection Agency
γ_{dry}	Dry unit weight (kN/m^3)
k	Turbulent kinetic energy (m^2/s^2)
k_{ah}	Air permeability of the granular fill material
$k_{ah(T1Struc)}$	Air permeability of the T1 Struc granular fill material (m^2)
$k_{ah(T2Perm)}$	Air permeability of the T2 Perm granular fill material (m^2)
k_{as}	Air permeability of the native soil
L	Flow length (m)
MARIA	Mechanized house for Advanced Research on Indoor Air
μ	Dynamic viscosity (Pa.s)
n_h	Porosity
P	Suction pressure developed in an SD system obtained from CFD simulations (Pa)
PFE	Pressure field extension
P_{sump}	Suction pressure at the sump (Pa)
PVC	Polyvinyl chloride
Q_m	Airflow rate
RANS	Reynolds-averaged Navier−Stokes
SD	Soil depressurisation
t	Thickness of the granular fill material (m)
$t_{(final)}$	Final thickness
$t_{(initial)}$	Initial thickness
$t_{(T2Perm)}$	Thickness of the T2 Perm granular fill material (m)
V	Flow velocity (m/s)
w_{crack}	Width of wall crack (mm)
WHO	World Health Organization
w_n	Moisture content
w_{nc}	Compaction moisture content
$w_{nc(opt)}$	Optimum compaction moisture content (%)
w_{sump}	Sump width (m)

Appendix 1 Data Adapted from External Studies

Table A1.1. Typical porosity (*n*) values for granular material used as hardcore in SD systems

Material type	*n*	Reference	Standard
Well-sorted sand (dense)	0.34	Terzaghi *et al*. (1996)	N/A
Poorly sorted sand (dense)	0.3		
Gravel (fine)	0.25–0.38	McWhorter and Sunada (1977)	N/A
Gravel (coarse)	0.24–0.36		
Sand (fine)	0.25–0.53		
Sand (coarse)	0.31–0.46		
Gravel	0.25–0.4	Freeze and Cherry (1979)	N/A
Sand	0.25–0.5		
Sandstone	0.05–0.3		
Well-sorted gravel	0.12–0.46	Fredlund and Rahardjo (1993)	N/A
Well-sorted sand	0.17–0.55		
Gravel (well sorted)	0.25–0.5	Fetter (2001)	ASTM D4253/4254
Sand (well sorted)	0.25–0.5		
Sand and gravel mixed	0.2–0.35		
Sand (very dense)	≤ 0.15	Budhu (2010)	ASTM D4253/4254
Sand (dense)	0.15–0.3		
Sand (medium)	0.3–0.6		
Gravel	0.2	AWWA (2014)	ASTM D4253/4254
Sand	0.25		
10-mm single-sized gravel (uncompacted)	0.37	BRE (1998)	N/A
10-mm single-sized gravel (compacted)	0.35		
20-mm single-sized gravel (uncompacted)	0.43		
20-mm graded gravel (uncompacted)	0.46		
40-mm graded gravel (uncompacted)	0.45		
40-mm graded gravel (compacted)	0.39		
Well-graded gravel (uncompacted)	0.32		
Well-graded gravel (compacted)	0.22		

N/A, not available.

Table A1.2. Typical air permeability (k_a) values for granular materials used as hardcore in SD systems

Material type	*k*a (m²)	Reference	Standard
Clean sand	10^{-10}–10^{-13}	Freeze and Cherry (1979), Lu and Likos (2004)	N/A
Gravel	10^{-7}–10^{-10}		
Gravel (dense)	2×10^{-8}	Bonnefous *et al*. (1992)	N/A
Gravel (medium)	10^{-7}		
Gravel (loose)	2×10^{-7}		
Gravel	5×10^{-9}	Andersen (2001)	N/A
Gravel	10^{-9}	Diallo (2013)	N/A
10-mm single-sized gravel (uncompacted)	2.1×10^{-8}	BRE (1998)	ASTM 90,
20-mm single-sized gravel (uncompacted)	9.9×10^{-8}		DoT 90
20-mm graded gravel (uncompacted)	9.3×10^{-8}		
40-mm graded gravel (uncompacted)	2.7×10^{-7}		
Well-graded gravel (uncompacted)	2.7×10^{-8}		

DoT, UK Department of Transport; N/A, not available.

Appendix 2 Data Developed in This Study

Table A2.1. Experimental testing programme for compactions and pressure measurements for the T1 Struc, T2 Perm and Hybrid materials

Material layer	Material type	$t_{(initial)}$ (mm)	Compaction	Suction pressure measurement			
				Type 1	Type 2	Type 3	Type 4
T1−Layer #1	T1 Struc	150	×				
T1−Layer #2		225	×	×			
T1−Layer #3		150	×	×			
T1−Layer #4		150	×				
T1−Layer #5		225	×	×	×		
T1−Layer #6		110	×	×			
T2−H−Layer #7	Hybrid	225	×	×	×		
T2−Layer #1	T2 Perm	150	×				
T2−Layer #2		150	×	×	×	×	
T2−Layer #3		150	×	×		×	×
T2−Layer #4		150	×	×			
T2−Layer #5		150	×	×			
T2−Layer #6		150	×	×, ×*	×		

×, active depressurisation; ×*, passive depressurisation.

Table A2.2. Summary of the test results for T1 Struc and T2 Perm

No.	Test ID	w_n (%)	γ dry (kN/m³)	n_h	$k_{ah} \times 10^{-10}$ (m²)			
					Darcy (1856)	Ergun (1952)	ASTM (2013)	D–F (1901)
Compacted T1 Struc granular fill material								
1	T1#1-1*	4.26	22.46	0.140	1.69±0.41	0.72±0.04	1.78±0.22	1.78±0.14
2	T1#1-2	3.81	22.46	0.140	1.86±0.25	0.70±0.02	1.95±0.17	1.81±0.42
3	T1#2-1*	5.58	23.38	0.100	Difficult to flow due to extremely low k_{ah}			
4	T1#3-1*	3.25	21.02	0.200	5.25±0.32	3.33±0.16	5.64±0.38	6.16±0.45
5	T1#3-2	2.68	21.02	0.200	6.51±0.23	3.89±0.10	6.88±0.22	6.15±0.19
6	T1#4-1*	3.73	22.40	0.142	2.27±0.18	0.90±0.03	2.40±0.12	3.78±0.30
7	T1#4-2	0.87	22.40	0.142	2.96±0.22	1.26±0.12	3.13±0.32	8.47±0.15
8	T1#4-3	4.25	22.40	0.142	0.68±0.022	0.35±0.03	7.05±0.17	0.41±0.03
9	T1#4-4	3.81	22.40	0.142	2.22±0.31	0.73± 0.02	2.27±0.26	1.64±0.13
10	T1#5-1*	4.34	21.70	0.175	0.97±0.042	0.58±0.04	1.08±0.41	0.75±0.06
11	T1#5-2	2.63	21.70	0.175	1.65±0.12	1.03±0.21	7.92±0.24	1.53±0.35
12	T1#6-1*	3.40	21.81	0.164	1.64±0.35	0.86±0.05	1.73±0.33	1.76±0.27
13	T1#6-2	2.55	21.81	0.164	2.57±0.21	1.62±0.13	2.73±0.32	2.51±0.16
14	T1#6-3	4.8	21.81	0.164	0.90±0.042	0.49±0.03	0.95± 0.03	0.70±0.02
15	T1#7-1*	3.17	21.74	0.167	2.26±0.37	1.09±0.30	2.31±0.28	1.83±0.45
16	T1#7-2	2.1	21.74	0.167	5.63±0.15	3.21±0.12	5.13±0.23	4.06±0.35
17	T1#7-3	4.70	21.74	0.167	0.35±0.033	0.35±0.02	0.35±0.03	0.35±0.04
18	T1#8-1*	3.94	22.53	0.136	1.07±0.35	0.38±0.04	1.12±0.28	0.98±0.06

Table A2.2. Continued

No.	Test ID	w_n (%)	γ dry (kN/m^3)	n_h	$k_{ah} \times 10^{-10}$ (m^2)			
					Darcy (1856)	Ergun (1952)	ASTM (2013)	D–F (1901)
19	T1#8-2	1.72	22.53	0.136	2.79±0.55	1.79±0.37	2.99±0.16	2.76±0.15
20	T1#8-3	4.17	22.53	0.136	0.29±0.044	0.12±0.03	0.24±0.01	0.36±0.02
21	T1#9-1*	3.66	22.46	0.140	0.90±0.011	0.34±0.02	0.96±0.01	0.84±0.02
22	T1#9-2	2.52	22.46	0.140	2.08±0.22	1.02±0.32	2.18±0.13	2.84±0.27
23	T1#9-3	4.00	22.46	0.140	0.23±0.015	0.19±0.05	0.22±0.03	0.20±0.03
24	T1#10-1*	3.61	21.87	0.162	2.00±0.19	0.99±0.03	2.15±0.17	1.69±0.15
25	T1#10-2	2.17	21.87	0.162	3.90±0.25	1.64±0.15	4.14±0.18	3.34±0.23
26	T1#11-1**	3.12	17.20	0.353	183±20.0	374±10.0	N/A	248±18.0
27	T1#12-1*	2.97	20.3	0.23	6.06±1.4	4.87±0.10	6.42±1.3	10.5±1.0
28	T1#13-1*	2.99	20.04	0.23	3.91±0.6	3.37±0.10	4.18±0.7	3.59±0.10
29	T1#14-1**	2.70	17.40	0.35	301±30.0	238±40	N/A	238±20.0
30	T1#15-1*	2.70	21.33	0.20	2.04±0.4	1.51±0.10	2.12±0.4	1.92±0.20
31	T1#16-1*	2.87	22.18	0.18	1.12±0.14	9.74±0.17	N/A	15.5±30.0
32	T1#17-1*	2.60	21.73	0.19	130±32	108±22.0	N/A	87.6±1.70
33	T1#18-1*	0.97	21.04	0.23	56.4±1.1	93.7±2.80	N/A	80.8±1.90
34	T1#19-1*	5.99	23.68	0.13	Difficult to flow due to extremely low k_{ah}			
35	T1#20-1*	3.66	22.19	0.18	2.86±0.24	1.80±0.11	3.04±0.25	2.74±0.06
36	T1#20-2	2.40	22.19	0.18	4.17±0.55	2.62±0.22	4.43±0.13	3.99±0.34
37	T1#20-3	3.75	22.19	0.18	2.52±0.35	1.59±0.22	2.68±0.31	2.42±0.23
38	T1#21-1*	1.32	21.05	0.22	38.5±4.7	38.4±10.0	N/A	34.0±5.0
39	T1#22-1*	2.54	21.36	0.21	17.5±2.3	13.7±2.0	N/A	24.3±4.4
40	T1#22-2	3.11	21.36	0.21	7.56±0.45	5.92±0.33	N/A	10.5±2.5
41	T1#23-1*	2.14	21.14	0.22	11.6±4.0	12.3±5.0	N/A	25.0±3.9
42	T1#24-1*	2.83	21.44	0.21	22.2±3.2	22.9±4.2	N/A	20.2±3.4
43	T1#24-2	3.87	21.44	0.21	2.27±0.17	2.34±0.21	N/A	2.07±0.45
44	T1#25-1*	2.41	21.35	0.21	12.4±2.4	12.9±3.7	N/A	18.4±4.7
45	T1#26-1*	1.45	21.01	0.23	14.3±1.0	12.7±3.3	N/A	20.9±1.7
46	T1#27-1*	3.51	21.92	0.19	4.68±0.32	3.17±0.24	4.96±0.35	4.80±0.54
47	T1#27-2	1.24	21.92	0.19	9.2±0.21	6.29±0.32	9.84±0.43	9.53±0.22
48	T1#27-3	1.24	21.92	0.19	4.13±0.18	2.81±0.20	4.38±0.20	4.23±0.15
49	T1#28-1*	1.64	20.95	0.23	31.0±3.40	36.4±4.90	N/A	35.1±3.60
Compacted T2 Perm granular fill material								
50	T2#1-1*	0.184	16.45	0.373	317±10	641±20	N/A	312±15.00
51	T2#2-1*	0.77	16.35	0.373	191±23	526±16	N/A	190±24.0
52	T2#3-1*	0.3	16.4	0.371	248±26	487±20	N/A	322±25.0
53	T2#4-1*	0.155	16.63	0.363	102±15	576±25	N/A	138±30.0
54	T2#5-1*	1.17	16.7	0.360	323±33	275±15	N/A	196±12.0
55	T2#6-1*	0.61	16.5	0.373	171±11	449±17	N/A	190±33.0

***, compacted material; **, uncompacted material; D–F, Darcy–Forchheimer; N/A, not available.**

Table A2.3. Summary of the k_{ah} values and overall compacted thickness of material obtained from phases 1 and 2

		Phase 2				
	Phase 1	Layer #2	Layer #3	Layer #4	Layer #5	Layer #6
T2 Perm material						
$t_{(final,\ T2\ Perm)}$ (mm)		294	434	569	703	840
Air permeability, k_{ah} (m^2) × 10^{-8}	2.25	2.21	2.25	1.88	1.76	1.15
T1 Struc material						
$t_{(final,\ T2\ Perm)}$ (mm)		120	410		674	757
Air permeability, k_{ah} (m^2) × 10^{-8}	0.024	0.62	0.45		0.42	0.49

Table A2.4. Boundary conditions for the CFD simulations

Boundary	Type	Momentum[a]
Sump	Outlet	$P_{relative} = -100$ Pa
Wall crack ($w_{crack} > 0$)	Inlet (or opening)	$P_{relative} = 0$ Pa
Imperfectly sealed slab	Inlet (or opening)	$P_{relative} = 0$ Pa
Ground surface	Inlet (or opening)	$P_{relative} = 0$ Pa
Wall crack ($w_{crack} = 0$)	Wall	No slip wall
Perfectly sealed slab	Wall	No slip wall
Bottom of the domain	Wall	No slip wall
Left side of the domain	Wall	No slip wall

[a] **$P_{relative}$ is the pressure relative to the reference pressure at 102,300 Pa (1.01 atm).**

Table A2.5. Summary of testing phases at the pilot house

Phase	Description	Dates
1	Closed period	25/06/2018–26/07/2018
2	Passive SD	26/07/2018–end of August 2018
No measurements (issues related to the pressure sensors)		
3	Closed period	10/10/2018–13/11/2018
4	Active SD (v_{ext} = 0–4 m/s)	13/11/2018–16/11/2018
No measurements (issues related to power supply in the house		
5	Closed period	13/12/2018–19/02/2019
6	Active SD (v_{ext} = 1.5 m/s)	19/02/2019–06/03/2019
7	Closed period	06/03/2019–14/03/2019
8	Active SD (v_{ext} = 2 m/s)	14/03/2019–02/04/2019
9	Closed period	02/04/2019–30/04/2019

Table A2.6. Radon concentrations (C_{Rn}) in the basement and on the ground floor for the SD testing phases indicated and radon reductions relative to the average radon levels for the closed periods

	CRn (Bq/m³)		Radon reduction (%)	
	Basement	Ground floor	Basement	Ground Floor
Average closed	54,625	26,421		
Phase 2: passive SD	7417	–	86	–
Phase 4: active SD (v_{ext} = 0–4 m/s)	662	328	99	99
Phase 6: active SD (v_{ext} = 1.5 m/s)	3326	3689	94	86
Phase 8: active SD (v_{ext} = 2 m/s)	3701	2279	93	91

AN GHNÍOMHAIREACHT UM CHAOMHNÚ COMHSHAOIL
Tá an Ghníomhaireacht um Chaomhnú Comhshaoil (GCC) freagrach as an gcomhshaol a chaomhnú agus a fheabhsú mar shócmhainn luachmhar do mhuintir na hÉireann. Táimid tiomanta do dhaoine agus don chomhshaol a chosaint ó éifeachtaí díobhálacha na radaíochta agus an truaillithe.

Is féidir obair na Gníomhaireachta a roinnt ina trí phríomhréimse:

Rialú: *Déanaimid córais éifeachtacha rialaithe agus comhlíonta comhshaoil a chur i bhfeidhm chun torthaí maithe comhshaoil a sholáthar agus chun díriú orthu siúd nach gcloíonn leis na córais sin.*

Eolas: *Soláthraímid sonraí, faisnéis agus measúnú comhshaoil atá ar ardchaighdeán, spriocdhírithe agus tráthúil chun bonn eolais a chur faoin gcinnteoireacht ar gach leibhéal.*

Tacaíocht: *Bímid ag saothrú i gcomhar le grúpaí eile chun tacú le comhshaol atá glan, táirgiúil agus cosanta go maith, agus le hiompar a chuirfidh le comhshaol inbhuanaithe.*

Ár bhFreagrachtaí

Ceadúnú
Déanaimid na gníomhaíochtaí seo a leanas a rialú ionas nach ndéanann siad dochar do shláinte an phobail ná don chomhshaol:
- saoráidí dramhaíola *(m.sh. láithreáin líonta talún, loisceoirí, stáisiúin aistrithe dramhaíola)*;
- gníomhaíochtaí tionsclaíocha ar scála mór *(m.sh. déantúsaíocht cógaisíochta, déantúsaíocht stroighne, stáisiúin chumhachta)*;
- an diantalmhaíocht *(m.sh. muca, éanlaith)*;
- úsáid shrianta agus scaoileadh rialaithe Orgánach Géinmhodhnaithe *(OGM)*;
- foinsí radaíochta ianúcháin *(m.sh. trealamh x-gha agus radaiteiripe, foinsí tionsclaíocha)*;
- áiseanna móra stórála peitril;
- scardadh dramhuisce;
- gníomhaíochtaí dumpála ar farraige.

Forfheidhmiú Náisiúnta i leith Cúrsaí Comhshaoil
- Clár náisiúnta iniúchtaí agus cigireachtaí a dhéanamh gach bliain ar shaoráidí a bhfuil ceadúnas ón nGníomhaireacht acu.
- Maoirseacht a dhéanamh ar fhreagrachtaí cosanta comhshaoil na n-údarás áitiúil.
- Caighdeán an uisce óil, arna sholáthar ag soláthraithe uisce phoiblí, a mhaoirsiú.
- Obair le húdaráis áitiúla agus le gníomhaireachtaí eile chun dul i ngleic le coireanna comhshaoil trí chomhordú a dhéanamh ar líonra forfheidhmiúcháin náisiúnta, trí dhíriú ar chiontóirí, agus trí mhaoirsiú a dhéanamh ar leasúchán.
- Cur i bhfeidhm rialachán ar nós na Rialachán um Dhramhthrealamh Leictreach agus Leictreonach (DTLL), um Shrian ar Shubstaintí Guaiseacha agus na Rialachán um rialú ar shubstaintí a ídíonn an ciseal ózóin.
- An dlí a chur orthu siúd a bhriseann dlí an chomhshaoil agus a dhéanann dochar don chomhshaol.

Bainistíocht Uisce
- Monatóireacht agus tuairisciú a dhéanamh ar cháilíocht aibhneacha, lochanna, uiscí idirchriosacha agus cósta na hÉireann, agus screamhuiscí; leibhéil uisce agus sruthanna aibhneacha a thomhas.
- Comhordú náisiúnta agus maoirsiú a dhéanamh ar an gCreat-Treoir Uisce.
- Monatóireacht agus tuairisciú a dhéanamh ar Cháilíocht an Uisce Snámha.

Monatóireacht, Anailís agus Tuairisciú ar an gComhshaol
- Monatóireacht a dhéanamh ar cháilíocht an aeir agus Treoir an AE maidir le hAer Glan don Eoraip (CAFÉ) a chur chun feidhme.
- Tuairisciú neamhspleách le cabhrú le cinnteoireacht an rialtais náisiúnta agus na n-údarás áitiúil *(m.sh. tuairisciú tréimhsiúil ar staid Chomhshaol na hÉireann agus Tuarascálacha ar Tháscairí)*.

Rialú Astaíochtaí na nGás Ceaptha Teasa in Éirinn
- Fardail agus réamh-mheastacháin na hÉireann maidir le gáis cheaptha teasa a ullmhú.
- An Treoir maidir le Trádáil Astaíochtaí a chur chun feidhme i gcomhair breis agus 100 de na táirgeoirí dé-ocsaíde carbóin is mó in Éirinn.

Taighde agus Forbairt Comhshaoil
- Taighde comhshaoil a chistiú chun brúnna a shainaithint, bonn eolais a chur faoi bheartais, agus réitigh a sholáthar i réimsí na haeráide, an uisce agus na hinbhuanaitheachta.

Measúnacht Straitéiseach Timpeallachta
- Measúnacht a dhéanamh ar thionchar pleananna agus clár beartaithe ar an gcomhshaol in Éirinn *(m.sh. mórphleananna forbartha)*.

Cosaint Raideolaíoch
- Monatóireacht a dhéanamh ar leibhéil radaíochta, measúnacht a dhéanamh ar nochtadh mhuintir na hÉireann don radaíocht ianúcháin.
- Cabhrú le pleananna náisiúnta a fhorbairt le haghaidh éigeandálaí ag eascairt as taismí núicléacha.
- Monatóireacht a dhéanamh ar fhorbairtí thar lear a bhaineann le saoráidí núicléacha agus leis an tsábháilteacht raideolaíochta.
- Sainseirbhísí cosanta ar an radaíocht a sholáthar, nó maoirsiú a dhéanamh ar sholáthar na seirbhísí sin.

Treoir, Faisnéis Inrochtana agus Oideachas
- Comhairle agus treoir a chur ar fáil d'earnáil na tionsclaíochta agus don phobal maidir le hábhair a bhaineann le caomhnú an chomhshaoil agus leis an gcosaint raideolaíoch.
- Faisnéis thráthúil ar an gcomhshaol ar a bhfuil fáil éasca a chur ar fáil chun rannpháirtíocht an phobail a spreagadh sa chinnteoireacht i ndáil leis an gcomhshaol *(m.sh. Timpeall an Tí, léarscáileanna radóin)*.
- Comhairle a chur ar fáil don Rialtas maidir le hábhair a bhaineann leis an tsábháilteacht raideolaíoch agus le cúrsaí práinnfhreagartha.
- Plean Náisiúnta Bainistíochta Dramhaíola Guaisí a fhorbairt chun dramhaíl ghuaiseach a chosc agus a bhainistiú.

Múscailt Feasachta agus Athrú Iompraíochta
- Feasacht chomhshaoil níos fearr a ghiniúint agus dul i bhfeidhm ar athrú iompraíochta dearfach trí thacú le gnóthais, le pobail agus le teaghlaigh a bheith níos éifeachtúla ar acmhainní.
- Tástáil le haghaidh radóin a chur chun cinn i dtithe agus in ionaid oibre, agus gníomhartha leasúcháin a spreagadh nuair is gá.

Bainistíocht agus struchtúr na Gníomhaireachta um Chaomhnú Comhshaoil
Tá an ghníomhaíocht á bainistiú ag Bord lánaimseartha, ar a bhfuil Ard-Stiúrthóir agus cúigear Stiúrthóirí. Déantar an obair ar fud cúig cinn d'Oifigí:
- An Oifig um Inmharthanacht Comhshaoil
- An Oifig Forfheidhmithe i leith cúrsaí Comhshaoil
- An Oifig um Fianaise is Measúnú
- Oifig um Chosaint Radaíochta agus Monatóireachta Comhshaoil
- An Oifig Cumarsáide agus Seirbhísí Corparáideacha

Tá Coiste Comhairleach ag an nGníomhaireacht le cabhrú léi. Tá dáréag comhaltaí air agus tagann siad le chéile go rialta le plé a dhéanamh ar ábhair imní agus le comhairle a chur ar an mBord.

EPA Research Report 332

OPTI-SDS: An Investigation of the OPTImum Specification for Soil Depressurisation Systems (Active and Passive) That Take Account of Irish Building Practices

Authors: Le Chi Hung, Jamie Goggins, Marta Fuente and Mark Foley

Identifying Pressures

In Ireland, radon is the second most important cause of lung cancer (after smoking) and is linked to up to 300 cases per year. It is estimated that some 9% of homes exceed the reference level of radon of 200 Bq/m^3 and about one-third of the country is categorised as being at high risk.

The National Radon Control Strategy (NRCS) for Ireland identified several knowledge gaps, including the optimum specifications for soil depressurisation (SD) systems (active and passive) that take account of Irish building practices. Few publications exist on this issue in the Irish context and this limits policy development and implementation, as well as hindering the use of novel technologies in the development of "radon-safe" new buildings. Studies in other countries have indicated that the effectiveness of passive sumps is enhanced by appropriate sealing across the base of the building (passive SD systems). Therefore, research is required in this field to take account of Irish building practices.

Informing Policy

Radon research has the potential to reduce the radiation burden to the population and hence reduce lung cancer rates. The European Radon Association (ERA) is attempting to consolidate international research efforts, most recently at the ERA meeting in February 2020 in Vienna. European Union partnerships have been established, with networks including universities, government agencies, and small and medium-sized enterprises, and the outcomes of these will inform international policies. Specific guidance on radon prevention measures for new homes in Ireland is contained in the "Building Regulations 1997, Technical Guidance Document C: Site Preparation and Resistance to Moisture". The NRCS was developed to address the long-term radon exposure risk and highlights the need to strengthen technical guidance to protect against and prevent radon exposure in new buildings. The OPTI-SDS project findings will inform the NRCS co-ordination groups' input into the revision of Technical Guidance Document C.

Developing Solutions

The OPTI-SDS project examined the characterisation of the T1 Struc and T2 Perm specified granular fill materials for SD systems for buildings. The project was divided into two experimental test phases. Furthermore, passive depressurisation tests were carried out to examine the performance of different common chimney cowls available on the market for use in passive depressurisation systems.

Computational fluid dynamic simulations were developed and validated to simulate the flow behaviour of the T1 Struc and T2 Perm materials. The key parameters for simulating the flow behaviour of the materials were confirmed to be air permeability, porosity and effective particle diameter. Benchmark input parameters for the design of the T1 Struc and T2 Perm materials are provided in this study.

Finally, a case study was conducted in a pilot house with high radon levels in Spain to examine the ability and efficiency of active and passive SD systems to mitigate radon levels. Radon concentration and pressure field extension under the slab were monitored to examine radon reductions as a function of depressurisation.

EPA Research: McCumiskey House, Richiew, Clonskeagh, Dublin 14.

Phone: 01 268 0100
Twitter: @EPAResearchNews
Email: research@epa.ie